Science of the Total Environment 812 (2022) 151334

Contents lists available at ScienceDirect

Science of the Total Environment

journal homepage: www.elsevier.com/locate/scitotenv

Adsorption isotherm models: A comprehensive and systematic review (2010−2020)

Mahdieh Mozaffari Majd [a], Vahid Kordzadeh-Kermani [b], Vahab Ghalandari [a], Anis Askari [c], Mika Sillanpää [d,e,f,*]

[a] Kerman Momtazan Cement Company, 32nd km Kerman-Tehran Highway, 7637158135, Kerman, Iran
[b] Department of Chemical Engineering, Iran University of Science and Technology, Narmak, Tehran 16846-13114, Iran
[c] Department of Chemical Engineering, Amirkabir University of Technology (Tehran Polytechnic), Tehran, Iran
[d] Faculty of Science and Technology, School of Applied Physics, University Kebangsaan Malaysia, 43600 Bangi, Selangor, Malaysia
[e] School of Chemistry, Shoolini University, Solan, Himachal Pradesh 173229, India
[f] Department of Biological and Chemical Engineering, Aarhus University, Nørrebrogade 44, 8000 Aarhus C, Denmark

HIGHLIGHTS

- The most widely used adsorption isotherm models are reviewed.
- The applicable definition and parameters of isotherms are organized in the table.
- Numerous practical examples of isotherms used in peer-reviewed studies are presented.

GRAPHICAL ABSTRACT

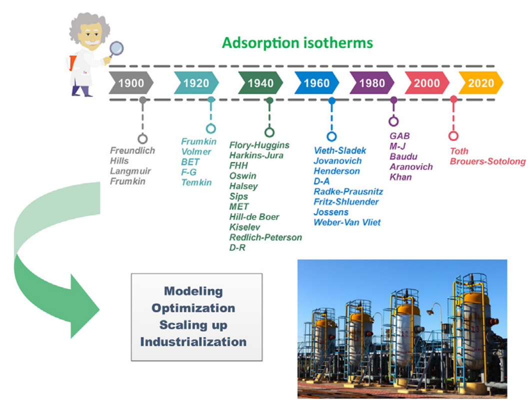

ARTICLE INFO

Article history:
Received 21 July 2021
Received in revised form 26 October 2021
Accepted 26 October 2021
Available online 6 November 2021

Editor: Jay Gan

Keywords:
Adsorption
Adsorption isotherms
Maximum adsorption capacity
Isotherm equation

ABSTRACT

Among numerous methods developed in purification and separation industries, the adsorption process has received considerable attention due to its inexpensive, facile, and eco-friendly nature. The importance of the adsorption process causes extraordinary endeavors for modeling the adsorption isotherms during the years; thus, myriads of research have been conducted and many reviews have been published. In this paper, we have attempted to gather the most widely used adsorption isotherms and their related definitions, along with examples of correlated work of the recent decade. In the present review, 37 adsorption isotherms with about 400 references have been collected from the research published in the period of 2010–2020. The adsorption isotherms utilized are alphabetically organized for ease of access. The parameters of each isotherm, as well as the applicable definitions, are presented in the table, in addition to being discussed in the text. Another table is provided for the practical use of researchers, featuring the usage of the related isotherms in peer-reviewed studies.

Contents

* Corresponding author at: Department of Biological and Chemical Engineering, Aarhus University, Nørrebrogade 44, 8000 Aarhus C, Denmark.
E-mail address: mikaesillanpaa@gmail.com (M. Sillanpää).

https://doi.org/10.1016/j.scitotenv.2021.151334
0048-9697/

1. Introduction

Among various methods evolved in purification and separation industries, the adsorption process has received remarkable attention due to its inexpensive, uncomplicated and eco-friendly nature. IUPAC defines adsorption as “the increase in the concentration of a substance at the interface of a condensed and a liquid or gaseous layer owing to the operation of surface forces” (Calvert, 1990). Adsorbate is the substance in the solid, liquid or gas phase, which is adsorbed, and the substance (surface) into which the adsorbate is adsorbed is called adsorbent. Adsorption processes are categorized into physical and chemical classes based on the nature of forces between adsorbate and adsorbent. Van der Waals forces play a critical role in physical adsorption, whereas chemical bonds are associated with chemical adsorption. The importance of the adsorption process encourages researchers from many disciplines to better understand this process. Numerous experimental and theoretical studies (molecular dynamics study and density functional theory (DFT) methods) have been conducted for this purpose (Ahmad et al., 2020; Majd et al., 2017; Zhuang et al., 2020). Among these various data, the adsorption isotherms and their corresponding equations characterize the adsorption processes in a complete and thorough manner. The adsorption isotherm describes and predicts the amount of adsorbed material as a function of pressure (or concentration) at a constant temperature (Karri and Sahu, 2018; Karri et al., 2017). Remarkable endeavors have been made for modeling the adsorption isotherms within the past decade and the efforts will continue to discover the unknown aspects of them.

About 15% of world's energy consumes in industrial separation processes especially in oil and gas refineries, food processing, and water treatment industries which include adsorption processes. The industrial adsorption process can be classified into two categories of bulk separation process and purification process. The bulk separation process includes processes like separation of paraffin/aromatics, N_2/O_2, water/ethanol, p-xylene/o-xylene, fructose/glucose and etc. The purification approach especially considers removing substances from different streams such as organic compounds from air, water from natural gas, sulfur compounds from hydrogen, solvents and odors from air, odor and taste from drinking water, and the decolorizing of sugar syrups, vegetable oils and petroleum fractions. The industrial adsorption process can be implemented in two modes of batch and continuous counter-current. In the batch process the feed stream passes through a fixed bed adsorbent stage until the adsorbent's saturation be obtained. After the saturation achieved the adsorbent bed is regenerated or replaced by fresh ones. The continuous adsorption process considers two parallel fixed beds that runs at adsorption and desorption modes simultaneously which their modes changed in turn by achieving saturation. Additionally, the moving bed method is known as a continuous process in which the adsorbent particles move in different zones of the adsorption equipment. The fluidized and expanded bed processes is also introduced for improving the process time and efficiency. The pressure swing adsorption (PSA) and the temperature swing adsorption (TSA) are two procedure that applied in industrial gas adsorption processes for establishing a continuous operation.

In the all mentioned industrial adsorption processes it is crucial to know the equilibrium data, the adsorption capacity of adsorbent, and the kinetics of the process for designing and optimizing purposes. Therefore, the adsorption isotherms provide valuable estimate data in different operation condition for researcher and engineers which can be applied for designing, optimizing and troubleshooting of an adsorption process.

In this paper, the most widely used adsorption isotherms and their related definitions, along with correlated research conducted in the recent decade are gathered. The adsorption isotherms presented are alphabetically organized for ease of access in Table 1. The parameters of each isotherm, as well as the applicable definitions, are defined in Table 2, in addition to being discussed in the text. Table 3 presenting different adsorption processes is provided for the practical use of researchers, featuring examples of the isotherms used in peer-reviewed studies. In all isotherm models q_e and C_e are defined as equilibrium adsorption capacity of adsorbent and equilibrium concentration of adsorbate, respectively.

To the best of our knowledge, this is the most comprehensive review that has been published to date on adsorption isotherms, and we hope that this review will be useful for researchers working in the related area.

2. Isotherm models

2.1. Aranovich isotherm model

The Aranovich isotherm is based on the theory of polymolecular adsorption isotherm and can be properly used for calculating the specific surface areas of disperse and porous adsorbents (Aranovich, 1992). The assumptions that Aranovich isotherm takes into account can be summarized as follows: the adsorbent surfaces are even, level and homogeneous; merely the interaction of “closest neighbors” exists; the energy of desorption is dependent upon layer's numeral value; and just configurational components of free energy are taken into consideration. Aranovich isotherm model can be considered as the modified form of BET model. This equation is the same as BET equation (Eq. (4)) (Wjihi et al., 2019) in all terms except for the power of the term $(1 - C_e/C_s)$ which is 0.5 for Aranovich while in the BET model it equals to 1. Furthermore, it can be applied to the broader range of adsorbate concentrations compared to BET model. The Aranovich equation can be expressed as (Aranovich, 1992; Do, 1998):

$$q_e = \frac{q_{m,Ar} C_{Ar} \frac{C_e}{C_{S,Ar}}}{\left(1 - \frac{C_e}{C_{S,Ar}}\right)^{\frac{1}{2}} \left(1 + C_{Ar} \frac{C_e}{C_{S,Ar}}\right)} \quad (1)$$

In which C_{Ar}, $C_{S,\ Ar}$, and $q_{m,\ Ar}$ are the Aranovich isotherm constant, saturation concentration of Aranovich isotherm and maximum adsorption capacity of Aranovich isotherm, respectively.

Furthermore, researchers (Szatanik-Kloc et al., 2018) studied the soil compaction impact on the surface properties of different cereal roots. They measured the water vapor adsorption-desorption isotherms and fitted the experimental data of the quantity of adsorbed water vapor per root's mass to Aranovich isotherm model to find out the specific surface area.

Using carbon adsorbents for adsorbing benzene and pyridine vapors was investigated elsewhere (Belyaeva and Krasnova, 2016). By means of the BET and Aranovich equations, general characteristics of adsorption were determined. It was concluded that it is more accurate to describe the adsorption isotherm of benzene vapors by the Aranovich model and pyridine vapors by the BET model.

Humpola and Odetti (Humpola et al., 2013) developed a method centered on gas isotherm measurements (nitrogen, carbon dioxide, methane, oxygen and argon) to calculate the adsorption capacities of different solid materials. They applied the method to characterize two granular activated carbons and a graphitized carbon black surface. They investigated the conformity of the system with the BET and the Aranovich isotherms. They conclude that the Aranovich isotherm can appropriately describe the adsorption behavior of granular activated carbon at high pressures.

2.2. Baudu isotherm model

The Baudu isotherm model considers the Langmuir coefficients (Eq. (37) (Langmuir, 1918) as a function of concentration (if $K_L = b_{0,\ Ba} C_e^{x_{Ba}}$, $q_{mL} = q_{m0,\ Ba} C_e^{y_{Ba}}$) (Baudu, 1990; Baudu et al., 1989). By substituting these functionalities in the Langmuir model, the four-parameter Baudu model will be obtained (Eq. (2)). This equation was proposed in 1990 by Baudu to model an adsorption system for removing various organic pollutants in aqueous solution using activated carbon. The x_{Ba} and y_{Ba} defines as Baudo constants and the terms of $(1 + x_{Ba} + y_{Ba})$ and $(1 + x_{Ba})$ should have a value under unity for model validity (Saadi et al., 2015). The $q_{m0,\ Ba} (mg/g)$ is the maximum adsorption capacity of the model and the $b_{0,\ Ba}$ is equilibrium constant. In the systems with low coverage of the surface, the Baudu model transforms to Eq. (3).

$$q_e = \frac{q_{m0,Ba} b_{0,Ba} C_e^{(1+x_{Ba}+y_{Ba})}}{1 + b_{0,Ba} C_e^{(1+x_{Ba})}} \quad (2)$$

$$q_e = \frac{q_{m0,Ba} b_{0,Ba} C_e^{(1+x_{Ba}+y_{Ba})}}{1 + b_{0,Ba}} \quad (3)$$

The researchers Svilovic et al. applied the Baudu isotherm for modeling the adsorption of copper cation on fly-ash and zeolite based adsorbents (Svilović et al., 2019). In the work of Syafiuddin et al. the adsorption of silver nanoparticles on various adsorbent such as glass beads, magnetic iron oxide, and biological materials were investigated and the Baudu isotherm model was determined as a reliable model for describing the adsorption of silver nano particles (Syafiuddin et al., 2018). In another research the adsorption of phenolic compounds and chlorophenols onto granular activated carbon was investigated. The researchers reported the conformity of experimental results with the Baudu isotherm (Hamdaoui and Naffrechoux, 2007).

2.3. Brunauer- Emmet-Teller (BET) isotherm model

In 1938 Brunauer, Emmet, and Teller (Brunauer et al., 1938) proposed an adsorption isotherm based on multimolecular adsorption theory for gaseous substances. Brunauer et al. defined five types of isotherm for a physical adsorption system (Khalfaoui et al., 2003). They considered two pressure regions for adsorbing gas constituents onto adsorbents. At the temperatures near the point of condensation, isotherms had concave shape for low pressures, and had convex shape over the pressure axis for high pressures.

The convex shape of isotherms in high pressure can be related to liquid state of constituents that condensed in capillaries of adsorbent in a molecular dimension scale. The capillary condensation mechanism causes a multimolecular adsorption layer occurs for systems comprised non-polar molecules adsorbate and ionic adsorbent. The adsorbent surface layer induces electrical dipoles to first layer of adsorption and so on the first layer polarizes the other layers of adsorption. Various forms of the BET isotherm were proposed (Ebadi et al., 2009). The most general form of the BET model presented in Eq. (4) (Wjihi et al., 2019):

Table 1
Adsorption isotherm models.

	Model name	Isotherm equation	Model parameters	Ref.
1	Aranovich	$q_e = \frac{q_{m,Ar} C_{Ar} \frac{C_e}{C_{s,Ar}}}{\left(1-\frac{C_e}{C_{s,Ar}}\right)^{\frac{1}{2}} \left(1+C_{Ar}\frac{C_e}{C_{S,Ar}}\right)}$	$q_{m,\ Ar}$, C_{Ar}, $C_{s,\ Ar}$	Aranovich (1992); Do (1998)
2	Baudu	$q_e = \frac{q_{m0,Ba} b_{0,Ba} C_e^{(1+x_{Ba}+y_{Ba})}}{1+b_{0,Ba} C_e^{(1+x_{Ba})}}$	$q_{m0,\ Ba}$, $b_{0,\ Ba}$, x_{Ba}, y_{Ba}	Baudu (1990); Baudu et al. (1989)
3	Brunauer- Emmet-Teller (BET)	$q_e = \frac{q_{m,BET} C_{BET} C_e}{(C_{s,BET}-C_e)\left[1+(C_{BET}-1)\left(\frac{C_e}{C_{s,BET}}\right)\right]}$	$q_{m,\ BET}$, C_{BET}, $C_{s,\ BET}$	Wjihi et al. (2019)
4	Brouers-Sotolongo	$q_e = q_{m,BS}(1- \exp(-K_{BS} C_e^{\alpha_{BS}}))$	$q_{m,\ BS}$, K_{BS}, α_{BS}	Brouers et al. (2005)
5	Dubinin-Astakhov (DA)	$q_e = q_{m,DA}\left[-\left(\frac{\varepsilon_{DA}}{E_{DA}}\right)^{n_{DA}}\right], \varepsilon_{DA} = RTln\left(\frac{C_{s,DA}}{C_e}\right)$	$q_{m,\ DA}$, E_{DA}, n_{DA}, ε_{DA}, $C_{s,\ DA}$	Dubinin and Astakhov (1971)
6	Dubinin-Radushkevich (DR)	$q = q_{m,DR} e^{-K_{DR}\varepsilon_{DR}^2}, \varepsilon_{DR} = RT\left(1+\frac{1}{C_e}\right)$	$q_{m,\ DR}$, K_{DR}, ε_{DR}	Dubinin (1960)
7	Flory-Huggins	$\frac{\theta_{FH}}{C_{0,FH}} = K_{FH}(1-\theta_{FH})^{n_{FH}}, \theta_{FH} = 1-\frac{C_e}{C_0}$	K_{FH}, n_{FH}, $C_{0,\ FH}$, θ_{FH}	Flory (1942); Huggins (1942)
8	Fowler Guggenheim	$C_e = \frac{\theta_{FG}}{K_{FG}(1-\theta_{FG})} exp(\frac{2\theta_{FG} W_{FG}}{RT}), (\theta_{FG} = q_e/q_{m,FG})$	θ_{FG}, K_{FG}, W_{FG}, $q_{m,\ FG}$	Fowler (1939)
9	Frenkel-Halsey-Hill (FHH)	$\ln\left(\frac{C_e}{C_{s,FHH}}\right) = -\frac{\alpha_{FHH}}{RT}\left(\frac{q_{s,FHH}}{q_e d_{FHH}}\right)^r$	$C_{s,\ FHH}$, α_{FHH}, $q_{s,\ FHH}$, r, d_{FHH}	Frenkel (1946); Hill (1952)
10	Freundlich	$q_e = k_F C_e^{n_F}$	K_F, n_F	Freundlich (1906)
11	Fritz-Shluender	3-Parameter $q_e = \frac{q_{m,FS1} K_{FS1} C_e}{1+q_{m,FS1} C_e^{m_{FS1}}}$	$q_{m,\ FS1}$, K_{FS1}, m_{FS1}	Fritz and Schluender (1974); Ramadoss and Subramaniam (2019)
		4-Parameter $q_e = \frac{C_{FS2} C_e^{\alpha_{FS2}}}{1+D_{FS2} C_e^{\beta_{FS2}}}$	C_{FS2}, α_{FS2}, D_{FS2}, β_{FS2}	
		5-Parameter $q_e = \frac{q_{m,FS3} K_{1,FS3} C_e^{m_{1,FS3}}}{1+K_{2,FS3} C_e^{m_{2,FS3}}}$	$q_{m,\ FS3}$, $K_{1,\ FS3}$, $K_{2,\ FS3}$, $m_{1,\ FS3}$, $m_{2,\ FS3}$	
12	Frumkin	$C_e = \frac{\theta_{Fm}}{K_{Fm}(1-\theta_{Fm})} \exp(-f_{Fm}\theta_{Fm}), \theta_{FM} = \frac{q_e}{q_m}$	θ_{Fm}, K_{Fm}, f_{Fm}	Frumkin (1925a); Grchev et al. (1991)
13	Guggenheim-Andersen-de Boer (GAB)	$q_e = \frac{q_{m,GAB} C_{GAB} K_{GAB} C_e}{(C_{s,GAB}-K_G C_e)[1+(C_{GAB}-1)K_G \frac{C_e}{C_{s,GAB}}]}$	$q_{m,\ GAB}$, C_{GAB}, K_{GAB}, $C_{s,\ GAB}$	Anderson (1946); De Boer (1953); Guggenheim (1966)
		Modified: $q_e = \frac{q'_{m,GAB} C'_{GAB} K'_{GAB}\left(\frac{C_e}{C'_{s,GAB}}\right)^{n'_{GAB}}}{\left(1-K'_{GAB}\left(\frac{C_e}{C'_{S,GAB}}\right)^{n'_{GAB}}\right)\left[1+(C'_{GAB}-1)K'_{GAB}\left(\frac{C_e}{C'_{s,GAB}}\right)^{n'_{GAB}}\right]}$	$q_{m,\ GAB}'$, C_{GAB}', K'_{GAB}, $C_{s,\ GAB}'$, n_{GAB}'	Zou et al. (2016)
14	Halsey	$q_e = e^{-(\ln K_{HL} - \ln C_e)/n_{HL}}$	K_{HL}, n_{HL}	Halsey (1948)
15	Harkins-Jura	$\frac{1}{q_e^2} = \frac{B_{HJ}}{A_{HJ}} - \frac{1}{A_{HJ}} logC_e$	A_{HJ}, B_{HJ}	Harkins and Jura (1944)
16	Henderson	$q_e = (\frac{-\ln(1-C_e)}{A_{He}})^{1/n_{He}}$	A_{He}, n_{He}	Henderson (1970)
		Modified: $q_e = [\frac{-\ln(1-C_e)}{A'_{He}(T+B'_{He})}]^{1/n'_{He}}$	A'_{He}, B'_{He}, n'_{He}	Mehta and Singh (2006)
17	Henry	$q_e = K_{HN} C_e$	K_{HN}	Erbil (2006)
18	Hill-De Boer	$K_{1,HB} C_e = \frac{\theta_{HB}}{1-\theta_{HB}} exp(\frac{\theta_{HB}}{1-\theta_{HB}} - \frac{K_{2,HB}\theta_{HB}}{RT})$ $\theta_{HB} = q_e/q_{m,HB}$	$K_{1,\ HB}$, $K_{2,\ HB}$, θ_{HB}, $q_{m,\ HB}$	De Boer (1953); Hill (1946)
19	Hills	$q_e = \left(\frac{q_{SH} \cdot C_e^{n_{SH}}}{K_{D,SH}+C_e^{n_{SH}}}\right)$	q_{SH}, n_{SH}, $K_{D,\ SH}$	Hill (1910)
20	Jossens	$C_e = \frac{q_e}{H_{Js}} \exp(F_{Js} q_e^{P_{Js}})$	H_{Js}, F_{Js}, P_{Js}	Jossens et al. (1978)
21	Jovanovich	$q_e = q_{m,\ Jv}[1 - e^{K_{Jv}C}{}_e]$	$q_{m,\ Jv}$, K_{Jv}	Jovanović (1969)
22	Khan	$q_e = \frac{q_{m,KH} b_{KH} C_e}{(1+b_{KH} C_e)^{a_{KH}}}$	$q_{m,\ KH}$, b_{KH}, a_{KH}	Khan et al. (1997); Khan et al. (1996)
23	Kiselev	$K_{1,\ KV} C_e = \frac{\theta_{KV}}{(1-\theta_{KV})(1+k_{n,KV}\theta_{KV})}, \theta_{KV} = \frac{q_e}{q_{S,KV}}$	θ_{KV}, $K_{1,\ KV}$, $K_{n,\ KV}$, $q_{S,\ KV}$	Kiselev (1958)
24	Koble-Corrigan	$q_e = \frac{a_{KC} C_e^{n_{KC}}}{1+b_{KC} C_e^{n_{KC}}}$	a_{KC}, b_{KC}, n_{KC}	Koble and Corrigan (1952)
25	Langmuir	$q_e = \frac{q_{m,L} K_L C_e}{1+K_L C_e}$	$q_{m,\ L}$, K_L	Langmuir (1918)
26	MacMillan-Teller (MET)	$q_e = q_{s,MET}(\frac{K_{MET}}{\ln(C_{s,MET}/C_e)})^{\frac{1}{3}}$	$q_{s,\ MET}$, K_{MET}, $C_{s,\ MET}$	McMillan and Teller (1951)
27	Marczewski-Jaroniec	$q_e = q_{m,MJ}\left(\frac{(K_{MJ} C_e)^{n_{MJ}}}{1+(K_{MJ} C_e)^{n_{MJ}}}\right)^{\frac{m_{MJ}}{n_{MJ}}}$	$q_{m,\ MJ}$, K_{MJ}, n_{MJ}, m_{MJ}	Derylo-Marczewska and Jaroniec (1987)
28	Oswin	$q_e = K_{OS}\left(\frac{C_e}{1-C_e}\right)^{n_{OS}}$	K_{OS}, n_{OS}	Oswin (1946)
		Modified: $q_e = (A'_{OS} + B'_{OS} T)(\frac{C_e}{1-C_e})^{n'_{OS}}$	A'_{OS}, B'_{OS}, n_{OS}'	Chen (1990)
29	Radke-Prausnitz	$q_e = \frac{q_{m,RP} K_{RP} C_e}{(1+K_{RP} C_e^{m_{RP}})}$	$q_{m,\ RP}$, K_{RP}, m_{RP}	Radke and Prausnitz (1972)
30	Redlich-Peterson	$q_e = \frac{K_{RN} C_e}{1+a_{RN} C_e^{\beta_{RN}}}$	K_{RN}, a_{RN}, β_{RN}	Redlich and Peterson (1959)
31	Sips	$q_e = \frac{q_{m,SP} K_{SP} C_e^{n_{SP}}}{1+K_{SP} C_e^{n_{SP}}}$	$q_{m,\ SP}$, K_{SP}, n_{SP}	Sips (1948)

Table 1 (*continued*)

	Model name	Isotherm equation	Model parameters	Ref.
32	Smith	$q_e = (A'_{ST} + B'_{ST}T) + C'_{ST}\ \ln(1-C_e)$ Modified: $q_e = (A'_{ST} + B'_{ST}T) + C'_{ST}\ ln(1 - C_e)$	A_{ST}, B_{ST} $A'_{ST}, B'_{ST}, C'_{ST}$	Smith (1947) Bala and Woods (1991); Nellist (1974)
33	Temkin	$q_e = \frac{RT}{b_{TM}}\ \ln K_{TM}C_e$	b_{TM}, K_{TM}	Temkin (1940)
34	Toth	$q_e = \frac{q_{m,TO}C_e}{\left(K_{TO} + C_e^{Z_{TO}}\right)^{1/Z_{TO}}}$	$q_{m,\ TO}, K_{TO}, Z_{TO}$	Toth (2002); Tóth (1995)
35	Vieth-Sladek	$q_e = K_{VS}C_e + \frac{q_{m,VS}\beta_{VS}C_e}{1+\beta_{VS}C_e}$	$K_{VS}, q_{m,\ VS}, \beta_{VS}$	Vieth and Sladek, 1965b
36	Volmer	$C_e = \frac{\theta_{VL}}{d_{VL}(1-\theta_{VL})}\ exp(\frac{\theta_{VL}}{1-\theta_{VL}}),\ \theta_{VL} = \frac{q_e}{q_{m,VL}}$	$d_{VL}, q_{m,\ VL}, \theta_{VL}, q_{m,\ VL}$	Volmer (1925)
37	Weber-Van Vliet	$C_e = P_{1,WB}q_e^{\left(P_{2,WB}q_e^{P_{3,WB}} + P_{4,WB}\right)}$	$P_{1,\ WB}, P_{2,\ WB}, P_{3,\ WB}, P_{4,\ WB}$	Van Vliet et al. (1980)

$$q_e = \frac{q_{mBET}C_{BET}C_e}{(C_{s,BET} - C_e)\left[1 + (C_{BET} - 1)\left(\frac{C_e}{C_{s,BET}}\right)\right]} \tag{4}$$

In Eq. (4), the parameters of $q_{mBET}\left(\frac{mg}{g}\right)$, $C_{s,\ BET}$ and $C_{BET}\left(\frac{L}{mg}\right)$ are defined as the maximum adsorption capacity of BET isotherm, monolayer saturation concentration of isotherm and BET adsorption constant, respectively. The BET model covers relative pressures (P/P_0) between the values of 0.05 to 0.3.

In a research the ammonia gas were adsorbed on straw-rice based biochar and the adsorption system obeyed the BET isotherm (Park et al., 2019). Other researchers also used hydroxyapatite nanoparticles for adsorbing water vapor adsorption and found out the BET isotherm is the best descriptive model for their system (Szałaj et al., 2019).

Some researchers modified the BET model based on statistical physics and assumed that the molecules of the first layer adsorbed on the surface with more energy than the remaining layers (Khalfaoui et al., 2003). In another work (Wjihi et al., 2019) the modified BET isotherm model was applied for a dye/nanosilica adsorption system. Also it was found that the methane gas adsorption to shale-oil, chiefly obeys the BET isotherm model (Yu et al., 2016b).

One of the main applications of the BET isotherm is the estimation of specific surface area and pore size and shape of porous adsorbents. In a low temperature instrument, the pressure of a gas is changed (normally nitrogen gas at 77 K) in an adsorption/desorption route, and partial pressures were measured. By comparing the shape of the obtained adsorption/desorption isotherm with the five reference BET isotherm curves, the shape and behavior of pores can be described (Ladavos et al., 2012).

2.4. Brouers–Sotolongo isotherm model

A state-of-art isotherm was proposed based on considering some theoretical assumption on the Langmuir isotherm in 2005 by Brouers et al. In the Brouers–Sotolongo (BS) isotherm model, it is considered that the adsorbent has sites with distributed sorption energies, which this distribution obeys from the Levy stable distributions theory (Brouers et al., 2005). The BS isotherm model is expressed by Eq. (5). In Eq. (5) the $q_{m,\ BS}$ is the maximum adsorption capacity (mg/g), the K_{BS} (L/mg) and α_{BS} are the model constants.

$$q_e = q_{m,BS}\left(1 - exp\left(-K_{BS}C_e^{\alpha_{BS}}\right)\right) \tag{5}$$

Various research are presented to show the reliability of the BS isotherm model. In the work of Unuabonah et al., the adsorption of phosphate from water by using modified clay was evaluated, and the BS isotherm model adequately described the experimental results (Unuabonah et al., 2017). In addition, it is reported that the adsorption of the methylene blue (MB) dye onto various activated carbon was in conformity with the BS isotherm model (Selmi et al., 2018; Vargas et al., 2011).

2.5. Dubinin-Astakhov isotherm model

The Dubinin-Astakov (DA) model is widely deployed in studying the adsorption of gases onto microporous activated carbons. The DA equation is written as follows (Dubinin and Astakhov, 1971):

$$q_e = q_{m,DA}\left[-\left(\frac{\varepsilon_{DA}}{E_{DA}}\right)^{n_{DA}}\right] \tag{6}$$

$q_{m,\ DA}$ is the maximum adsorption capacity of the DA isotherm (mg/g), ε_{DA} is the DA isotherm adsorption potential (kJ/mol), n_{DA} is the heterogeneity parameter in DA isotherm model (Burevski, 1982), and E_{DA} is the characteristic energy of the system in DA isotherm model (kJ/mol). The expression (7) is used to measure the adsorption potential (Dubinin and Astakhov, 1971) (Ross and Riley, 1990), where $C_{s,\ DA}$ is maximum solubility of the adsorbate.

$$\varepsilon_{DA} = RTln\left(\frac{C_{s,DA}}{C_e}\right) \tag{7}$$

Yan and Niu developed natural-based adsorbents for the adsorption of norfloxacinfrom from aqueous solutions (Yan and Niu, 2018). The experimental results and the DA model were well-matched, and the DA model was applied to determine the site energy distribution mechanism.

Singh and Kumar investigated the CO_2 adsorption on a commercially available activated carbon (the Norit Darco form), which was made from lignite granular content. (Singh and Kumar, 2016). The Langmuir and DA isotherm models were applied to describe the CO_2 adsorption, and the DA isotherm model was found to be consistent with experimental results.

Cheng and Hu worked on the adsorption of acetylene (C_2H_2) on different metal organic frameworks (MOFs) (Cheng and Hu, 2016). Their findings revealed that DA equation was better than Langmuir and BET models to demonstrate C_2H_2 adsorption on MOFs.

At various temperatures, Singh et al. studied the adsorption isotherms and the kinetics of CO_2 on native coconut shell based activated carbon (CSAC) (Singh et al., 2018). Experimental evidence of CO_2 absorption is associated with the Langmuir and the DA models and according to obtained results, the DA model is appropriate for adsorption isotherms.

Dhaneswara et al. synthesized a Mesoporous Silica adsorbent with different concentrations of Pluronic 123 surfactant and studied the effect of these different concentrations on the N_2 adsorption behavior of silica (Dhaneswara et al., 2018). They mentioned that the DA isotherm could be utilized to calculate the silica's adsorption potential at a relative pressure of 0.3.

Table 2
Nomenclature.

Notation	Description
A_{HJ}	Harkins-Jura isotherm constant
A_{He}	Henderson isotherm constant
A_{ST}	Smith isotherm constant
$A_{He'}$	Modified-Henderson isotherm constant
A'_{OS}	Modified-Oswin isotherm parameter
A'_{ST}	Modified-Smith isotherm constant
B_{HJ}	Harkins-Jura isotherm constant
B_{ST}	Smith isotherm constant
$B_{He'}$	Modified- Henderson isotherm constant
B'_{OS}	Modified Oswin isotherm parameter
B'_{ST}	Modified-Smith isotherm constant
$C_{0,\ FH}$	Flory-Huggins isotherm constant
C_{Ar}	Aranovich isotherm constant
C_{BET}	BET adsorption constant
C_{FS2}	Constant of 4-parameters Fritz-Shluender isotherm
C_{GAB}	Chemical potential difference between adsorption layers of GAB isotherm
$C_{s,\ Ar}$	Saturation concentration of Aranovich isotherm
$C_{s,\ BET}$	Monolayer saturation concentration of BET isotherm
$C_{s,\ DA}$	Maximum solubility of the adsorbate
$C_{s,\ FHH}$	Frenkel-Halsey-Hill isotherm constant
$C_{s,\ GAB}$	GAB isotherm constant
$C_{s,\ MET}$	Monolayer saturation concentration of MET isotherm
C'_{GAB}	Chemical potential difference between adsorption layers of modified-GAB isotherm
$C'_{s,\ GAB}$	Modified-GAB isotherm constant
C'_{ST}	Modified-Smith isotherm constant
D_{FS2}	Constant of 4-parameters Fritz-Shluender isotherm
E_{DA}	Characteristic energy of the system of Dubinin-Astakhov isotherm
F_{Js}	Jossens isotherm constant
H_{Js}	Jossens isotherm constant
$K_{1,\ FS3}$	5-parameters Fritz-Shluender isotherm constant
$K_{1,\ HB}$	Hil-De Boer isotherm constant
$K_{1,\ KV}$	Kiselev isotherm constant
$K_{2,\ FS3}$	5-parameters Fritz-Shluender isotherm constant
$K_{2,\ HB}$	Energetic constant of the interaction between adsorbed molecules of the Hil-De Boer isotherm
K_{BS}	Brouers–Sotolongo isotherm model constant
$K_{D,\ SH}$	Hill isotherm constant
K_{DR}	Dubinin-Radushkevich isotherm constant
K_F	Fitting constant of Freundlich isotherm
K_{FG}	Fowler Guggenheim isotherm Equilibrium consta
K_{FH}	Flory-Huggins isotherm equilibrium constant
K_{FS1}	3-parameters Fritz-Shluender isotherm equilibrium constant
K_{Fm}	Frumkin isotherm equilibrium constant
K_{GAB}	Free enthalpy of adsorbate molecules in the second layer of adsorption of GAB isotherm
K_{HL}	Halsey isotherm constant
K_{HN}	Henry adsorption constant
K_{MET}	MET isotherm constant
K_{MJ}	Marczewski–Jaroniec isotherm equilibrium constant
$K_{n,\ KV}$	Kiselev isotherm constant
K_{OS}	Oswin isotherm parameter
K_{RN}	Redlich-Peterson isotherm constant
K_{RP}	Radke-Prausnitz isotherm equilibrium constant
K_{SP}	Sips isotherm constant
K_{TM}	Temkin isotherm constant
K_{TO}	Toth isotherm constant
K_{VS}	Vieth-Sladek isotherm constant
K_L	Langmuir isotherm equilibrium constant
K_{Jv}	Jovanovich constant
K'_{GAB}	Free enthalpy of adsorbate molecules in the second layer of adsorption of modified-GAB isotherm
$P_{1,\ WB}$	Weber-Van Vliet isotherm parameter
$P_{2,\ WB}$	Weber-Van Vliet isotherm parameter
$P_{3,\ WB}$	Weber-Van Vliet isotherm parameter
$P_{4,\ WB}$	Weber-Van Vliet isotherm parameter
P_{Js}	Jossens isotherm constant
R	Universal gas constant
T	Absolute Temperature
W_{FG}	Interaction energy between adsorbed substances of Fowler Guggenheim isotherm
Z_{TO}	Toth dimensionless parameter
a_{KC}	Koble-Carrigan isotherm constant
a_{KH}	Khan isotherm exponent

Table 2 (*continued*)

Notation	Description
a_{RN}	Redlich-Peterson isotherm constant
$b_{0,\ Ba}$	Baudu isotherm Equilibrium constant
b_{KC}	Koble-Carrigan isotherm constant
b_{KH}	Khan isotherm constant
b_{TM}	Temkin isotherm constant
d_{FHH}	Sign of the interlayer spacing of Frenkel-Halsey-Hill isotherm
d_{VL}	Volmer affinity constant
f_{Fm}	Adsorbate interaction coefficient of the Frumkin isotherm
$m_{1,\ FS3}$	5-parameters Fritz-Shluender isotherm constant
$m_{2,\ FS3}$	5-parameters Fritz-Shluender isotherm constant
m_{FS1}	3-parameters Fritz-Shluender isotherm constant
m_{MJ}	Marczewski–Jaroniec isotherm equilibrium constant
m_{RP}	Radke-Prausnitz isotherm exponent
n_{DA}	Dubinin-Astakhov isotherm heterogeneity parameter
n_{FH}	The number of adsorbates that occupies adsorption sites of the Flory-Huggins isotherm
n_{HL}	Halsey isotherm constant
n_{He}	Henderson isotherm constant
n_{KC}	Koble-Carrigan isotherm exponent
n_{MJ}	Marczewski–Jaroniec isotherm equilibrium constant
n_{OS}	Oswin isotherm constant
n_{SH}	Hill isotherm constant
n_{SP}	Sips isotherm exponent
n'_{He}	Modified- Henderson isotherm constant
n'_{OS}	Modified-Oswin isotherm constant
n'_{GAB}	Modified-GAB isotherm constant
$q_{m,\ Ar}$	Maximum adsorption capacity of Aranovich isotherm
$q_{m0,\ Ba}$	Maximum adsorption capacity of Baudu model
$q_{m,\ BET}$	Maximum adsorption capacity of BET isotherm
$q_{m,\ BS}$	Maximum adsorption capacity of the Brouers–Sotolongo isotherm
$q_{m,\ DA}$	Maximum adsorption capacity of the Dubinin- Astakhov isotherm
$q_{m,\ DR}$	Maximum adsorption capacity of the Dubinin-Radushkevich isotherm
$q_{m,\ FS1}$	Maximum adsorption capacity of the 3-parameters Fritz-Shluender isotherm
$q_{m,\ FS3}$	Maximum adsorption capacity of the 5-parameters Fritz-Shluender isotherm
$q_{m,\ GAB}$	Maximum adsorption capacity of the GAB isotherm
$q_{m,\ GAB'}$	Maximum adsorption capacity of the modified-GAB isotherm
$q_{m,\ FG}$	Maximum adsorption capacity of the Flory-Huggins isotherm
$q_{m,\ HB}$	Maximum adsorption capacity of the Hill-De Boer isotherm
$q_{m,\ Jv}$	Maximum adsorption capacity of Jovanovich isotherm
$q_{m,\ KH}$	Maximum adsorption capacity of Khan isotherm
$q_{m,\ MJ}$	Maximum adsorption capacity of Marczewski–Jaroniec isotherm
$q_{m,\ RP}$	Maximum adsorption capacity of the Radke-Prausnitz isotherm
$q_{m,\ SP}$	Maximum adsorption capacity of Sips isotherm
$q_{m,\ TO}$	Maximum adsorption capacity of the Toth isotherm
$q_{m,\ VL}$	Maximum adsorption capacity of the Volmer isotherm
$q_{m,\ VS}$	Maximum adsorption capacity of the Vieth-Sladek isotherm
$q_{s,\ FHH}$	Frenkel-Halsey-Hill isotherm constant
$q_{s,\ MET}$	Theoretical saturation capacity of the MET isotherm
$q_{S,\ KV}$	Maximum monolayer adsorption capacity of Kiselev isotherm
q_{SH}	Maximum adsorption capacity of the Hill isotherm
r	Inverse power of distance from the surface of the Frenkel-Halsey-Hill isotherm
x_{Ba}	Baudo isotherm constant
n_F	Freundlich isotherm fitting constant
y_{Ba}	Baudo isotherm constant
α_{BS}	Brouers–Sotolongo isotherm constant
α_{FHH}	Frenkel-Halsey-Hill isotherm constant
α_{FS2}	4-parameters Fritz-Shluender isotherm constant
β_{FS2}	4-parameters Fritz-Shluender isotherm constant
β_{RN}	Redlich-Peterson isotherm exponent
β_{VS}	Vieth-Sladek isotherm constant
ε_{DA}	Adsorption potential of Dubinin-Astakhov isotherm
ε_{DR}	Polanyi potential of Dubinin-Radushkevich isotherm
θ_{FG}	Surface coverage degree of the Fowler Guggenheim isotherm
θ_{FH}	Surface coverage degree of the Flory-Huggins isotherm model
θ_{Fm}	Surface coverage degree of Frumkin isotherm
θ_{HB}	Surface coverage degree of the Hill-De Boer isotherm
θ_{KV}	Surface coverage degree of Kiselev isotherm
θ_{VL}	Surface coverage degree of the Volmer isotherm

2.6. The Dubinin–Radushkevich isotherm model

The Dubinin–Radushkevich (DR) isotherm model assumes that the adsorption is related to the volume of adsorbent pores. In this model,

Table 3
Isotherm models for different adsorbents and adsorbates.

	Isotherm model	Adsorbent	Adsorbate	Ref.
1	Aranovich	Carbon (granular activated charcoal) Carbon (crushed activated semi-coke)	Benzene vapor, pyridine vapor	Belyaeva and Krasnova (2016)
2	Baudu	Fly ash-based geopolymer, fly ash-based geopolymer	Copper ions	Svilović et al. (2019)
		Glass beads, aged iron oxide magnetic particles, Fe_3O_4@ polydopamine core-shell microspheres, *Aeromonas punctata*	Silver nanoparticles	Syafiuddin et al. (2018)
		Granular activated carbon	Phenol, chlorophenols	Hamdaoui and Naffrechoux (2007)
		Cystoseira myricaas	Hg(II)	Zarei and Niad (2017)
		Ulva lactuca	Praseodymium	Vijayaraghavan (2015)
		SD/$MnFe_2O_4$ composite	As(III) and As(V)	Podder and Majumder (2015c)
		Leurotus platypus	Zn(II)	Das et al. (2014)
		Activated carbon	Basic red 9	Sivarajasekar and Baskar (2014a)
		Dead biomass of yeast	Zn(II)	Das et al. (2012)
		Caryota urens seeds	Zn(II)	Saravanan et al. (2018)
3	BET	Nanosilica	Crystal violet	Wjihi et al. (2019)
		Rice straw-derived biochar	NH_3-N	Park et al. (2019)
		Hydroxyapatite nanoparticles	H_2O	Szałaj et al. (2019)
		Marcellus Shale	CH_4	Yu et al. (2016a)
		Fly Ash	Moisture	Navea et al. (2017)
		Date kernels	Moisture	Alyousef et al. (2020)
		Graphite nanoplatelets	Toxic dyes	Oliveira et al. (2019)
		Polysaccharide-based	MTBE	Tsui et al. (2018)
		Saccharomyces cerevisiae	Cr (VI)	De Rossi et al. (2018)
4	Brouers–Sotolongo	Activated carbons	MB and methyl orange	Selmi et al. (2018); Vargas et al. (2011)
		Triple-metal nanosorbent	Reactive Blue 19	Kostić et al. (2018)
		Low-cost lignocellulosic	Basic red 2 and basic violet 3	Wakkel et al. (2019)
		Modified durian seed	Methyl red dye	Ahmad et al. (2015)
		Coconut shell-activated carbon	2,4-Dichlorophenoxyacetic acid	Njoku et al. (2015)
		Pomegranate peel activated carbon	Remazol brilliant blue reactive dye	Ahmad et al. (2014b)
		Magnetite nanoparticles	Organic dyes	Madrakian et al. (2012)
		Reed-based beads	Cd(II)	Karoui et al. (2021)
		Algae	Pb(II)	Brouers and Al-Musawi (2015)
		Activated carbons	MB and methyl orange (MO)	Brouers and Al-Musawi (2015)
5	DA	Barley straw-based adsorbents	Norfloxacin	Yan and Niu (2018)
		Macroporous resin	Chloride, nitrate, sulfate ions	Dron and Dodi (2011)
		Activated carbons	methane	Luo et al. (2011)
		Activated carbons	Toluene, acetone, n-hexane, n-decane, methanol	Ushiki et al. (2013)
		Coconut shell derived carbon (CDC)	Toluene and chlorobenzene	Zhao et al. (2018)
		Microporous activated carbon powder of type Maxsorb III	CO_2	Jribi et al. (2017)
		Activated carbons	CO_2	Singh and Kumar (2017)
6	DR	Common Reed (CR) activated (Activated carbons)	Cu(II), Cd(II)	Abdelnaeim et al. (2016)
		Moroccan natural clays	MB, malachite green (MG), methyl orange (MO)	Elmoubarki et al. (2015)
		Carbon-magnetite composite (CB-FM)	CO_2	Raganati et al. (2018)
		Irvingia gabonensis nut (ADN)	Cu(II)	Inyinbor et al. (2019)
		Biochar (BC)	Trichloroethylene (TCE)	Ahmad et al. (2013)
		Babassu coconut (*Orbignya speciosa*) epicarp (BCE) (biomass)	textile dyes(Blue Remazol R160 (BR 160), Rubi S2G (R S2G), Red Remazol 5R (RR 5), Violet Remazol 5R (VR 5), Indanthrene Olive Green (IOG) dye)	Vieira et al. (2011)
		Activated carbon	Fluoride	Araga et al. (2017)
7	Flory-Huggins	Activated lignin-chitosan blend	MB	Rezakazemi and Shirazian (2019)
		Stainless steel	Pyrazolo [3,4-b] Pyridine	James et al. (2011)
		Concrete steel-reinforcement	*Phyllanthus muellerianus* leaf-extract	Okeniyi et al. (2014)
		Peanut hulls	MB	Farooq et al. (2019)
		Chikni Mitti (Kaolinite)	Ni^{+2}, Cr^{+6}	Jalees et al. (2019a)
		Mild steel	Three imidazole derivatives (benzimidazole, 2-methyl benzimidazole and 2-aminobenzimidazole)	Ghanbari et al. (2010)
		Microwave activated carbonized coconut shell	Urea	Pillai et al. (2014)
		Chir pine leaves (*Pinus roxburghii*)	Arsenic ions	Shafique et al. (2012)
		Cellulose membranes	Phosphate anions	Nechifor et al. (2015)
		Palm oil fruit shells	Copper ions	Hossain et al. (2012)
		Aluminum	*Gloriosa superba* gum	Eddy et al. (2014)
		Mild steel	*Euphorbia heterophylla* L.extract	Akinbulumo et al. (2020)
		Marine sediment	Mn(VII)	Mahmoud et al. (2020)
		Kaolinite	Rhodamine B	Khan et al. (2012)
		Polymeric adsorbent (Amberlite XAD 7)	Oil	Albatrni et al. (2019)

(continued on next page)

Table 3 (*continued*)

	Isotherm model	Adsorbent	Adsorbate	Ref.
8	Fowler-Guggenheim	Recycled Concrete	Phosphate	Wu et al. (2019)
		Ocimum gratissimum	Indigo carmine dye	Dada et al. (2020)
		Graphene oxide nanomaterials	Non-ionic surfactant	Prediger et al. (2018)
		Compost	Heavy metals	Pennanen et al. (2020)
		Agro-waste	Hexavalent chromium	Mokkapati et al. (2018)
		Microcrystalline cellulose	Xyloglucan	Myśliwiec et al. (2016)
		Graphene	Br_2	Chen et al. (2014)
		Dealuminated Faujasite Zeolite	Aromatic Compounds	Koubaissy et al. (2011)
		Natural Clays	α-Endosulfan	Yonli et al. (2014)
9	Frenkel-Halsey-Hill	Namontmorillonite and illite clay	Water	Hatch et al. (2014)
		glass	Moisture, Ethanol	Laaksonen (2015)
		Zeolite 3A and Zeolite 13X	Water vapor	Kim et al. (2016)
		Superporous hydrogel composites	Water vapor	Mittal et al. (2020)
10	Freundlich	Polyaniline (PAn) nanocomposite	Manganese ion	Hallajiqomi and Eisazadeh (2017)
		Activated carbon (AC)	Rhodium 6G, MB	Jarrah (2017)
		Superparamagnetic nanoparticles (Fe_3O_4)	Polysaccharide	Nanta et al. (2018)
		Sylopute	Paclitaxel	Kim and Kim (2019)
		MCM-41/PD composite	Cr(VI)	Selim et al. (2018)
		Rice husk, Palm leaf, Water hyacinth	Cu(II), Co(II), Fe(III)	Sadeek et al. (2015)
		Alginate-Au-Mica bionanocomposite	Pb(II)	Ahmad and Mirza (2017)
		Bentonite and modified Bentonite clay	Cu^{2+}, Cd^{2+}	Akpa and Unuabonah (2011)
		Modified natural bentonit	Congo red (CR)	Toor and Jin (2012)
		Modified zeolite	Reactive Red 239 (RR-239),Reactive Blue 250 (RB-250)	Alver and Metin (2012)
		Modified bentonite clay (organoclay)	MB, crystal violet (CV), Rhodamine B(RB)	Anirudhan and Ramachandran (2015)
		Iron oxide activated red mud	Cd(II)	Khan et al. (2015)
		Hg(II)-ion-imprinted polymer (IIP)	Hg(II)	Singh and Mishra (2010)
		AB-8 resin	Polyphenols	Gao et al. (2013)
		Trichoderma reesei	Co^{2+}, Cu^{2+}, Ni^{2+}, Pb^{2+}, Zn^{2+}	Ghaedi et al. (2013)
		Crystalline tin oxide nanoparticle	Uranium and thorium ions	Nilchi et al. (2013)
		Filamentous green algal Spirogyra sp.	C.I. Acid Orange 7(AO7), C.I. Basic Red 46(BR46) and C.I. Basic Blue 3 (BB3) dyes	Khataee et al. (2013)
		Banana peel	MB	Amela et al. (2012)
		Graphene	Acid red 1 and MB dyes	Kim et al. (2015)
		Sugar beet pulp	MB	Vučurović et al. (2012)
		Rice bran (RB) composites	Malachite Green (MG) dye	Bhatti et al. (2017)
		Activated carbon	Tartrazine	Gautam et al. (2015)
		Brown macroalga Stoechospermum marginatum	Acid Blue 25(AB25), Acid Orange 7(AO7), Acid Black 1 (AB1)	Daneshvar et al. (2012)
		Ground burnt patties	Phosphate	Rout et al. (2014)
		Rice hull-based activated carbon	Eriochrome Black T (EBT)	de Luna et al. (2013)
		Oil palm (*Elaeis guineensis*) leaves	MB	Setiabudi et al. (2016)
11	Fritz-Shluender	Treated Martil sand	Cu(II)	Nebaghe et al. (2016)
		Sulfur-chelating based cellulose	Cd (II)	Zheng et al. (2019)
		Colpomenia sinuosa	Cd (II)	Zarei and Niad (2020)
		Cu_2O	Azo dyes	Nassaji Jahromi et al. (2020)
		Camelorum tree particles	Hg(II)	Hashem et al. (2016)
		P. eldarica leaves	Pb(II), Cu(II), Ni(II)	Asgarzadeh et al. (2016)
		Orange peel	Gray BF-2R dye	Nascimento et al. (2014)
		Metallurgical slag	As(III), As(V)	Schouwenaars et al. (2017)
		Silver-doped TiO2	Reactive Blue 255	Fard and Fazaeli (2018)
		Saccharum Bengalense	Pb(II)	Din et al. (2014)
12	Frumkin	Mild steel	Three imidazole derivatives (benzimidazole, 2-methyl benzimidazole, 2-aminobenzimidazole)	Ghanbari et al. (2010)
		Concrete steel-reinforcement	*Phyllanthus muellerianus* leaf-extract	Okeniyi et al. (2014)
		Pterospermum acerifolium shells	MB, hexavalent chromium	Rangabhashiyam and Balasubramanian (2018)
		Glycerol-based carbon	MB	Narvekar et al. (2018)
		Mild steel	*Azadirachta indica* extract	Sharma et al. (2010)
		Sandstone and carbonate rock	Zwitterionic surfactant	Kumar and Mandal (2019)
		Ag nanoparticles dispersed in agarose gel	Methamphetamine hydrochloride	Souza et al. (2018)
		Moderate density fiberboard saw dust	Cyanide	Hisham et al. (2016)
		Aluminum alloy	*Commiphora pedunculata* gum	Ameh and Eddy (2014)
		Hydromagnesite stromatolite	Basic Yellow 28, Acid Red 336	Karakuş et al. (2020)
		Carboxymethylated bacterial cellulose	Lead	Rossi et al. (2018)
13	GAB	Soy-melon	H_2O	Oluwamukomi (2009)
		Template carbon	Ethane	Zou et al. (2016)
		Shale rocks	Moisture	Shen et al. (2018)
		Euterpe oleracea	Moisture	García-Tejeda and Barrera-Figueroa (2019)
		Longmaxi shale	Moisture	Ma et al. (2020)
		Potato	Moisture	Singh and Talukdar (2020)
		Microencapsulated extra virgin olive oil	Moisture	Zungur Bastıoğlu et al. (2017)

Table 3 (*continued*)

	Isotherm model	Adsorbent	Adsorbate	Ref.
		Sugar beet seeds	Moisture	de Oliveira et al. (2017)
		Nano-tailored mesoporous silica	Moisture	Mikšík et al. (2020)
14	Halsey	Multi-walled carbon nanotubes (MWCNTs)	Ammonium ions (NH_4^+)	Moradi (2016)
		Derived and thiourea-functionalized silica	Cadmium	Omotunde et al. (2018)
		Water chestnut (*Trapa natans* L.) peel	Rhodamine B	Khan et al. (2013)
		MWCNT–COOH–cellulose–MgO NP nanocomposite	MB	Khalili et al. (2018)
		Nanobentonite impregnated Nanocellulose/Chitosan aerogel	Cr (VI), Co (III), Cu (II)	Shahnaz et al. (2020)
		Perovskite lanthanum aluminate	Fluoride & Direct Blue 53 dye	Manjunatha et al. (2019)
15	Harkins-Jura	Ag-Cr-AC nanocomposites	Binary dye system of Reactive Red,Crystal Violet	Saad et al. (2017)
		Cereus sp.(biosorbent)	Congo red	Jeyavishnu and Alagesan (2020)
		Natural bentonite, zeolite, and sepiolite	Acid Orange 95 (AO 95)	(Tümsek and Oz, 2013)
16	Henderson	Hydromagnesite stromatolite	Basic Blue 3, Basic Yellow 28, Acid Red 336 dyes	Karakuş et al. (2020)
		Freeze-dried powders (avocado, maltodextrin, inulin)	Moisture	Stępień et al. (2020)
		Modified cassava flour	Moisture	Hawa et al. (2020)
		Quinoa grains	Moisture	Arslan-Tontul (2020a)
		Air-dried papaya	Moisture	Thalerngnawachart and Duangmal (2016)
		Bamboo	Moisture	Chen et al. (2020)
		Untreated lignite	MB	Gürses et al. (2014)
		Penaeus Vannamei meat	Moisture	Shi et al. (2016)
		Soil	Moisture	Arthur et al. (2016)
17	Henry	Zeolite ITQ-29.	CO_2 and CH_4	Poursaeidesfahani et al. (2019)
18	Hil-De-Boer	Trimellitated-sugarcane bagasse (STA)	Auramine-O (AO) and safranin-T (ST)	Fideles et al. (2018)
19	Hill	Biocomposite powder	Ciprofloxacin and MB	Karoui et al. (2020)
		Biochar	Trichloroethylene	(Ahmad et al., 2014a)
		Municipal solid waste biochar (MSW-BC)	Ciprofloxacin (CPX)	Ashiq et al. (2019)
		Chitosan/zeolite composite	Reactive Red 120	Dehghani et al. (2017)
		Modified corn husk leaves	Hg(II)	Lin et al. (2019)
20	Jossens	Polyamide 6.6 fibers	Red Astrazon 5BL	Makhlouf et al. (2012)
		Polyamide 6.6 microfibres	Astrazon Red 5 BL	Makhlouf et al. (2015)
		Arachis hypogea husk	Cr(VI)	Bayuo et al. (2020)
21	Jovanovic	Waste activated sludge	Eriochrome Black T	Aly-Eldeen et al. (2018)
		Clay minerals	Thiamine	Ghaleh et al. (2020)
22	Khan	Activated lignin-chitosan blend	MB	Rezakazemi and Shirazian (2019)
		Ion exchange resin DOWEX HCR-S	Zink	Fil et al. (2012)
		Activated carbon derived from immature cotton seeds	Basic red 9	Sivarajasekar and Baskar (2014b)
		Quaternary amine modified orange peel powder	Reactive Red 120 azo dye	Munagapati et al. (2019)
		Granular activated carbon	4-Chlorophenol adsorption	Bilgili et al. (2012)
		Palm-date stones	Cationic dyes (basic violet 3, basic red 2)	Wakkel et al. (2019)
		Granular activated carbon/$MnFe_2O_4$ composite	As(III), As(V)	Podder and Majumder (2016b)
		Marine sediment	Mn(VII)	Mahmoud et al. (2020)
		Graphene oxide nanoparticles	Antidiabetic pharmaceutical (metformin)	Balasubramani et al. (2020)
		Functionalized nano-clay composite	Naproxen	Rafati et al. (2016)
		Nano zero valent iron stacked activated carbon	Malachite green dye	Kumar et al. (2018)
		Amino functionalized silica nano hollow sphere	Imidacloprid pesticide	Kalhor et al. (2018)
		Sandstone minerals	A novel saponin-based surfactant (*Glycyrrhiza Glabra*)	Arabloo et al. (2015)
23	Kiselev	Titanium dioxide	Phenol, Copper, Zinc, Cadmium and Iron	Bekkouche et al. (2012)
		Banana bunch, sorghum stem and casuarinas fruit	Cr(VI)	Mokkapati et al. (2018)
		G blue-green marine algae	Divalent nickel	Ramadoss and Subramaniam (2019)
		Cereus sp.	Congo red	Jeyavishnu and Alagesan (2020)
24	Koble–Corrigan	Cashew nut shell	Congo red	Kumar et al. (2010b)
		Bentonite and zeolite	Pb(II)	Hamidpour et al. (2011)
		Lotus leaf	MB	Han et al. (2011)
		Bamboo charcoals	Yellow 161 dye	Wang and Yan (2011)
		Bark of *Eucalyptus tereticornis* L.	Imidacloprid and atrazine	Mandal and Singh (2016)
		Martil sand	Copper(II)	Nebaghe et al. (2016)
		Salix psammophila	Activated carbon-based sulfamethazine sodium	(Liu et al., 2019b)

(continued on next page)

Table 3 (*continued*)

	Isotherm model	Adsorbent	Adsorbate	Ref.
		Citrate modified sugarcane bagasse	MB	Mpatani et al. (2020)
		Coal fly ash	MB	Supelano et al. (2020)
25	Langmuir	Brewers' spent grain (BSG)	Congo Red (CR) dye, Malachite Green (MG) dye	Chanzu et al. (2019)
		Faujasite-type Y zeolite (NaY) wa	Phenol	Mohammed et al. (2019)
		Fe_3O_4@BDC@AGPA nanocomposite	Pb(II) ion	Alsuhybani et al. (2020)
		Boron doped carbon nanotubes (BCNTs)	Hydrogen	Sawant et al. (2019)
		TMS-SMSs(thiol-modified mesoporous silica submicrospheres)	Tl(I) ion	Soltani et al. (2019)
		Magnetic-SBA-15/CPAA	Acid Blue 25	Ghanei et al. (2018)
		Carbon composite lignin-based	Congo Red (CR) dye, Eriochrome blue black R dye	Wang et al. (2018)
		Activated carbon	Toluene	Pei and Zhang (2012)
		Citric acid-magnetite	Ni(II) ions	Baseri and Tizro (2017)
		Meso-porous silica SBA-3	Disulfiram	Sandberg et al. (2018)
		Ag modified calcium hydroxyapatite (CaHAp)	Pyridine	Srilakshmi and Saraf (2016)
		Sandstone rock surface	Hydrolyzed polyacrylamide (HPAM) polymers	Ali and Mahmud (2015)
		Graphene	Nitrate ion	Ganesan et al. (2013)
		Indion NSSR resin	Nitrate ion	Milmile et al. (2011)
		Orange peel activated carbon (OPAC)	chlorophenoxyacetic acid herbicides	Pandiarajan et al. (2018)
		Carbon steel	Ascorbyl palmitate (AP)	Deyab (2014)
		Ash and Fe nanoparticles loaded ash (nFe-A)	Pb(II) ion	Ghasemi et al. (2014)
		Mild steel	Cefazolin	Singh and Quraishi (2010)
		MgO decked few layer Graphene Coated Fullers' Earth (MgO-FLG-FE)	*Acid Blue 9* (AB9) and *Safranin O* (SO) dye	Reddy et al. (2018)
		Palm shell activated carbon supported with cerium oxide (Ce/PSAC)	SO_2 and NO	Sumathi et al. (2010)
		Bone char	Cr(VI)	Hyder et al. (2015)
		Unmodified groundnut hull (UGS) and the modified groundnut hull (MGS)	Cr(VI)	Owalude and Tella (2016)
		Hydroxyapatite (HA)	Bovine serum albumin (BSA)	Swain and Sarkar (2013)
		Empty bunch- activated carbon (EBC-AC)	MB	Egbosiuba et al. (2020)
		Sodium alginate lginate–carboxymethyl cellulose (SA-CMC)	Pb(II) ion	Ren et al. (2016)
		Organobentonite	Rhodamine B(RhB), Acid red 1	Huang et al. (2017)
		NaOH-modified rejected tea (N-RT)	MB	Nasuha and Hameed (2011)
26	MET	Metallurgical slag	Arsenic ions	Mercado-Borrayo et al. (2014a)
		Iron nanoparticles	Boron	Mercado-Borrayo et al. (2014b)
27	Marczewski-Jaroniec	Cotton seeds (activated carbon)	Basic red 9	Sivarajasekar and Baskar (2014b)
		Activated *Gossypium hirsutum* seeds	Basic violet 10	Sivarajasekar and Baskar (2015)
		SD/$MnFe_2O_4$ composite	As(III) and As(V)	Podder and Majumder (2015a); Podder and Majumder (2015b)
		Sawdust/$MnFe_2O_4$ composite	As(III) and As(V)	Podder and Majumder (2016a)
		Blue-green marine algae	Ni(II)	Ramadoss and Subramaniam (2019)
		Colpomenia sinuosa	Cadmium	Zarei and Niad (2020)
		Cellulose biochar	Cr (VI), As (V), Cu (II), and Pb (II)	Neeli et al. (2020)
28	Oswin	Tunisian clay	Moisture	Jhider and Bagané (2019)
		Chili pepper	Moisture	Getahun et al. (2020)
		Full-fatted grape seeds flour	Moisture	Bogoeva and Durakova (2020)
		Coffee blends	Moisture	(GHH et al., 2020)
		Pd- and Ru-Doped C60 Fullerene	Hydrogen	Saha and Deng (2011)
		Red onion slices	Moisture	Gazor and Eyvani (2011)
		Autoclaved aerated concrete	Moisture	Gazor and Eyvani (2011)
		Ficus deltoidea leaves	Moisture	Jamaluddin et al. (2020)
29	Radke–Prausnitz	Flamboyant pods (*Delonix regia*)	MB	Vargas et al. (2011)
		Exfoliated graphite	C.I. Acid Blue 92	Goshadrou and Moheb (2011)
		Bentonite, sepiolite, and zeolite	Acid Orange 95	(Tümsek and Oz, 2013)
		Nano-clay composite	Ibuprofen	Rafati et al. (2018)
		Carbon nanotubes	Pb^{2+}	Eyni et al. (2019)
		Graphene oxide nanosheets	Total Organic Carbon	Parsa et al. (2020)
30	Redlich–Peterson	Pistachio shell activated carbons	MB and basic brown	Wu et al. (2010)
		Kraft lignin	Cr(VI)	Brdar et al. (2012)
		Raw and modified Ball clay	MB	Auta and Hameed (2012)
		Buckwheat hulls	Hg(II)	Wang et al. (2013)
		Kaolinite	Zn(II) and Cu(II)	Shahmohammadi-Kalalagh and Babazadeh (2014)
		Powdered activated carbon	Remazol Brillant Yellow 3GL	Açıkyıldız et al. (2015)

Table 3 (*continued*)

	Isotherm model	Adsorbent	Adsorbate	Ref.
		Poly(AA-*co*-VPA) hydrogel cross-linked with N-maleyl chitosan	Crystal violet and MB	Nakhjiri et al. (2018)
		Polyacrylic acid-based Hydrogel and Chitosan-based Hydrogel	Cadmium ions	Vilela et al. (2019)
		Fibrous silica nanospheres	Crystal violet	Roghanizad et al. (2020)
		Olive stone and date pit	Cr(VI)	Mangwandi et al. (2020)
		Yeast β-glucan	Hexanal, 1-octen-3-ol and nonanal	Zhang et al. (2020)
31	Sips	Thiol-functionalized silica nano hollow sphere	Hg^{2+}, Pb^{2+} and Cd^{2+}	Rostamian et al. (2011)
		Date stones	MB	Ahmed and Dhedan (2012)
		Aminated pumpkin seed powder	Methyl orange	Subbaiah and Kim (2016)
		Activated carbon	Amoxicillin	de Franco et al. (2017)
		Superparamagnetic nanoparticles	Polysaccharide	Nanta et al. (2018)
		Lanthanum and cerium modified mesoporous alumina	Fluoride ions	He et al. (2019)
		Piaçava fibers	MB	Marques et al. (2019)
		Biomass-based carbon	Bisphenol A	Juhola et al. (2020)
		NaY Zeolite	CO_2, CO, N_2, CH_4, and H_2	Feng et al. (2020)
		Activated carbon	N_2, CH_4 and CO_2	Bagheri et al. (2021)
32	Smith	Crambe grain	Moisture	Cruz et al. (2017)
		Canola	Moisture	Zare et al. (2011)
		Pomegranate arils	Moisture	Mundada and Hathan (2012)
		Manihot esculenta Crantz	Moisture	Contreras et al. (2017)
		Hemerocallis Fulva	Moisture	Ma et al. (2016)
		Extruded snack product (rice and corn flour)	Moisture	Sharma et al. (2019)
		Tapioca flour	Moisture	Chisté et al. (2012)
		Piper retrofractum Vahl	Moisture	Sun et al. (2017)
		Whole chia seeds	Moisture	Arslan-Tontul (2020b)
33	Temkin	Cashew nut shell	Congo red	Kumar et al. (2010b)
		Ethylenediamine-modified cross-linked magnetic chitosan	Chromium (VI)	Hu et al. (2011)
		Unmineable coal	CO_2 and CH_4	Garnier et al. (2011)
		Almond shell	Toluidine blue O	Duran et al. (2011)
		Sugar beet pulp	MB	Vučurović et al. (2012)
		Rice hull based activated carbon	Eriochrome Black T (EBT) dye	de Luna et al. (2013)
		Lignite and coconut shell-based activated carbon fiber	Zn (II)	Shrestha et al. (2013)
		Spinel magnesium aluminate nanoparticles	MB	Ismail et al. (2013)
		Tragacanth gum-graft-polyamidoxime	Co(II), Zn(II), Cr(III), Cd(III)	Masoumi and Ghaemy (2014)
		Lagerstroemia speciosa bark	Cr(VI)	Srivastava et al. (2015)
		Algal biochar	Co (II)	Bordoloi et al. (2017)
		Aspergillus niger	Zn(II), CO(II), Cd(II)	Hajahmadi et al. (2015)
		MgO nanomaterials	Textile dye	Mahmoud et al. (2016)
		Diaion HP-20	Paclitaxel	Shin and Kim (2016)
		Chitosan (prawn shells)	Malachite green, Reactive red, Direct yellow	Subramani and Thinakaran (2017)
		Lobeira fruit (*Solanum lycocarpum*)	Pb(II)	Araújo et al. (2018)
		Sawdust	Chromium (VI)	Chakraborty et al. (2021)
		Chikni Mitti (Kaolinite)	Pb^{+2} and Ni^{+2}	Jalees et al. (2019b)
		magnetic spinel ZnFe2O4 nanomaterial	Evans Blue dye	Vergis et al. (2019)
		Pine cone	Malachite green	Kavci (2021)
		Haloxylon recurvum Plant	Acid Brown	Hassan et al. (2020)
		Eichhornia crassipes	Crystal violet	Patil et al. (2020)
		Boron doped ordered mesoporous carbon	Pb (II)	Liu et al. (2020)
34	Toth	Modified silica gel	CO_2, N_2, O_2, Ar	Wilson et al. (2020)
		Polymerized ionic liquid composite	CO_2	Rocky et al. (2019)
		Carbon based adsorbents (activated carbon, multi-walled carbon nanotubes)	H_2	Feng et al. (2019)
		Activated carbon (Maxsorb III)	HFC404A	Ghazy et al. (2020)
		Carboxylated Camelthorn Biomass	Cd(II)	Hashem et al. (2020)
		Carbon-magnetite composite	CO_2	Raganati et al. (2018)
		Zeolite 13×	H_2O	Son et al. (2019)
		MOF-5	H_2	Sridhar and Kaisare (2020)
		Ajuga Pseudo-Iva	Methyl violet	Behloul et al. (2018)
		Lipophilic activated carbons	Sudan-IV	Diaz de Tuesta et al. (2020)
35	Vieth-Sladek	Activated lignin-chitosan blend	MB	Rezakazemi and Shirazian (2019)
		Activated carbon obtained from immature cotton seeds	Basic red 9	Sivarajasekar and Baskar (2014b)
		Eucalyptus camaldulensis	Bisphenol-A	Balci and Erkurt (2017)

(continued on next page)

Table 3 (*continued*)

	Isotherm model	Adsorbent	Adsorbate	Ref.
		bark/magnetite composite		
		Activated carbons derived by the pyrolysis of cassava peel	Copper ions	Moreno-Piraján and Giraldo (2010)
		Activated carbon developed by pyrolysis of potato peel	Copper (II)	Moreno-Piraján and Giraldo (2011)
		Nutraceutical industrial fennel seed spent	Ethidium bromide (EtBr)	Sulthana et al. (2018)
		Activated carbon taken from flamboyant pods (*Delonix regia*)	Food dyes (Acid Yellow 6, Acid Yellow 23, and Acid Red 18)	Vargas et al. (2012)
		Activated carbon produced from flamboyant pods (*Delonix regia*)	MB	Vargas et al. (2011)
		Palm oil fruit shells	Copper ions	Hossain et al. (2012)
		Granular activated carbon/$MnFe_2O_4$ composite	As(III) and As(V)	Podder and Majumder (2016b)
		Graphene oxide nanoparticles	Antidiabetic pharmaceutical (metformin)	Balasubramani et al. (2020)
36	Volmer	Stainless steel	Pyrazolo [3, 4-b] Pyridine	James et al. (2011)
		Aluminum	*Gloriosa superba* gum	Eddy et al. (2014)
		granular activated carbons	Benzene, Phenol, Toluene, Nitrobenzene, and Chlorobenzene	Davoudinejad and Ghorbanian (2013)
37	Weber-Van Vliet	Macrofungus Pleurotus platypus	Ag(I)	Das et al. (2010)
		Cotton seeds (activated carbon)	Basic red 9	Sivarajasekar and Baskar (2014b)
		Clinoptilolite and Bentonite	Cd(II)	Kashi et al. (2017)
		Graphene oxide nanoparticles	Antidiabetic pharmaceutical	Balasubramani et al. (2020)

the structure of pores in adsorbent is considered and it is applicable for heterogeneous surfaces (Dubinin, 1960; Hu and Zhang, 2019). The DR isotherm model is commonly used to describe physical or chemical adsorption processes (Alberti et al., 2012). The corresponding equation is:

$$q_e = q_{m,DR} e^{-K_{DR}\varepsilon_{DR}^2} \tag{8}$$

$$\varepsilon_{DR} = RT\left(1 + \frac{1}{C_e}\right) \tag{9}$$

where $q_{m,\ DR}$ is the maximum adsorption capacity of the DR isotherm model, K_{DR} is constant of the DR isotherm model (mol^2/kJ^2), ε_{DR} is Polanyi potential DR isotherm model ($kJmol^{-1}$).

Abdelnaeim et al. prepared activated carbon from Common reed (*P. australis*) and evaluated its ability to remove Cu and Cd ions from aqueous solutions. (Abdelnaeim et al., 2016). Both heavy metal ions were observed to be strongly adsorbed because the surface of the activated carbon was enriched with phosphorous and quinones groups during the synthesis process and the equilibrium data are better defined by the DR model.

Using Moroccan natural clays, Elmoubarki et al. investigated the elimination of dyes from aqueous solutions (Elmoubarki et al., 2015). The pH of the solution played a significant role, and in the case of anionic dyes, the DR isotherm fitted well.

Under fixed bed operating conditions, Raganati et al. researched the adsorption of carbon dioxide (CO_2) on carbon black with fine magnetite particles (CB-FM) composite (Raganati et al., 2018). Among a variety of isotherm models, the DR model was successful, and it provided information on the mechanism of CO_2 adsorption on CB-FM.

Inyinbor et al. used a novel adsorbent made from the Irvingia gabonensis nut (ADN) waste to scavenge the copper ions from an aqueous solution reaching over 90% extraction efficiency (Inyinbor et al., 2019). Eventually, the DR isotherm described a chemical adsorption process for their systems.

2.7. Flory-Huggins isotherm model

Flory-Huggins solution theory provides an effective and simple mathematical model for the thermodynamics of polymer mixtures. The dissolution process is obtained by putting together entropy and enthalpy, where it could be defined by the Flory-Huggins equation (Senichev and Tereshatov, 2014). This theory presumes that polymer segments and solvent species occupy lattice sites and single sites, respectively; hence, the calculation of the entropy of varied long-chain molecules will become possible.

Flory–Huggins model (Flory, 1942; Huggins, 1942), which is able to demonstrate whether the adsorption process is feasible and spontaneous, describes the surface coverage degree characteristics of the adsorbate onto the adsorbent. This model can be stated as:

$$\frac{\theta_{FH}}{C_{0,FH}} = K_{FH}(1-\theta_{FH})^{n_{FH}} \tag{10}$$

In which θ_{FH} represents surface coverage degree ($\theta_{FH} = 1-\frac{C_e}{C_0}$), n_{FH} shows the number of adsorbates that occupy adsorption spots, and K_{FH} denotes the Flory-Huggins equilibrium constant. Furthermore, K_{FH} is often employed for the determination of the spontaneity free Gibbs energy due to its relation to the following equation (Augustus et al., 2017; Vijayaraghavan et al., 2006):

$$\Delta G^\circ = -RT\ \ln K_{FH} \tag{11}$$

In one research, the microwave activated carbon taken from coconut shell was utilized for urea removal from human urine (Pillai et al., 2014). The adsorption data was fitted to five different isotherm models, among which the Flory–Huggins isotherm was the best match due to error analysis. Furthermore, the negative value of ΔG° obtained by this model confirmed the adsorption was feasible and spontaneous.

Shafique et al. also investigated Chir pine leaves (*Pinus roxburghii*) application as an adsorbent for arsenic removal from aqueous solutions (Shafique et al., 2012). They reported that Langmuir and Flory–Huggins were the best ones based on the coefficient of correlation.

Moreover, Okeniyi et al. employed electrochemical techniques to study *Phyllanthus muellerianus* leaf-extract performance for inhibiting concrete steel-reinforcement corrosion within H_2SO_4 solution (Okeniyi et al., 2014). Additionally, their adsorption isotherm modeling indicated that the experimental results coincided with the Flory-Huggins and Frumkin models which both propose the physical adsorption process of the extract on the steel-rebar surface.

2.8. Fowler Guggenheim isotherm model

The Fowler-Guggenheim (F-G) isotherm model was proposed in 1939 as a simple route for adsorption modeling by lateral interaction consideration of the adsorbed molecules (Fowler, 1939). The F-G isotherm is expressed by Eq. (12).

$$C_e = \frac{\theta_{FG}}{K_{FG}(1-\theta_{FG})} exp\left(\frac{2\theta_{FG}W_{FG}}{RT}\right) \tag{12}$$

In the Eq. (12) the parameter K_{FG} define as the equilibrium constant (L/mg) and W_{FG} is the energy of interaction between adsorbed substances. The θ_{FG} parameter is the Surface coverage degree and is defined as the ratio of the number of adsorbed molecules to the number of active sites of adsorbent in a unit surface area (Brancher et al., 2019; Mbaye et al., 2016). In the reference (Liu et al., 2019a) it is mentioned that the fractional surface coverage can be calculated by ($\theta_{FG} = q_e/q_m$), where q_m is the maximum capacity of adsorption calculated by Langmuir isotherm. This isotherm model is valid for the range of ($\theta_{FG} > 0.6$) (Jeyavishnu and Alagesan, 2020). The W_{FG} has a positive value when the adsorbate-adsorbate interaction is attractive and indicates the heat of adsorption increases by increasing adsorption capacity. Also, the negative value of the W_{FG} expresses the adsorbate-adsorbate interaction is repulsive and the heat of adsorption decreases by increasing adsorption capacity. By neglecting lateral interaction between adsorbate molecules ($W_{FG} = 0$), the F-G isotherm is transformed to the Langmuir model.

Some researchers introduced a modification for the F-G isotherm by considering the surface tension effect, using thermodynamic models and imposing surface structure coefficient, and applied it for the system which included adsorbing oxygen molecules by liquid metals (Ricci et al., 1988).

In the study of Wu et al., the removal of phosphate from polluted water by using recycled concrete was investigated. It was found that the F-G successfully describes the system behavior in a wide range of pH (Wu et al., 2019).

Another research examined the F-G isotherm in a system for adsorption of indigo carmine dye onto special plant leaves. The researchers expressed an exothermic biosorption process as the result of the F-G model (Dada et al., 2020). Also, the F-G model provided a suitable fit for the equilibrium adsorption results of a system for adsorbing non-ionic surfactant (Triton X-100) from an aqueous solution (Prediger et al., 2018).

2.9. Frenkel-Halsey-Hill isotherm model

The Frenkel-Halsey-Hill (FHH) isotherm is a popular isotherm, which was introduced to characterize the process of multilayer adsorption on the smooth solid surface. The isotherm's equation can be written as follows (Frenkel, 1946) (Hill, 1952):

$$\ln\left(\frac{C_e}{C_{s,FHH}}\right) = -\frac{\alpha_{FHH}}{RT}\left(\frac{q_{s,FHH}}{q_e d_{FHH}}\right)^r \tag{13}$$

In this equation, α_{FHH}, d_{FHH}, $C_{s,\ FHH}$ and r are the isotherm constant, the indication of the interlayer distance, Frenkel-Halsey-Hill isotherm constant and the inverse power of spacing from the surface, respectively.

Hung et al. measured the adsorption capacity of kaolinite, black carbon, and montmorillonite, which are insoluble components, utilizing FHH and BET isotherm theories. At high saturation conditions, the adsorbent's surface was analyzed using FHH and BET isotherms to demonstrate the multilayer adsorption process (Hung et al., 2015). Liu an Nie applied Frenkel-Halsey-Hill isotherm to study the fractal characteristics and dimensions of several coal samples, which were utilized to adsorb CH_4. The finding revealed that samples had various abilities for CH_4 adsorption, and the FHH model is suitable for characterizing the pores heterogeneity (Liu and Nie, 2016). One type of zeolite and superporous hydrogel of polyacrylamide were made to adsorb moisture of the air. These adsorbents displayed type-III isotherm and followed FHH isotherm model. The moisture adsorption capacity was observed to reduce when the temperature increases (Mittal et al., 2020).

2.10. Freundlich adsorption isotherm model

Freundlich isotherm is the first isotherm model proposed by Herber Freundlich based on experimental results. This model is applicable in the studies of adsorption on rough and multisite (heterogonous) surfaces (Freundlich, 1906). Freundlich isotherm is as follows:

$$q_e = k_F C_e^{n_F} \tag{14}$$

where k_F and n_F are adsorption potential and strength constants of Freundlich isotherm model, respectively. By having the (n_F) parameter, Freundlich isotherm can describe the heterogeneity of the surface, i.e., the homogenous surfaces have $n_F = 1$, which represents the adsorption is proportional to the percent of sites occupied.

Hallajiqomi and Eisazadeh investigated the polyaniline (PAn) nanocomposite's ability to extract manganese under various conditions (pH, adsorbent dosage, and contact time) in their study (Hallajiqomi and Eisazadeh, 2017). The Freundlich adsorption isotherm model was more successful in predicting the amount of adsorbed manganese on polyaniline nanocomposite.

Jarrah utilized residual fuel oil to make mesoporous activated charcoal which then he used to adsorb the MB and rhodamine 6G (R6G) from their single and binary aqueous solutions (Jarrah, 2017). The first layer of dye was adsorbed due to the electrostatic attraction and the second layer was then mechanically adsorbed on top of the first. Freundlich isotherm model was fitted very well to the obtained results of this research.

Nanta et al. used superparamagnetic nanoparticles as adsorbents to remove high polysaccharide concentrations from rice noodle manufacturing wastewater (Nanta et al., 2018). Their study showed that the Freundlich isotherm better suited the equilibrium data. Additionally, the experiments of Kim et al. confirmed that the Freundlich adsorption isotherm was the best fit for the paclitaxel drug adsorption on commercial synthetic adsorbent (Sylopute) (Kim and Kim, 2019).

Selim et al. studied Cr(VI) adsorption from aqueous solutions by a synthetic PD/MCM-41 composite (Selim et al., 2018). The findings of this study verified the conformity of the adsorption isotherm with the Freundlich isotherm.

2.11. Fritz-Shluender isotherm model

In the research of Fritz and Schlunder, the competitive adsorption of p-nitrophenol and phenol on activated carbon was investigated. They proposed empirical mathematical isotherm models for bisolute and single solute adsorption for a wide range of applications. The three, four, and five-parameter Fritz-Shluender (F-S) isotherm models are expressed in Eqs. (15)–(17) (Fritz and Schluender, 1974; Ramadoss and Subramaniam, 2019).

$$q_e = \frac{q_{m,FS1}\ K_{FS1} C_e}{1 + q_{m,FS} 1 C_e^{m_{FS1}}} \tag{15}$$

$$q_e = \frac{C_{FS2} C_e^{\alpha_{FS2}}}{1 + D_{FS2} C_e^{\beta_{FS2}}} \tag{16}$$

$$q_e = \frac{q_{m,FS3} K_{1,FS3} C_e^{m_{1,FS3}}}{1 + K_{2,FS3} C_e^{m_{2,FS3}}} \tag{17}$$

In the three-parameter model (Eq. (15)) the $q_{m,\ FS1}$ define as the maximum adsorption capacity (mg/L) and the K_{FS1} is equilibrium constant (L/mg). The four-parameter model (Eq. (16)) was obtained from the Langmuir-Freundlich model and the α_{FS2} and β_{FS2} parametrs have the value lower than unity ($\alpha, \beta < 1$). By adjusting the α_{FS2} and β_{FS2} to the value of unity, the model transforms to the Langmuir model. The $K_{1,\ FS3}$, $K_{2,\ FS3}$, $m_{1,\ FS3}$ and $m_{2,\ FS3}$ are the constants for the five-parameter (Eq. (17)) F-S model and the $q_{m,\ FS3}$ shows the maximum adsorption capacity (mg/g) (m_1, $m_2 < 1$).

Nebaghe et al. proposed a modification for the F-S model by adding additional parameters to the model. They validate their model by experimental results from adsorption of Cu(II) onto treated sand with a good agreement (Nebaghe et al., 2016).

In some research the three and four-parameter F-S were applied for reliable estimation of the adsorption of Cd(II) onto treated cellulose-based and other bio-based adsorbent (Zarei and Niad, 2020; Zheng et al., 2019).

2.12. Frumkin isotherm model

The Frumkin isotherm represents the monolayer adsorption onto a homogenous surface, considering the interaction among the adsorbed species. Its equation is depicted below (Frumkin, 1925b; Grchev et al., 1991):

$$C_e = \frac{\theta_{Fm}}{K_{Fm}(1-\theta_{Fm})}\exp\left(-f_{Fm}\theta_{Fm}\right) \tag{18}$$

In which θ_{Fm} $\left(\theta_{FM} = \frac{q_e}{q_m}\right)$ is the surface coverage degree ($0 \le \theta_{Fm} \le 1$), and K_{Fm} and f_{Fm} describe Frumkin equilibrium constant and adsorbate interaction coefficient of the Frumkin equation, respectively. Parameter f_{Fm} correlates with the attractive or repulsive forces between the adsorbed molecules based on the amount of its positive or negative values, respectively; but providing that f_{Fm}equals to zero, meaning no interaction exists among adsorbate molecules, the Frumkin model turns to the Langmuir equation.

The adsorption characteristics of *Azadirachta indica* extract in terms of a mild steel corrosion inhibitor in nitric acid solutions have been analyzed in a study (Sharma et al., 2010), and it turned out that the Frumkin model described it the best.

Narvekar et al. (Narvekar et al., 2018) investigated the MB adsorption on a synthesized glycerol-based carbon. They came to conclusion that at higher equilibrium concentration, Frumkin adsorption model was the best match of the adsorption data, potentially because of the existence of large interaction between the adsorbate species.

Souza et al. (Souza et al., 2018) examined the methamphetamine hydrochloride (MA) adsorption on dispersed Ag nanoparticles in agarose gel. Their obtained results revealed that MA adsorbed onto the Ag nanoparticle surface, making ionic pairs with the adsorbed chloride and followed the Frumkin model with positive f_{Fm} parameter representing the attractive lateral interaction.

In another study, the adsorption behavior of zwitterionic surfactant onto sandstone and carbonate samples was studied by Kumar and Mandal (Kumar and Mandal, 2019). They found out that the surfactant adsorption onto sandstone followed the Frumkin model, indicating attraction forces between the adsorbed molecules, while the surfactant adsorption onto carbonate surface followed Sips model.

2.13. GAB (Guggenheim-Andersen-de Boer) isotherm model

The three-parameter GAB isotherm model is generally defined as a modification and refinement for the BET model by considering the heat of adsorption (Anderson, 1946; De Boer, 1953; Guggenheim, 1966). By using the GAB model, the broader range of relative pressures and chemical activities will be considered that makes it more practical in water adsorption systems. The GAB model has an additional K_{GAB} parameter and is expressed by eq. 19. By making a regression of a dataset over these two models and adjusting a predetermined value for the K_{GAB} parameter, it is always observed that the ($q_{m,\ BET} < q_{m,\ GAB}$) and ($C_{BET} > C_{GAB}$). This deviation highlights the importance of a modification for the BET model (Timmermann, 2003).

$$q_e = \frac{q_{m,GAB}C_{GAB}K_{GAB}C_e}{\left(C_{s,GAB} - K_G C_e\right)\left[1 + (C_{GAB}-1)K_G\frac{C_e}{C_{s,GAB}}\right]} \tag{19}$$

For this purpose, Anderson had made efforts by adsorbing nitrogen on spheres of glass (at 78 K), while de Boer proposed ($K_{GAB} < 1$) for a nitrogen-TiO_2 adsorption system. Also, Guggenheim tried to adsorb nitrogen on Fe/Al_2O_3 and finally van der Berg analyzed the adsorption of water on wheat starch and proposed the acronym of GAB for the modified model (CVD, 1981). The K_{GAB} expressed the free enthalpy of adsorbate molecules in the second layer of adsorption and it always had a value lower than unity. The C_{GAB} parameter shows the chemical potential difference between adsorption layers. By adjusting ($K_{GAB} = 1$) the GAB model will transform to the BET model.

The GAB model has become very popular in the field of food technology (Maroulis et al., 1988). It has been applied in several food, fruit and cereal materials for modeling and estimating the equilibrium moisture content (Maroulis et al., 1988; Oluwamukomi, 2009; San Martin et al., 2001). In a paper, researchers performed a modification for the GAB model by addition and applying the n_{GAB}' parameter as the power of the $\left(\frac{C_e}{C_{s,GAB}}\right)$ parameter in the Eq. (19) and transformed it to a four-parameter model. The modified form of the GAB model is expressed by Eq. (20), and it was applied for modeling the adsorption of ethane on templated carbon in different temperatures (Zou et al., 2016).

$$q_e = \frac{q'_{m,GAB}C'_{GAB}K'_{GAB}\left(\frac{C_e}{C'_{s,GAB}}\right)^{n'_{GAB}}}{\left(1 - K'_{GAB}\left(\frac{C_e}{C'_{S,GAB}}\right)^{n'_{GAB}}\right)\left[1 + (C'_{GAB}-1)K'_{GAB}\left(\frac{C_e}{C'_{s,GAB}}\right)^{n'_{GAB}}\right]} \tag{20}$$

2.14. Halsey isotherm model

The Halsey isotherm is applicable for heterogeneous surfaces and multilayer adsorption processes (Halsey, 1948). The following is the Halsey equation:

$$q_e = e^{-(\ln K_{HL} - \ln C_e)/n_{HL}} \tag{21}$$

where K_{HL} and n_{HL} are Halsey isotherm model constant. Using multi-walled carbon nanotubes (MWCNTs), Moradi investigated methods to remove ammonium ions from an aqueous solution (Moradi, 2016). Experimental results of this research showed that the Halsey isotherm model could better describe the adsorption process. Omotunde et al. investigated the adsorption of cadmium from an aqueous solution using derived and thiol-functionalized silica (Omotunde et al., 2018). The equilibrium adsorption effects are matched well in the Halsey, Freundlich, Langmuir and Temkin isotherms.

2.15. Harkins-Jura isotherm model

Harkins-Jura isotherm model is based on the concept of multilayer adsorption on adsorbents with heterogeneous pores. It is applicable for adsorption processes involving adsorbents of varying pore sizes (Harkins and Jura, 1944; Jeyavishnu and Alagesan, 2020). In Eq. (22), A_{HJ} and B_{HJ} are Harkins Jura isotherm model constants:

$$\frac{1}{q_e^2} = \frac{B_{HJ}}{A_{HJ}} - \frac{1}{A_{HJ}}\log C_e \tag{22}$$

Saad et al. conducted research on the removal of binary dye systems of Reactive Red and Crystal Violet using Ag-Cr-AC nanocomposites as an adsorbent (Saad et al., 2017). It was shown that among the examined isotherms, two dyes had two different adsorption systems. The Langmuir isotherm has described the Reactive Red adsorption, and the adsorption of Crystal Violet followed the Harkins-Jura isotherm model.

In another study, the removal of Congo red from aqueous solution media was investigated using a novel adsorbent prepared from *Cereus* sp. by Jeyavishnu and Alagesan. They verified the experimental data adherence to many isotherm models, including the Harkins-Jura (Jeyavishnu and Alagesan, 2020).

2.16. Henderson isotherm model

In 1952 Henderson proposed an empirical isotherm model for estimating moisture content of biomaterials (Henderson, 1970). The biomaterials generally have capillaries in their structure and these capillaries show different behavior in the adsorption process. In a humid atmosphere, biomaterials have different adsorption-desorption isotherm (hysteresis) and the capillaries' structure may have reformed during adsorption-desorption cycles, and the presence of inert gases may affect the adsorption process. Henderson performed experiments to evaluate equilibrium moisture content of a special variety of rice in different humid conditions. The main application of Henderson model is in food drying systems. The Henderson isotherm model is expressed by Eq. (23), where the A_{He} and n_{He} define as model constants related to adsorbent material (Karakuş et al., 2020).

$$q_e = \left(\frac{-\ln(1-C_e)}{A_{He}}\right)^{1/n_{He}} \tag{23}$$

A modification for Henderson isotherm model was introduced by Thompson et al. (1968)) for the corn drying system by considering the temperature effect in the model. The modified Henderson model is showed by Eq. (24) and the A_{He}', $B_{He}'$and n_{He}' are the model constants (Mehta and Singh, 2006).

$$q_e = \left[\frac{-\ln(1-C_e)}{A'_{He}(T+B'_{He})}\right]^{1/n'_{He}} \tag{24}$$

In the research of (Karakuş et al., 2020), the adsorption of different dyes onto hydromagnesite stromatolite was studied and the Henderson isotherm showed an appropriate description for the system. Also, it was found that the Henderson isotherm can be applied for adsorption of moisture on freeze-dried powdery food material and various flours (Hawa et al., 2020; Stępień et al., 2020). Additionally, tomato pulp was dried in different drying equipment and the modified Henderson isotherm was determined as the best model for estimating moisture content in all drying systems (Chawla et al., 2008). Moreover, the drying of cucumber seeds obeyed the modified Henderson isotherm as well (Corrêa et al., n.d.).

2.17. Henry isotherm model

Henry adsorption isotherm model is the most basic adsorption isotherm and it is represented by Eqs. (25) and (26) for liquid and gaseous systems, respectively (Erbil, 2006):

$$q_e = K_{HN}C_e \tag{25}$$

$$q_e = K_{HN}P \tag{26}$$

where K_{HN} is defined as the Henry adsorption constant. In 2018, Poursaeidesfahani et al., investigated the adsorption of an equimolar mixture of carbon dioxide and methane onto a zeolite-based adsorbent (ITQ-29). The obtained Henry coefficient were in agreement with experimental results (Poursaeidesfahani et al., 2019). The findings of Soukup *et al.* on hydrogen adsorption research were well matched by Henry adsorption isotherm (Soukup et al., 2017).

2.18. Hill-De Boer isotherm model

The Hill-De Boer isotherm model is represented by Eq. (27), and describes the case of mobile adsorption and lateral interaction among adsorbed molecules (De Boer, 1953; Hill, 1946):

$$K_{1,HB}C_e = \frac{\theta_{HB}}{1-\theta_{HB}} exp\left(\frac{\theta_{HB}}{1-\theta_{HB}} - \frac{K_{2,HB}\theta_{HB}}{RT}\right) \tag{27}$$

where $K_{1,\ HB}$ is the Hill-De Boer constant (L/mg), θ_{HB} is the Surface coverage degree ($\theta_{HB} = q_e/q_{m,\ HB}$, and $q_{m,\ HB}$ is maximum adsorption capacity of the Hill-De Boer isotherm), and $K_{2,\ HB}$ is the energetic constant of the interaction between adsorbed molecules (kJ/mol). Research of Ludmila Vidoca et al. on the extraction of carotenoids from hybrid palm oil by adsorption onto polymeric resin Diaion HP-20 confirmed that Jovanovich and Hill-De Boer are the best models examined in their study (Vidoca et al., 2020).

2.19. Hill isotherm model

The Hill isotherm model considers adsorption as a cooperative process. In this view, adsorbed adsorbate on adsorbent could have affected other sites (Hill, 1910). This adsorption isotherm model equation is originally derived from the non-ideal competitive adsorption (NICA) isotherm (Koopal et al., 1994). The non-linear form of the Hill isotherm model is written as follows:

$$q_e = \left(\frac{q_{SH}\cdot C_e^{n_{SH}}}{K_{D,SH}+C_e^{n_{SH}}}\right) \tag{28}$$

where q_{SH} is Hill isotherm maximum uptake saturation (mg/L), n_{SH} is Hill cooperativity coefficient of the binding interaction, and $K_{D,\ SH}$ defines the Hill isotherm constant.

The experiments of Karoui et al. on extracting binary ciprofloxacin antibiotic (CIP) and MB dye showed that the Hill isotherm was one of the isotherm models which can explain biosorption process of MB (Karoui et al., 2020).

2.20. Jossens isotherm model

The energy distribution of adsorbent-adsorbate interactions is used by the Jossens isotherm model to anticipate the adsorption process in adsorption sites. This isotherm presumes the surface of adsorbent is heterogeneous with adherence to the interactions that exist among the adsorbate and the adsorbent. The equation of Jossen isotherm is given by the following expression (Jossens et al., 1978):

$$C_e = \frac{q_e}{H_{Js}} \exp\left(F_{Js}q_e^{P_{Js}}\right) \tag{29}$$

In this equation, H_{Js}, F_{Js}, which only vary with temperature, and P_{Js} are the parameters of the Jossens isotherm. It should be noted that Jossens model becomes Henry's law at low concentrations. Jossens isotherm model was used to describe the influence of hot water on dyeing process (Makhlouf et al., 2015). The capacity of an unmodified biosorbent for adsorbing chromium (VI) from an aqueous solution was analyzed by Bayuo et al. In this work, Jossens and Redlich–Peterson isotherms were utilized to evaluate the biosorption of hexavalent chromium onto the unmodified biosorbent (Bayuo et al., 2020).

2.21. Jovanovich isotherm model

Jovanovich isotherm model can be considered as a modification of the Langmuir model (Langmuir, 1918) in which adsorption-adsorption interactions are added. The equation for this adsorption isotherm model is less often used in physical adsorption and it can be used for both mobile and monolayer localized adsorption (Jovanović, 1969). At high concentration the Jovanovich equation model will approach equilibrium, and as the concentration reduces; it approaches to Henry's law. Additionally, the Jovanovich equation approaches saturation more slowly than the Langmuir equation. The non-linearized version of the Jovanovich equation is:

$$q_e = q_{m,Jv}\left[1 - e^{K_{Jv}C_e}\right] \tag{30}$$

where, $q_{m,\ Jv}$ describes the maximum adsorption capacity of Jovanovich isotherm and K_{Jv} is Jovanovich constant (L/g). Using the factorial modeling method, Aly-Eldeenn et al. investigated the sorption of Eriochrome Black T dye from aqueous solution on a waste sludge adsorbent (Aly-Eldeen et al., 2018).Their experimental results were fitted the Jovanovic model better than the Halsey model. Ghaleh et al. investigated the thiamine adsorption on sodium montmorillonite (Mt). Their results showed that the Jovanovich isotherm adsorption model fitted appropriately to the experimental data (Ghaleh et al., 2020).

2.22. Khan isotherm model

Khan isotherm model (Khan et al., 1997; Khan et al., 1996) is a general model recommended for the pure solutions; i.e., its equation is for bi-adsorbate adsorption from pure dilute aqueous solutions. This model owns a distinguishing feature like reflecting both characteristics of Langmuir isotherm on the one hand and the Freundlich model on the other hand. Khan isotherm was developed for single and multicomponent adsorption systems and it is written as follows:

$$q_e = \frac{q_{m,KH} b_{KH} C_e}{(1 + b_{KH} C_e)^{a_{KH}}} \tag{31}$$

where $q_{m,\ KH}$ expresses the maximum adsorption capacity of Khan isotherm, and b_{KH} and a_{KH} are Khan isotherm constant and exponent, respectively. Providing that a_{KH} is unity, the equation turns to the Langmuir model and in high equilibrium concentrations it approaches the Freundlich isotherm.

Quaternary amine modified orange peel powder (QAMOPP) was applied as an adsorbent for Reactive Red 120 (RR120) adsorption in one study. Adsorption data of RR120 were fitted with non-linearized isotherms and it was detected that the Langmuir and Khan were the best to predict RR120 removal by QAMOPP (Munagapati et al., 2019).

Furthermore, 4-chlorophenol (4-CP) adsorption onto granular activated carbon (GAC) was investigated and modeled by six isotherm equations. It was observed that even though, except for Freundlich model, all of the other applied equilibrium models coincided well with empirical findings, Khan isotherm model was the finest for representing the 4-CP adsorption on GAC based on the R^2 values. Also, since all isotherm models were applicable to this system, it can be deduced that both heterogeneous surface conditions and monolayer adsorption occur in the study (Bilgili et al., 2012).

In order to remove the cationic dyes (basic violet 3 (BV3) and basic red 2 (BR2)) from wastewater Wakkel et al. developed an inexpensive and environment-friendly adsorbent named as palm-date stones. Between the applied models, Toth, Khan and Redlich–Peterson adapted properly to basic violet 3 equilibrium results while Hill and Koble–Corrigan were the best representatives of BR2 adsorption (Wakkel et al., 2019). In another work, the ability of an ion exchange resin to remove zinc from aqueous solution was examined at different conditions. By using nine isotherm models, the adsorption data were analyzed, and Khan isotherm model turned out to be the most fitted model (Fil et al., 2012).

2.23. Kiselev isotherm model

In the concentrated monomolecular layer, the Kiselev isotherm is recognized as the adsorption model, and it is given by the following expression (Kiselev, 1958):

$$K_{1,KV} C_e = \frac{\theta_{KV}}{(1 - \theta_{KV})(1 + K_{n,KV}\theta_{KV})} \tag{32}$$

In this equation, $K_{1,\ KV}$, $K_{n,\ KV}$ and θ_{KV} are the constant of Kiselev equilibrium, the complex formation constant and the Surface coverage degree which is equal to ($q_e/q_{S,\ KV}$), respectively.

Titanium oxide was used to adsorb phenol and, four heavy metals including copper, zinc, cadmium and iron. Kiselev isotherm proved that the adsorption behavior of phenol and other metals ions onto TiO_2 is different, and adsorption energy values were obtained by Temkin model. This work gives a better comprehension of adsorption onto the surface of TiO_2 so as to specify bisolute and single-solute adsorption of metallic ions (Marczewski, 2011). Kiselev model isotherm as well as several isotherm models were employed to assess the potential of a powerful resin (cation-exchange) to remove nickel from aqueous medium. In the study of Yousef et al. the Hill isotherm had an strong agreement with the experimental results (Yousef et al., 2016).

2.24. Koble–Corrigan isotherm model

Koble-Carrigan isotherm model contains three parameters, and it is obtained as consequence of combining Freundlich and Langmuir isotherms to represent adsorption equilibrium data (Alahmadi et al., 2014). The following expression indicates the nonlinear form of the Koble-Corrigan isotherm equation (Koble and Corrigan, 1952):

$$q_e = \frac{a_{KC} C_e^{n_{KC}}}{1 + b_{KC} C_e^{n_{KC}}} \tag{33}$$

Koble-isotherm Carrigan's constants are a_{KC} and b_{KC} in this equation, and n_{KC} is an exponent of this isotherm. Koble-Carrigan isotherm becomes Freundlich isotherm at high concentrations of adsorbate. If n_{KC} is smaller than 1, it means that it is unable to specify the experimental data considering high concentration coefficient or small error amounts; therefore, the isotherm is reliable when n_{KC} is more than or equal to 1 (Koble and Corrigan, 1952). Natural bentonite and zeolite were evaluated to eliminate lead (Pb(II)) from aqueous solutions. Although the removal of lead ions by bentonite and zeolite involves several mechanisms and complicated, experimental equilibrium data demonstrated that the Koble–Corrigan isotherm is able to explain the interaction between lead and other minerals significantly. The results indicated that natural bentonite and zeolite utilized in this work have a suitable adsorption capacity for lead; hence, it may be capable to remove lead from polluted environment (Hamidpour et al., 2011). The idea of using lotus leaf to eliminate MB from the aqueous medium was investigated by Han et al. under various conditions. The experimental data demonstrated that lotus leaf could be capable adsorbent to eliminate MB significantly. In addition, the adsorption mechanism was discussed using Koble–Corrigan, Langmuir, and Freundlich, and the finding showed that system's adsorption behavior were appropriately predicted by Koble–Corrigan model (Han et al., 2011). Wang et al. showed that the bamboo activated carbons could be used to eliminate dyes and color from wastewater as a capable and economic adsorbent. In this work, Koble-Corrigan, Jovanovic, Freundlich, Langmuir, and Khan isotherms were used to fit with equilibrium results, and among these isotherms, Koble-Corrigan and Jovanovic isotherm models had the best and worst performance, respectively. Relying on thermodynamic criteria, the adsorption mechanism was spontaneous and endothermic with a physical essence (Wang and Yan, 2011). In a research, a bio-based activated carbon (derived from *Salix psammophila*) was utilized to eliminate sulfamethazine sodium from aqueous medium. To explain the adsorption mechanism of the system, multiple isotherm models were used, and the isotherm model of Koble-Corrigan matched well with the experimental equilibrium results. Also, this work illustrated that this adsorbent is an efficient and low-cost adsorbent to adsorb sulfamethazine sodium from aqueous solution (Liu et al., 2019b).

2.25. Langmuir isotherm model

The Langmuir isotherm model, one of the first proposed isotherm, assumes the adsorbate and adsorbent in ideal manner and this model is deployed for homogenous surfaces. Another assumption of this isotherm model is the reversibility of adsorption-desorption process (Langmuir, 1916; Langmuir, 1918). The Langmuir isotherm can be obtained from these assumptions, implying that:

$$q_e = \frac{q_{m,L} k_L C_e}{1 + k_L C_e} \tag{34}$$

where $q_{m,\ L}$ is maximum adsorption capacity of Langmuir isotherm (mg/g), k_L is Langmuir isotherm constant or affinity constant (dm^3/mg).

The results of Chanzu et al. research demonstrated the exothermic adsorption of Congo Red (CR) and malachite green dyes (MG) from aqueous solution on Brewer's spent grain (BSG). Their results were fitted closely to the Langmuir adsorption isotherm model (Chanzu et al., 2019).

Mohammed et al. studied phenol adsorption onto zeolite NaY adsorbent from a synthetic wastewater at various temperatures and pH (Mohammed et al., 2019).Their findings verified that the phenol adsorption on zeolite NaY conformed to the Langmuir adsorption isotherm model.

Alsuhybani et al. studied the ability of modified magnetic nanoparticles to remove harmful lead ions from aqueous solutions and found the success of Langmuir adsorption isotherm model for describing the adsorption mechanism (Alsuhybani et al., 2020). Sawant et al. synthesized boron doped carbon nanotubes (BCNTs) and investigated their hydrogen adsorption behavior in comparison to undoped single and multiwalled carbon nanotubes (Sawant et al., 2019). They discovered a significant improvement in the hydrogen storage value of doped CNTs as compared to other undoped CNTs. The Langmuir adsorption isotherm was discerned to be appropriate for explaining adsorption isotherm.

Soltani et al. used thiol-modified mesoporous silica sub microspheres (TMS-SMSs) to remove poisonous Tl(I) ions from aqueous solution (Soltani et al., 2019). The adsorption of Tl(I) onto TMS-SMSs confirmed a Langmuir adsorption isotherm. Ghanei et al.and investigations on the adsorption of Acid Blue 25 on their synthesized Magnetic-SBA-15/CPAA revealed the Langmuir adsorption isotherm is the best choice for explaining this adsorption process (Ghanei et al., 2018).

Wang et al. investigated the adsorption ability of lignin-based carbon composite to remove various dyes (Wang et al., 2018). Obtained results verified that under neutral conditions, the adsorbent has strong adsorption properties. The adsorption Congo red of (CR) and Eriochrome blue black R dyes were well-matched to Langmuir adsorption isotherm. The research of Ahsaine et al. confirmed the best match of experimental evidence from adsorption of MB and Crystal Violet on their synthesized activated carbon for the Langmuir isotherm model, suggesting homogeneous distribution of adsorption sites (Ahsaine et al., 2018).

2.26. MacMillan-Teller (MET) isotherm model

MET isotherm model (McMillan and Teller, 1951) is derived from the insertion of the effects of surface tension into the BET isotherm; in other words, the model, which is correct in the multilayer adsorption region, considers both effects of the adsorbate surface energy and inclusion of the attractive forces of adsorbent over the first layer. Although this isotherm is tested in aqueous solutions, its utilization is for gases. The model's equation is defined as:

$$q_e = q_{s,MET} \left(\frac{K_{MET}}{ln\,(C_{s,MET}/C_e)} \right)^{\frac{1}{3}} \tag{35}$$

where $q_{s,\ MET}$ is theoretical saturation capacity of the isotherm, K_{MET} is MET isotherm constant, and $C_{S,\ MET}$ indicates the monolayer saturation concentration of adsorbate. When $C_{s,\ MET}/C_e$ comes close to unity, the logarithmic part may be estimated as follows:

$$q_e = q_{m,MET} \left(\frac{K_{MET} C_e}{C_{s,MET} - C_e} \right)^{\frac{1}{3}} \tag{36}$$

It is worth mentioning that the experimental data would fit appropriately to the isotherm model when the relative pressure is higher than 0.8. In one research, for adsorption of arsenic, metallurgical slag was practiced as a functional low-cost adsorbent. Then the adsorption data was modeled with 12 nonlinear isotherm models, including the MET model, to estimate data and analyze them statistically to find the best fit (Mercado-Borrayo et al., 2014a).

Furthermore, boron removal by metallurgical slag and iron nanoparticles was studied by Mercado-Borrayo et al. (2014b). They applied MET model along with 11 other adsorption isotherm models to find the one that described the experimental data more properly.

Rezakazemi and Shirazian (2019) applied MET isotherm as well as 23 other isotherm models to do a thorough analysis of numerous approaches for the MB removal from water by the lignin and chitosan blend.

2.27. Marczewski-Jaroniec isotherm model

The Marczewski-Jaroniec isotherm model is hypothesized to be based on the local Langmuir model and energy distribution in the adsorbent's active sites. The equation of this isotherm is expressed as follows (Derylo-Marczewska and Jaroniec, 1987):

$$q_e = q_{m,MJ} \left(\frac{(K_{MJ} C_e)^{n_{MJ}}}{1 + (K_{MJ} C_e)^{n_{MJ}}} \right)^{\frac{m_{MJ}}{n_{MJ}}} \tag{37}$$

In this equation, $q_{m,\ MJ}$ is the maximum adsorption capacity that obtained by this model, K_{MJ} is the equilibrium constant, and n_{MJ} and m_{MJ} are the model's parameters, which specify the surface's heterogeneity of adsorbent. Also, the distribution in the direction of higher and lower adsorption energy is also defined by n_{MJ} and m_{MJ}. Marczewski-Jaroniec Isotherm becomes Langmuir-Freundlich isotherm when $n_{MJ} = m_{MJ}$, and it becomes Langmuir isotherm when n_{MJ} and $m_{MJ} = 1$. The low-cost blue-green marine algae (BGMA) adsorbent that was utilized to remove Ni(II) from aqueous medium. The results indicated that the competition between Ni(II) and solvent to occupy the BGMA's active sites is weak because the isotherm is L-shaped based on equilibrium experimental data. The Marczewski–Jaroniec isotherm model and several other isotherms were utilized to specify the mechanism of adsorption (Ramadoss and Subramaniam, 2019).

2.28. Oswin isotherm model

The empirical two parameter Oswin isotherm model was proposed by Oswin in 1946 to estimate the moisture in water-sensitive materials and foods in packagings (Oswin, 1946). The Oswin isotherm model is shown by Eq. (38). The K_{OS} and n_{OS} are defined as the model parameters.

$$q_e = K_{OS} \left(\frac{C_e}{1 - C_e} \right)^{n_{OS}} \tag{38}$$

Chen introduced a modification for the Oswin isotherm model in 1990 by considering the K_{OS} as a function of temperature. He validated the model by estimating the water adsorption and moisture content of several biological and cereal materials in a limited range of humidity. The modified Oswin isotherm model is expressed by Eq. (39), where the A'_{OS}, B'_{OS} and n'_{OS} are the model parameters and the T is the temperature in (°C) (Chen, 1990).

$$q_e = (A'_{OS} + B'_{OS}T)\left(\frac{C_e}{1 - C_e}\right)^{n'_{OS}} \quad (39)$$

In a study, researchers evaluated the moisture adsorption of the Tunisian clay as a hygroscopic material and compare the results with different isotherms. They reported the Oswin model as a mathematical description of the system and found that the system behavior was highly depended on the temperature (Jhider and Bagané, 2019). The modified Oswin model also applied for modeling the moisture content of food materials. It has been used for estimating equilibrium moisture content of grape seeds flour, coffee blends and chili pepper (Bogoeva and Durakova, 2020; Getahun et al., 2020; Henrique Horta de Oliveira et al., 2020).

2.29. Radke–Prausnitz isotherm model

For modeling adsorption systems, the Radke-Prausnitz isotherm is widely used as it has some special properties at low adsorbate concentrations. The following expression describes the Radke-Prausnitz isotherm (Radke and Prausnitz, 1972):

$$q_e = \frac{q_{m,RP} K_{RP} C_e}{(1 + K_{RP} C_e^{m_{RP}})} \quad (40)$$

In this equation, $q_{m,\ RP}$, K_{RP} and m_{RP} are maximum adsorption capacity, equilibrium constant, and model exponent of Radke-Prausnitz isotherm, respectively. This isotherm becomes a linear isotherm at low adsorbate concentrations, while it converts to the Freundlich isotherm at high adsorbate concentrations, and even converts to the Langmuir isotherm if $m_{RP} = 0$. The other special characteristic of Radke-Prausnitz isotherm is that it can use in a vast range of concentration. The parameters of this model are acquired by nonlinear statistical fit of experimental data (Subramanyam and Ashutosh, 2012) (Ravnote and Adsorpcijo, 2013).

Exfoliated graphite was utilized to remove C.I. Acid Blue 92 dye, and the experimental data demonstrated that this adsorbent can adsorb the dye effectively. To examine the adsorption equilibrium data, Radke-Prausnitz, Langmuir, and Freundlich isotherms were utilized, and the results indicated that the adsorption mechanism was nonlinear and could be predicted by the models of Radke-Prausnitz and Langmuir (Goshadrou and Moheb, 2011).

For the elimination of MB and tartrazine from the aqueous medium, activated charcoal was used. To analyze dye adsorption data, several isotherm models were utilized, and various non-linear error functions were tested for isotherm equations. Based on the results, Radke- Prausnitz isotherm, which is a three-parameter model, has good agreement with equilibrium data, and non-linear regression produced the optimum parameter values (Sarici-Özdemir and Önal, 2014).

Rafati et al. studied the ability of a functionalized nano-clay composite to adsorb ibuprofen under various conditions. Experimental data proved that this adsorbent is able to remove ibuprofen from water and wastewater. In addition, nine isotherm were used to assess the adsorption equilibrium data, and results showed that Radke–Prausnitz was one of the optimum models that can be described the behavior of adsorption system (Rafati et al., 2018). Sahin et al. studied the possibility of using Zr-based MOF/graphene nanoplatelets for recovering the β-carotene from n-hexane solution. Under optimum conditions, the highest adsorption efficiency was observed (about 60%). It was a process of nonspontaneous, endothermic and chemisorption, which was evaluated by Radke—Prausnitz isotherm models (Şahin and SaS, 2020).

2.30. Redlich–Peterson isotherm model

As a result of combining Freundlich and Langmuir isotherms, Redlich–Peterson model is obtained that include three parameters. The empirical equation of model includes an exponential and a linear concentration relationships in the denominator and numerator respectively that shows the equilibrium of adsorption over a wide variety of concentration, which may be implemented both in homogeneous and heterogeneous systems of adsorption (Redlich and Peterson, 1959) (Prasad and Srivastava, 2009) (Ng et al., 2002). Redlich–Peterson model approaches Freundlich model when the β_{RN} value tends to zero, while at low concentration it approaches Langmuir model since the β_{RN} value tends to one. The model of the Redlich-Peterson isotherm is described by the following (Redlich and Peterson, 1959):

$$q_e = \frac{K_{RN} C_e}{1 + a_{RN} C_e^{\beta_{RN}}} \quad (41)$$

In this equation K_{RN} and a_{RN} are the constants of Redlich-Peterson model, and β_{RN} is exponent, which can be varied from 0 to 1.

A significant number of research indicated that the Redlich–Peterson isotherm model is more accurate compared with Freundlich and Langmuir isotherm models. Wu et al. proposed an effective exponential linear equation that was suitable and accurate to fit with adsorption experimental data in compare to logarithmical linear equation of Redlich–Peterson isotherm. The proposed equation was used for predicting the behavior of three dyes adsorption on certain kinds of pistachio shell activated carbons, and its performance was appropriate (Wu et al., 2010).

An investigation found that it is possible to use the Redlich-Peterson isotherm to obtain the function of site energy distribution which could be used to specify the surface heterogeneity of various adsorbents (Kumar et al., 2010a). Isotherm models were utilized to explain Kraft lignin's behavior in equilibrium condition to adsorb Cr (VI), and the results indicated that Redlich–Peterson isotherm is the effective model among three-parameter models (Brdar et al., 2012).

To assess the removal of an anionic dye on an industrial activated charcoal, the linear and non-linear shape of the Redlich-Peterson, Freundlich and Langmuir isotherms were utilized. The findings revealed that the experimental data are correctly matched to the isotherms of Redlich-Peterson and Langmuir. In addition, the obtained coefficients from non-linear equation were less than the obtained coefficients from linear equation (Açıkyıldız et al., 2015). Nakhjiri et al. studied the possibility of removal of crystal violet and MB from aqueous mediums by one type of hydrogel. The Redlich-Peterson, Langmuir, Freundlich, and Temkin models were utilized in various temperature to test the system's adsorption behavior, and it is observed that the experimental data can be described well by Redlich-Peterson model (Nakhjiri et al., 2018).

2.31. Sips isotherm model

Sips isotherm model, which is obtained by combining Freundlich and Langmuir isotherms, is a hybrid model. It is an appropriate isotherm to predict the adsorption behavior of the heterogeneous structures, and avoiding from the restriction of the increasing concentration of adsorbate that Freundlich isotherm is encountered. Sips isotherm becomes Freundlich and Langmuir isotherms at low and high concentrations respectively; hence, it can predict a monolayer adsorption system properly (Pérez-Marín et al., 2007) (Günay et al., 2007). Generally, the operating conditions of system, like pH, concentration, and temperature govern the parameters of Sips model. The isotherm model of Sips is given by the following (Sips, 1948):

$$q_e = \frac{q_{m,SP} K_{SP} C_e^{n_{SP}}}{1 + K_{SP} C_e^{n_{SP}}} \tag{42}$$

In this equation, $q_{m,\ SP}$, K_{SP} and n_{SP} are the maximum adsorption capacity, Sips isotherm constants, and Sips isotherm exponent, respectively.

A novel nano hollow sphere was used by Rostamian et al. to remove heavy toxic metals from water in batch mode. Sips and Redlich-Peterson models were fitted with the experimental data, and these isotherms indicated a good performance to predict the adsorption equilibrium data (Rostamian et al., 2011).

Zinc chloride was used for chemical activation of an activated carbon, which was made from agricultural wastes, and this activated carbon was applied to adsorb MB dye at a fixed temperature. Three isotherm models were used to evaluate the equilibrium adsorption data, including Sips, Freundlich, and Langmuir isotherms, and the results showed that the Sips model represented the adsorption equilibrium data well (Ahmed and Dhedan, 2012).

For the adsorption of CO_2 at high pressures, two commercial activated carbons, modified by KOH and $ZnCl_2$, were used. Among the various isotherm models, Sips was the best isotherm model that offered the best consistency of experimental data fitting. (Sreńscek-Nazzal et al., 2015).

The potential of two kind of modified mesoporous alumina to remove fluoride ion (F^-) was evaluated in column and batch adsorption systems. Thermodynamic results showed the adsorption of F^- is endothermic and spontaneous. Moreover, Sips isotherm model fitted well with equilibrium experimental data (He et al., 2019). Piaçava fibers were used to adsorb the MB dye, and the results were fitted with various isotherms. Based on adsorption results, the piaçava fibers are appropriate adsorbents for removing MB dye from colored effluents. In this research, Elvoich model provided sufficient fit to experimental kinetic data, and also the Sips model predicted the equilibrium data properly (Marques et al., 2019).

The capacity of two commercial activated carbons for N_2, CH_4 and CO_2 adsorption was experimentally and theoretically tested by Ghalandari et al. In this research, the Sips isotherm was used to evaluate the equilibrium data and it was observed that it is an appropriate isotherm to predict the adsorption mechanism of high-pressure systems. Furthermore, the extended Sips model was used to predict the multi-component adsorption of three binary mixtures of CO_2/N_2, CH_4/N_2 and CO_2/CH_4 and its performance was effective (Ghalandari et al., 2020).

2.32. Smith isotherm model

The Smith adsorption isotherm was introduced by Smith in 1947 for estimating the water adsorption of some polymeric materials. He developed the model by using the results of the adsorption of water vapor onto the cellophane, nylon, and cotton materials and also compared the model with the BET model. The Smith equation properly model the sigmoid shape isotherms (Maleki Majd et al., 2013). The Smith isotherm model is expressed by Eq. (43) (Smith, 1947). The A_{ST} and B_{ST} define as the model constants.

$$q_e = A_{ST} + B_{ST}\, ln\,(1 - C_e) \tag{43}$$

A modification for the Smith isotherm was proposed by Nellist in 1974 based on the results from drying the grass seeds experiments and evaluating the adsorption/desorption behavior of material that considered the temperature in the model. The modified Smith equation is shown by Eq. (47) (A'_{ST}, B'_{ST} and C'_{ST} are model constants) (Bala and Woods, 1991; Nellist, 1974).

$$q_e = (A\prime_{ST} + B\prime_{ST} T) + C\prime_{ST}\, ln\,(1 - C_e) \tag{44}$$

The Smith isotherm and the Modified smith isotherm were generally applied for calculating the moisture adsorption/desorption of food materials. Some researchers reported that these models can successfully modeled the drying Pomegranate Arils, Canola (*Brassica napus* L.), Crambe grains materials (Cruz et al., 2017; Mundada and Hathan, 2012; Zare et al., 2011).

2.33. Temkin isotherm model

The adsorption process is assumed as a multi-layer process by the Temkin model that includes a factor, which clearly considers interactions between adsorbent and adsorbate (Temkin, 1940). The Temkin model ignores the very high and low amount of concentrations, and also it presumes that the differential adsorption heat could reduce linearly in the layer for entire molecules as a consequence of increment coverage (Aharoni and Ungarish, 1977) (Kim et al., 2004). Although the Temkin model is not appropriate to predict the liquid phase adsorption, which is complicated adsorption system, it is suitable to anticipate the gas phase adsorption. The Temkin model equation is expressed as follows (Krishni et al., 2014):

$$q_e = \frac{RT}{b_{TM}} \ln K_{TM} C_e \tag{45}$$

In this equation, b_{TM} and K_{TM} are constants of Temkin isotherm (b_{TM} is related to sorption heat). Hadi et al. used several two-parameter isotherms to predict the adsorption behavior of several acid dyes on Granular Activated Carbon. The finding indicated that the experimental data are better matched to the isotherms of Langmuir and the Temkin (Hadi et al., 2010).

Hu et al. synthesized the tragacanth gum-*graft*-polyamidoxime to make a significant adsorbent to eliminate metal ions, which existed in an aqueous medium. They found that the Temkin isotherm has appropriate performance to correlate the experimental data, and Co (II) was adsorbed more than Zn(II), Cr(III) and Cd(II) (Hu et al., 2011).

In a batch system, *Aspergillus niger* was used to remove Zn (II), Co (II) and Cd (II) from an aqueous medium, and the obtained data were used for multicomponent competitive isotherms. The result indicated that Temkin and Langmuir were the best isotherms, which demonstrated the biosorption data (Srivastava et al., 2015). To eliminate Pb(II) from aqueous systems, Lobeira fruit was used, and the results illustrated that it is a suitable adsorbent for this system. Furthermore, the Temkin isotherm was used to obtain the value of adsorption heat that demonstrates the ionic interaction does not exist between and Pb(II) and the lobeira fruit, and their interaction is maybe physical in nature (Araújo et al., 2018).

Paluri et al. used the zinc chloride to active the banana root to produce a biomass activated carbon capable of adequately adsorbing MB in an aqueous medium, appropriately. In order to achieve the optimal isotherm, the linear and non-linear equations of Temkin, Freundlich and Langmuir isotherms were fitted with the equilibrium data, and several various error functions were utilized. The finding showed that the nonlinear equations has better performance in terms of determination coefficient or functions of error, and the best model was Temkin isotherm (Paluri et al., 2020).

2.34. Toth isotherm model

Toth isotherm model was introduced in 1995 by scientist József Tóth as an empirical model based on quasi Gaussian energy distribution theory (Toth, 2002; Tóth, 1995). This model modifies the Langmuir model and improves the accuracy of predications by considering submonolayer coverage. The model is mainly used for gaseous systems with low and high range of substrates concentration on heterogeneous surfaces, while other models like Freundlich and Sips have limitations in high and low pressures. The Toth model has three parameters and is described by Eq. (46). In the Toth isotherm it is assumed that the major active sites for adsorption have lower energy the mean value.

$$q_e = \frac{q_{m,TO} C_e}{\left(K_{TO} + C_e^{z_{TO}}\right)^{1/z_{TO}}} \tag{46}$$

The $q_{m,\ TO}$ is defined as the maximum adsorption capacity (mg/g). The parameter K_{TO} is defined as a constant for the model and the z_{TO} is a dimensionless parameter that is known as Toth constant and represents the inhomogeneity of the adsorbent surface and usually has a quantity lower than 1. If the value of the z is equal to 1, the Toth model transforms to Langmuir model that shows a homogeneous adsorption were occurred.

Recently, researchers were imposed modification on the Toth model. In the work of (Forssén and Fornstedt, 2015) the effect of small perturbation on the Toth isotherm were investigated and (Serna-Guerrero and Sayari, 2010) separated the Toth equation model as two chemical and physical separate parts. Also some researchers rearranged the model for use in the aqueous solution systems and applied it for modeling of organic adsorption systems (Terzyk et al., 2003).

The Toth isotherm model showed a good representation for adsorption systems like hydrogen-activated carbon and carbon nanotube, chlorofluorocarbons-activated carbon and carbon dioxide- polymer composite systems(Feng et al., 2019; Rocky et al., 2019; Wilson et al., 2020). It also had applications in adsorption cooling systems (Ghazy et al., 2020).

2.35. Vieth-Sladek isotherm model

Vieth-Sladek isotherm model (Vieth and Sladek, 1965) includes two different sections to simultaneously compute both equilibrium solubilities and the diffusion rates through solid adsorbents from transient sorption. The initial section is expressed by means of a linear component (Henry's law) and the second part happens to be a non-linear component (Langmuir isotherm). The linear part illustrates the physisorption of gas particles over the amorphous adsorbent surfaces and the non-linear part describes the adherence of gas particles to the sites present on the surfaces of porous adsorbent. This model is shown as follows:

$$q_e = K_{VS} C_e + \frac{q_{m,VS} \beta_{VS} C_e}{1 + \beta_{VS} C_e} \tag{47}$$

where $q_{m,\ VS}$ indicates the maximum adsorption capacity and K_{VS} and β_{VS} show the Vieth–Sladek constants. This model is considered applicable widely not only in the measurement of diffusion through polymers but also in the quantification of effective gas diffusivities into porous catalysts(Vieth and Sladek, 1965).

Vargas et al. (2012) used ten isotherm models for fitting the experimental results of the adsorption of three commonly used food dyes including Acid Yellow 6 (AY-6), Acid Yellow 23 (AY-23), and Acid Red 18 (AR-18) on activated carbon developed from flamboyant pods and they concluded that the Vieth–Sladek isotherm was characterized as the most efficient model to define the adsorption process.

In another work, *Eucalyptus camaldulensis* bark/magnetite composite was employed as an inexpensive adsorbent for the Bisphenol-A removal (Balci and Erkurt, 2017). Between the applied adsorption isotherms, the best prediction of maximum adsorption capacity based on the experimental findings is attained by means of the Vieth–Sladek isotherm model. Additionally, for adsorbing As(III) and As(V) in the synthetic wastewater, Podder and Majumder (2016b)) used the granular activated carbon/$MnFe_2O_4$ composite. In their work, 30 different isotherm models were applied, and it was found that the Vieth–Sladek model is the most appropriate model to estimate the equilibrium adsorption behavior of As(III) and As(V). They came to the conclusion that the adsorption of both As(III) and As(V) follows the monolayer adsorption process and will not establish a multilayer onto the aforementioned composite. Furthermore, in another research, a nutraceutical industrial fennel seed spent adsorbent was applied for removing ethidium bromide (EtBr) out of an aqueous solution (Sulthana et al., 2018). By using nine isotherm models (including two- and three-parameter models) to analyze the equilibrium results, the Vieth-Sladek model was known to be a good match to the measurements.

2.36. Volmer isotherm model

The Volmer isotherm model, which is a distributed monolayer adsorption model, was developed according to the assumption stating adsorbed molecules can move on the adsorbent surfaces, but they do not have any interactions with each other. Its equation is presented as follows (Do, 1998; Volmer, 1925):

$$C_e = \frac{\theta_{VL}}{d_{VL}(1-\theta_{VL})} \, exp\left(\frac{\theta_{VL}}{1-\theta_{VL}}\right) \tag{48}$$

In which d_{VL} is the Volmer affinity constant and is dependent on the temperature, $\theta_{VL} = q_e/q_{m,\ VL}$ indicates the surface coverage degree ranging from zero to one. Also, the $\left[exp\left(\frac{\theta_{VL}}{1-\theta_{VL}}\right)\right]$ term in Volmer equation explains the adsorbed molecules' mobility.

Afonso et al. also obtained the Volmer equation by means of adsorption kinetics (Afonso et al., 2016). They calculated the rate of adsorption by using the kinetic gas theory, and the rate of desorption by considering desorption as an activated process having the activated energy equivalent to the heat of adsorption. Finally, by assuming that at adsorption equilibrium the rate of adsorption and the rate of desorption are equal, Volmer equation is acquired. Eddy et al. (2014) showed that *Gloriosa superba* gum could be a suitable adsorption inhibitor (through the mechanisms of physical and chemical adsorption) for the corrosion of Al in HCl solutions. They used several adsorption models to describe the adsorption behavior of *Gloriosa superba* gum; however, they utilized the fitness of Parsons, Flory-Huggins, and Volmer adsorption isotherm models to clarify the presence of interaction among the particles of inhibitor.

In another research, Davoudinejad and Ghorbanian (2013) derived three new isotherm models using Adsorption Effective Surface (AES) method by utilizing derivation of Langmuir isotherm in combination with Kiselev, Volmer, and Fowler-Guggenheim models. They studied the adsorption equilibrium isotherms of Benzene, Phenol, Toluene, Nitrobenzene, and Chlorobenzene from solutions on granular activated carbons and modeled the experimental data with AES models and other corresponding equations. One of their findings was that in high adsorption values the Volmer model, in comparison with Langmuir and AES models, offers better outcomes.

Furthermore, photocatalytic degradation of Direct Red 264 azo dye in typical wastewater with CdS and Ag/CdS nanophotocatalysts using UV-C and visible light irradiation was studied by Fard et al. (2016). Additionally, they analyzed the experimental isothermic results using Volmer isotherm model along with 18 other two-, three-, and four-parameter isotherm models.

2.37. Weber-Van Vliet isotherm model

Weber and Van Vliet proposed an empirical equation, which contains four parameters, and it can predict the action of adsorption for a vast range of systems. The following expression is used to indicate this isotherm (Van Vliet et al., 1980):

$$C_e = P_1\ q_e^{\left(P_2 q_e^{P_3} + P_4\right)} \tag{49}$$

The Weber-Van Vliet model parameters that can be specified by several nonlinear curve fitting approaches are P_1, P_2, P_3, and P_4 (Van Vliet et al., 1980; Vijayaraghavan, 2015) (Parker, 1995). Weber–van Vliet isotherm model was utilized to anticipate the equilibrium biosorption of silver on macrofungus *Pleurotus platypus*. The findings revealed that this adsorbent is capable of eliminating silver from aqueous phase as an efficient and inexpensive biosorbent (Das et al., 2010). One type of high surface activated carbons, which was made from cotton seeds, was used to adsorb the basic red 9 (BR9) from the aqueous medium. Several isotherm models, like Weber-van Vliet were employed to evaluate the adsorption system (Sivarajasekar and Baskar, 2014b).

Elmi Fard et al. demonstrated that Weber–Van Vliet and 5-parameter Fritz–Schlunder are the best isotherms to explain the equilibrium behavior of degradation of RB 255 dye with Ag/TiO_2 nanoparticles under light irradiation(Fard and Fazaeli, 2018). The capacity of blue-green marine algae (BGMA) to adsorb Ni(II) under batch condition was studied by Ramadoss et al. The experimental data indicated that BGMA is not a capable adsorbent to adsorb Ni(II), and the isotherm of the adsorption system is L-shaped. Weber–van Vliet, Marczewski–Jaroniec, and Baudu were tested to predict experimental data (Ramadoss and Subramaniam, 2019).

3. Industrial approach and optimization

As mentioned before, the adsorption isotherms play important role in industrial problems. In the following, some examples of applying the adsorption isotherms for industrial simulation and optimization purposes are described. In the work of Jareteg et al. an industrial temperature-swing adsorption process was numerically simulated using finite-volume method. The simulation was conducted for a fixed-bed activated carbon which applied for eliminating benzene from biomass-derived gases in an isothermal and steady conditions. They applied the nonlinear DR isotherm for mass transfer calculations and applied it for a cyclic adsorption/desorption sequence. Additionally, they mentioned that this isotherm can be successfully describe the non-linear behavior of such industrial systems (Jareteg et al., 2020a; Jareteg et al., 2020b).

In the research of Kuah et al. a multi-stage pressure vacuum swing adsorption was proposed for propane and polymer grade propylene gases. They applied 4A zeolite adsorbent for this purpose and the modified Langmuir isotherm was applied for simulating the adsorption units. They optimized their process economically based on an industrial feed at a 99.34% efficiency, and estimated that the proposed process can halve the production price of propylene in comparison with the conventional distillation method (Kuah et al., 2018).

Jafari et al. mathematically modeled the industrial natural gas dehydration unit using 3A zeolite to investigate the temperature effect on the regeneration process as well as the competing of different species. They utilized the Langmuir adsorption isotherm, performed a molecular simulation, and concluded that by lowering, the regeneration temperature the regeneration time of the adsorbent was reduced, which decreased the flaring gas considerably (Jafari et al., 2020).

The adsorption of ammonia from air was investigated and analyzed in the research of Cardenas et al. for designing and optimizing an industrial process. They considered the zinc sulphate-doped activated carbon as adsorbent and applied the Sips adsorption isotherm for predicting equilibrium data. They modeled the process by considering a fixed bed column structure and validated their model using industrial data. They proposed their model for industrial approaches of studying different operating conditions and optimization (Cardenas et al., 2021).

4. Conclusion

The importance of the adsorption process causes extraordinary endeavors for modeling the adsorption isotherms over the years. Numerous adsorption isotherms have been proposed and this path continues. Henry's isotherm, the most basic adsorption isotherm, is applicable for low concentrations of the adsorbate. Freundlich (the first proposed isotherm equation based on empirical results) and Langmuir (the first scientifically derived isotherm) are more complicated isotherms compared to Henry's isotherm, but they have limitations. So, every other model that has been proposed after them has tried to overcome the limitations of previous models. The Langmuir model is applicable for homogenous surface and ignores adsorbate/adsorbate interactions, where Freundlich, Harkins-Jura, Halsey, Dubinin–Radushkevich, Sips, Jossens, and Marczewski–Jaroniec and Toth models are appropriate for heterogeneous adsorption systems. BET, MET, Halsey, Harkins-Jura, Temkin, FHH and GAB are examples of isotherm models applied for multilayer adsorption. Our findings show that MET, Aronovich, Redlich–Peterson, Radke-Prausnitz, and Jossens models are more suitable isotherms that can be used in a wide range of adsorbate concentrations. Weber–van Vliet and Brouers_Sotolongo are the best fits for vast range of systems. In the case of mobile adsorption using Hil-De-Boer and Jovanovich are recommended.

The other achievement of this review which should be notified is that some isotherms are more appropriate for special adsorbate; for examples, Temkin, Kiselev, and Marczewski–Jaroniec, Vieth-Sladek, Baudu, Fritz-Schluender, Freundlich models are more suitable for heavy metals; Redlich–Peterson, Radke-Prausnitz, Jossens, and Weber–van Vliet, Frumkin, Khan, Vieth-Sladek, are best-fitted models for different dyes; BET, MET, Aronovich, Sips, Toth, Temkin, GAB are appropriate models for gaseous materials including CH_4, $CO_{2;}$ and FHH, GAB, Henderson, Oswin, Smith models are proper matches for water vapor.

CRediT authorship contribution statement

Mahdieh Mozaffari Majd: Conceptualization, Project administration, Writing – original draft, Writing – review & editing. **Vahid Kordzadeh-Kermani:** Writing – original draft, Writing – review & editing. **Vahab Ghalandari:** Conceptualization, Writing – original draft. **Anis Askari:** Writing – original draft. **Mika Sillanpää:** Supervision, Writing – review & editing.

Declaration of competing interest

The authors declare that they have no known competing financial interests or personal relationships that could have appeared to influence the work reported in this paper.

References

Calvert, J.G., 1990. Glossary of atmospheric chemistry terms (Recommendations 1990). Pure Appl. Chem. 62, 2167–2219.

Ahmad, R., Ali, Z., Khan, A.A., Rehman, N.U., 2020. Terbium extraction by functionalized surface: experimental and DFT approach. Adsorption 26, 117–125.

Majd, M.M., Dabbagh, H., Farrokhpour, H., Chermahini, A.N., 2017. Theoretical study on the adsorption and relative stability of conformers of l-ascorbic acid on γ-alumina (100) surface. J. Mol. Struct. 1147, 185–191.

Zhuang, S., Chen, R., Liu, Y., Wang, J., 2020. Magnetic COFs for the adsorptive removal of diclofenac and sulfamethazine from aqueous solution: adsorption kinetics, isotherms study and DFT calculation. J. Hazard. Mater. 385, 121596.

Karri, R.R., Sahu, J., 2018. Modeling and optimization by particle swarm embedded neural network for adsorption of zinc (II) by palm kernel shell based activated carbon from aqueous environment. J. Environ. Manag. 206, 178–191.

Karri, R.R., Sahu, J., Jayakumar, N., 2017. Optimal isotherm parameters for phenol adsorption from aqueous solutions onto coconut shell based activated carbon: error analysis of linear and non-linear methods. J. Taiwan Inst. Chem. Eng. 80, 472–487.

Aranovich, G., 1992. The theory of polymolecular adsorption. Langmuir 8, 736–739.

Do, D.D., 1998. Adsorption analysis: equilibria and kinetics (with cd containing computer MATLAB programs. World Scientific. Vol 2 Academic Press Inc.

Baudu, M., 1990. Etude des interactions solutes-fibres de charbon actif: applications et regeneration. Rennes 1.
Baudu, M., Le Cloirec, P., Martin, G., 1989. Modélisations des isothermes d'adsorption Sur charbon actif de composés aromatiques en solution aqueuse. Chem.Eng. J. 41, 81–89.
Wjihi, S., Peres, E.C., Dotto, G.L., Lamine, A.B., 2019. Physicochemical assessment of crystal violet adsorption on nanosilica through the infinity multilayer model and sites energy distribution. J. Mol. Liq. 280, 58–63.
Brouers, F., Sotolongo, O., Marquez, F., Pirard, J.P., 2005. Microporous and heterogeneous surface adsorption isotherms arising from levy distributions. Physica A: Statistical Mechanics and its Applications 349, 271–282.
Dubinin, M., Astakhov, V., 1971. Development of the concepts of volume filling of micropores in the adsorption of gases and vapors by microporous adsorbents. Bull. Acad. Sci. USSR, Div. Chem. Sci. 20, 8–12.
Dubinin, M., 1960. The potential theory of adsorption of gases and vapors for adsorbents with energetically nonuniform surfaces. Chem. Rev. 60, 235–241.
Flory, P.J., 1942. Thermodynamics of high polymer solutions. J. Chem. Phys. 10, 51–61.
Huggins, M.L., 1942. Some properties of solutions of long-chain compounds. J. Phys. Chem. 46, 151–158.
Fowler, R.H., 1939. Statistical thermodynamics. The University press, pp. 439–450.
Frenkel, J., 1946. Kinetic Theory of Liquids. Clarendon Press, Oxford.
Hill, T.L., 1952. Theory of physical adsorption. Advances in Catalysis. 4. Elsevier, pp. 211–258.
Freundlich, H., 1906. Over the adsorption in solution. J. Phys. Chem. 57, 1100–1107.
Fritz, W., Schluender, E.-U., 1974. Simultaneous adsorption equilibria of organic solutes in dilute aqueous solutions on activated carbon. Chem. Eng. Sci. 29, 1279–1282.
Ramadoss, R., Subramaniam, D., 2019. Removal of divalent nickel from aqueous solution using blue-green marine algae: adsorption modeling and applicability of various isotherm models. Sep. Sci. Technol. 54, 943–961.
Frumkin, A., 1925a. The capillary curve of higher fatty acids and the constitutive equation of the surface layer. Zeit Fur Phy Chem Stoch Und Ver 116, 466–484.
Grchev, T., Cvetkovska, M., Stafilov, T., Schultze, J., 1991. Adsorption of polyacrylamide on gold and iron from acidic aqueous solutions. Electrochim. Acta 36, 1315–1323.
Anderson, R.B., 1946. Modifications of the brunauer, Emmett and Teller equation1. J. Am. Chem. Soc. 68, 686–691.
De Boer, J., 1953. The Dynamic Character of Adsorption. Oxford University Press, Oxford.
Guggenheim, E.A., 1966. Applications of Statistical Mechanics. Clarendon Press., pp. 80–85.
Zou, L., Gong, L., Xu, P., Feng, G., Liu, H., 2016. Modified GAB model for correlating multilayer adsorption equilibrium data. Sep. Purif. Technol. 161, 38–43.
Halsey, G., 1948. Physical adsorption on non-uniform surfaces. J. Chem. Phys. 16, 931–937.
Harkins, W.D., Jura, G., 1944. Surfaces of solids. XIII. A vapor adsorption method for the determination of the area of a solid without the assumption of a molecular area, and the areas occupied by nitrogen and other molecules on the surface of a solid. J. Am. Chem. Soc. 66, 1366–1373.
Henderson, S.M., 1970. Equilibrium moisture content of small grain-hysteresis. Trans. ASAE 13, 0762–0764.
Mehta, S., Singh, A., 2006. Adsorption isotherms for red chilli (Capsicum annum L.). Eur. Food Res. Technol. 223, 849–852.
Erbil, H.Y., 2006. Surface Chemistry of Solid and Liquid Interfaces. Blackwell Pub, Oxford eMAMalden MA.
Hill, T.L., 1946. Statistical mechanics of multimolecular adsorption II. Localized and mobile adsorption and absorption. J. Chem. Phys. 14, 441–453.
Hill, A.V., 1910. The possible effects of the aggregation of the molecules of haemoglobin on its dissociation curves. . Physiol. 40, 4–7.
Jossens, L., Prausnitz, J., Fritz, W., Schlünder, E., Myers, A., 1978. Thermodynamics of multi-solute adsorption from dilute aqueous solutions. Chem. Eng. Sci. 33, 1097–1106.
Jovanović, D., 1969. Physical adsorption of gases. Kolloid-Zeitschrift und Zeitschrift für Polymere 235, 1214–1225.
Khan, A., Ataullah, R., Al-Haddad, A., 1997. Equilibrium adsorption studies of some aromatic pollutants from dilute aqueous solutions on activated carbon at different temperatures. J. Colloid Interface Sci. 194, 154–165.
Khan, A.R., Al-Waheab, I., Al-Haddad, A., 1996. A generalized equation for adsorption isotherms for multi-component organic pollutants in dilute aqueous solution. Environ. Technol. 17, 13–23.
Kiselev, A., 1958. Vapor adsorption in the formation of adsorbate molecule complexes on the surface. Kolloid Zhur 20, 338–348.
Koble, R.A., Corrigan, T.E., 1952. Adsorption isotherms for pure hydrocarbons. Ind. Eng. Chem. 44, 383–387.
Langmuir, I., 1918. The adsorption of gases on plane surfaces of glass, mica and platinum. J. Am. Chem. Soc. 40, 1361–1403.
McMillan, W., Teller, E., 1951. The assumptions of the BET theory. J. Phys. Chem. 55, 17–20.
Derylo-Marczewska, A., Jaroniec, M., 1987. Adsorption of organic solutes from dilute solutions on solids. Surf. Colloid Sci. 14, 301.
Oswin, C.R., 1946. The kinetics of package life. III. The isotherm. J. Soc. Chem.Ind. 65, 419–421.
Chen, C.-C., 1990. Modification of Oswin EMC/ERH equation. Journal of Agricultural Research of China 367–376.
Radke, C., Prausnitz, J., 1972. Adsorption of organic solutes from dilute aqueous solution of activated carbon. Ind. Eng. Chem. Fundamentals 11, 445–451.
Redlich, O., Peterson, D.L., 1959. A useful adsorption isotherm. J. Phys. Chem. 63, 1024.
Sips, R., 1948. On the structure of a catalyst surface. J. Chem. Phys. 16, 490–495.
Smith, S.E., 1947. The sorption of water vapor by high polymers. J. Am. Chem. Soc. 69, 646–651.
Bala, B.K., Woods, J.L., 1991. Physical and thermal properties of malt. Dry. Technol. 9, 1091–1104.
Nellist, M.E., 1974. The Drying of Ryegrass Seeds in Deep Layers.
Temkin, M., 1940. Kinetics of ammonia synthesis on promoted iron catalysts. Acta Physiochim. URSS 12, 327–356.
Toth, J., 2002. Adsorption Theory, Modeling and Analysis.
Tóth, J., 1995. Uniform interpretation of gas/solid adsorption. Advances in Colloid and Interface Science. 55. Elsevier, pp. 1–239.
Vieth, W.R., Sladek, K., 1965. A model for diffusion in a glassy polymer. J. Colloid Sci. 20, 1014–1033.
Volmer, M., 1925. Thermodynamische folgerungen ans der zustandsgleichung für adsorbierte stoffe. Z. Phys. Chem. 115, 253–260.
Van Vliet, B., Weber Jr., W.J., Hozumi, H., 1980. Modeling and prediction of specific compound adsorption by activated carbon and synthetic adsorbents. Water Res. 14, 1719–1728.
Szatanik-Kloc, A., Horn, R., Lipiec, J., Siczek, A., Szerement, J., 2018. Soil compaction-induced changes of physicochemical properties of cereal roots. Soil Tillage Res. 175, 226–233.
Belyaeva, O.V., Krasnova, T.A., 2016. Adsorption of benzene and pyridine vapors by various carbon adsorbents. Sci. Evol. 3–7.
Humpola, P.D., Odetti, H.S., Flores, E.S., Vicente, J.L., 2013. Description of different solid adsorbent surfaces adsorption mechanisms based on a sequential decomposition of isotherms. Surf. Rev. Lett. 20, 1350022.
Saadi, R., Saadi, Z., Fazaeli, R., Fard, N.E., 2015. Monolayer and multilayer adsorption isotherm models for sorption from aqueous media. Korean J. Chem. Eng. 32, 787–799.
Svilović, S., Mužek, M.N., Nuić, I., Vučenović, P., 2019. Taguchi design of optimum process parameters for sorption of copper ions using different sorbents. Water Sci. Technol. 80, 98–108.
Syafiuddin, A., Salmiati, S., Jonbi, J., Fulazzaky, M.A., 2018. Application of the kinetic and isotherm models for better understanding of the behaviors of silver nanoparticles adsorption onto different adsorbents. J. Environ. Manag. 218, 59–70.
Hamdaoui, O., Naffrechoux, E., 2007. Modeling of adsorption isotherms of phenol and chlorophenols onto granular activated carbon: part II. Models with more than two parameters. J. Hazard. Mater. 147, 401–411.
Brunauer, S., Emmett, P.H., Teller, E., 1938. Adsorption of gases in multimolecular layers. J. Am. Chem. Soc. 60, 309–319.
Khalfaoui, M., Knani, S., Hachicha, M., Lamine, A.B., 2003. New theoretical expressions for the five adsorption type isotherms classified by BET based on statistical physics treatment. J. Colloid Interface Sci. 263, 350–356.
Ebadi, A., Mohammadzadeh, J.S.S., Khudiev, A., 2009. What is the correct form of BET isotherm for modeling liquid phase adsorption? Adsorption 15, 65–73.
Park, M.H., Jeong, S., Kim, J.Y., 2019. Adsorption of NH3-N onto rice straw-derived biochar. J. Environ. Chem. Eng. 7, 103039.
Szałaj, U., Świderska-Środa, A., Chodara, A., Gierlotka, S., Łojkowski, W., 2019. Nanoparticle size effect on water vapour adsorption by hydroxyapatite. Nanomaterials 9, 1005.
Yu, W., Wu, K., Sepehrnoori, K., 2016b. A semianalytical model for production simulation from nonplanar hydraulic-fracture geometry in tight oil reservoirs. SPE J. 21, 1028–1040.
Ladavos, A., Katsoulidis, A., Iosifidis, A., Triantafyllidis, K., Pinnavaia, T., Pomonis, P., 2012. The BET equation, the inflection points of N2 adsorption isotherms and the estimation of specific surface area of porous solids. Microporous Mesoporous Mater. 151, 126–133.
Unuabonah, E.I., Agunbiade, F.O., Alfred, M.O., Adewumi, T.A., Okoli, C.P., Omorogie, M.O., et al., 2017. Facile synthesis of new amino-functionalized agrogenic hybrid composite clay adsorbents for phosphate capture and recovery from water. J. Clean. Prod. 164, 652–663.
Selmi, T., Seffen, M., Sammouda, H., Mathieu, S., Jagiello, J., Celzard, A., et al., 2018. Physical meaning of the parameters used in fractal kinetic and generalised adsorption models of brouers-sotolongo. Adsorption 24, 11–27.
Vargas, A.M., Cazetta, A.L., Kunita, M.H., Silva, T.L., Almeida, V.C., 2011. Adsorption of methylene blue on activated carbon produced from flamboyant pods (Delonix regia): study of adsorption isotherms and kinetic models. Chem. Eng. J. 168, 722–730.
Burevski, D., 1982. The application of the dubinin-astakhov equation to the characterization of microporous carbons. Colloid Polym. Sci. 260, 623–627.
Ross, D.L., Riley, C.M., 1990. Aqueous solubilities of some variously substituted quinolone antimicrobials. Int. J. Pharm. 63, 237–250.
Yan, B., Niu, C.H., 2018. Adsorption behavior of norfloxacin and site energy distribution based on the dubinin-astakhov isotherm. Sci. Total Environ. 631, 1525–1533.
Singh, V.K., Kumar, E.A., 2016. Measurement and analysis of adsorption isotherms of CO2 on activated carbon. Appl. Therm. Eng. 97, 77–86.
Cheng, P., Hu, Y.H., 2016. Dubinin-astakhov model for acetylene adsorption on metal-organic frameworks. Appl. Surf. Sci. 377, 349–354.
Singh, V.K., Kumar, E.A., Saha, B.B., 2018. Adsorption isotherms, kinetics and thermodynamic simulation of CO2-CSAC pair for cooling application. Energy 160, 1158–1173.
Dhaneswara, D., Siti Agustina, A., Dewantoro Adhy, P., Delayori, F., Fatriansyah, J.F., 2018. The Effect of Pluronic 123 Surfactant concentration on The N 2 Adsorption Capacity of Mesoporous Silica SBA-15: Dubinin-Astakhov Adsorption Isotherm Analysis. Journal of Physics: Conference Series1011. IOP Publishing Ltd, p. 012017.
Hu, Q., Zhang, Z., 2019. Application of dubinin-radushkevich isotherm model at the solid/solution interface: a theoretical analysis. J. Mol. Liq. 277, 646–648.
Alberti, G., Amendola, V., Pesavento, M., Biesuz, R., 2012. Beyond the synthesis of novel solid phases: review on modelling of sorption phenomena. Coord. Chem. Rev. 256, 28–45.
Abdelnaeim, M.Y., El Sherif, I.Y., Attia, A.A., Fathy, N.A., El-Shahat, M., 2016. Impact of chemical activation on the adsorption performance of common reed towards Cu (II) and Cd (II). Int. J. Miner. Process. 157, 80–88.

Elmoubarki, R., Mahjoubi, F., Tounsadi, H., Moustadraf, J., Abdennouri, M., Zouhri, A., et al., 2015. Adsorption of textile dyes on raw and decanted Moroccan clays: kinetics, equilibrium and thermodynamics. Water Resour. Ind. 9, 16–29.

Raganati, F., Alfe, M., Gargiulo, V., Chirone, R., Ammendola, P., 2018. Isotherms and thermodynamics of CO2 adsorption on a novel carbon-magnetite composite sorbent. Chem. Eng. Res. Des. 134, 540–552.

Inyinbor, A.A., Adekola, F.A., Dada, O.A., Oluyori, A.P., Olatunji, G.A., Fanawopo, O.F., et al., 2019. Novel acid treated biomass: applications in Cu2+ scavenging, rhodamine B/Cu2+ binary solution and real textile effluent treatment. Environ. Technol. Innov. 13, 37–47.

Senichev, V.Y., Tereshatov, V.V., 2014. Simple solvent characteristics. Elsevier, pp. 117–149.

Augustus, E.N., Samuel, A.S., Nimibofa, A., Donbebe, W., 2017. Removal of Congo red from aqueous solutions using fly ash modified with hydrochloric acid. <span/>Curr. J.Appl. Sci. Technol 1–7.

Vijayaraghavan, K., Padmesh, T., Palanivelu, K., Velan, M., 2006. Biosorption of nickel (II) ions onto Sargassum wightii: application of two-parameter and three-parameter isotherm models. J. Hazard. Mater. 133, 304–308.

Pillai, M.G., Simha, P., Gugalia, A., 2014. Recovering urea from human urine by bio-sorption onto microwave activated carbonized coconut shells: equilibrium, kinetics, optimization and field studies. J. Environ. Chem. Eng. 2, 46–55.

Shafique, U., Ijaz, A., Salman, M., Uz Zaman, W., Jamil, N., Rehman, R., et al., 2012. Removal of arsenic from water using pine leaves. Journal of the Taiwan Institute of Chemical Engineers 43, 256–263.

Okeniyi, J.O., Loto, C.A., Popoola, A.P., 2014. Electrochemical performance of Phyllanthus muellerianus on the corrosion of concrete steel-reinforcement in industrial/microbial simulating-environment. Port. Electrochim. Acta 32, 199–211.

Brancher, R.D., Stefanov, S., Graur, I., Frezzotti, A., 2019. Kinetic theory description of gas adsorption-desorption on a solid surface. AIP Conference Proceedings. 2132. AIP Publishing LLC, p. 170003.

Mbaye, M.T., Maiga, S.M., Gatica, S.M., 2016. Commensurate phases of kr adsorbed on single-walled carbon nanotubes. J. Low Temp. Phys. 185, 129–137.

Liu, L., Luo, X.-B., Ding, L., Luo, S.-L., 2019a. Application of nanotechnology in the removal of heavy metal from water. Nanomaterials for the Removal of Pollutants and Resource Reutilization. Elsevier, pp. 83–147.

Jeyavishnu, K., Alagesan, V., 2020. Cereus sp. As potential biosorbent for removal of Congo red from aqueous solution: isotherm and kinetic investigations. Environ. Monit. Assess. 192, 1–15.

Ricci, E., Passerone, A., Joud, J., 1988. Thermodynamic study of adsorption in liquid metal-oxygen systems. Surf. Sci. 206, 533–553.

Wu, L., Tang, J., Zhang, S., Wang, J., Ding, X., 2019. Using recycled concrete as an adsorbent to remove phosphate from polluted water. J. Environ. Qual. 48, 1489–1497.

Dada, A.O., Adekola, F.A., Odebunmi, E.O., Dada, F.E., Bello, O.M., Akinyemi, B.A., et al., 2020. Sustainable and low-cost Ocimum gratissimum for biosorption of indigo carmine dye: kinetics, isotherm, and thermodynamic studies. Int. J. Phytoremed. 22, 1524–1537.

Prediger, P., Cheminski, T., de Figueiredo, Neves T., Nunes, W.B., Sabino, L., Picone, C.S.F., et al., 2018. Graphene oxide nanomaterials for the removal of non-ionic surfactant from water. J. Environ. Chem. Eng. 6, 1536–1545.

Hung, H.-M., Wang, K.-C., Chen, J.-P., 2015. Adsorption of nitrogen and water vapor by insoluble particles and the implication on cloud condensation nuclei activity. J. Aerosol Sci. 86, 24–31.

Liu, X., Nie, B., 2016. Fractal characteristics of coal samples utilizing image analysis and gas adsorption. Fuel 182, 314–322.

Mittal, H., Al Alili, A., Alhassan, S.M., 2020. Adsorption isotherm and kinetics of water vapors on novel superporous hydrogel composites. Microporous Mesoporous Mater. 299, 110106.

Hallajiqomi, M., Eisazadeh, H., 2017. Adsorption of manganese ion using polyaniline and it's nanocomposite: kinetics and isotherm studies. J. Ind. Eng. Chem. 55, 191–197.

Jarrah, N., 2017. Competitive adsorption isotherms of rhodium 6G and methylene blue on activated carbon prepared from residual fuel oil. J. Environ. Chem. Eng. 5, 4319–4326.

Nanta, P., Kasemwong, K., Skolpap, W., 2018. Isotherm and kinetic modeling on superparamagnetic nanoparticles adsorption of polysaccharide. J. Environ. Chem. Eng. 6, 794–802.

Kim, Y.-S., Kim, J.-H., 2019. Isotherm, kinetic and thermodynamic studies on the adsorption of paclitaxel onto sylopute. J. Chem. Thermodyn. 130, 104–113.

Selim, A.Q., Mohamed, E.A., Mobarak, M., Zayed, A.M., Seliem, M.K., Komarneni, S., 2018. Cr (VI) uptake by a composite of processed diatomite with MCM-41: isotherm, kinetic and thermodynamic studies. Microporous Mesoporous Mater. 260, 84–92.

Nebaghe, K., El Boundati, Y., Ziat, K., Naji, A., Rghioui, L., Saidi, M., 2016. Comparison of linear and non-linear method for determination of optimum equilibrium isotherm for adsorption of copper (II) onto treated Martil sand. Fluid Phase Equilib. 430, 188–194.

Zarei, S., Niad, M., 2020. The isotherm, kinetic and thermodynamic studies of the cadmium uptake by colpomenia sinuosa. Sep. Sci. Technol. 55, 257–265.

Zheng, L., Yang, Y., Meng, P., Peng, D., 2019. Absorption of cadmium (II) via sulfur-chelating based cellulose: characterization, isotherm models and their error analysis. Carbohydr. Polym. 209, 38–50.

Frumkin, A., 1925b. Electrocapillary curve of higher aliphatic acids and the state equation of the surface layer. Z. Phys. Chem. 116, 466–470.

Sharma, S.K., Mudhoo, A., Jain, G., Sharma, J., 2010. Corrosion inhibition and adsorption properties of Azadirachta indica mature leaves extract as green inhibitor for mild steel in HNO3. Green Chem. Lett. Rev. 3, 7–15.

Narvekar, A.A., Fernandes, J., Tilve, S., 2018. Adsorption behavior of methylene blue on glycerol based carbon materials. J. Environ. Chem. Eng. 6, 1714–1725.

Souza, M.A., de Oliveira, K.V., Oliveira, F.C., Silva, L.P., Rubim, J.C., 2018. The adsorption of methamphetamine on ag nanoparticles dispersed in agarose gel–detection of methamphetamine in fingerprints by SERS. Vib. Spectrosc. 98, 152–157.

Kumar, A., Mandal, A., 2019. Critical investigation of zwitterionic surfactant for enhanced oil recovery from both sandstone and carbonate reservoirs: adsorption, wettability alteration and imbibition studies. Chem. Eng. Sci. 209, 115222.

Timmermann, E.O., 2003. Multilayer sorption parameters: BET or GAB values? Colloids Surf. A Physicochem. Eng. Asp. 220, 235–260.

CVD, Berg, 1981. Vapour sorption equilibria and other water-starch interactions: a physico-chemical approach.

Maroulis, Z.B., Tsami, E., Marinos-Kouris, D., Saravacos, G.D., 1988. Application of the GAB model to the moisture sorption isotherms for dried fruits. J. Food Eng. 7, 63–78.

Oluwamukomi, M.O., 2009. Adsorption isotherm modeling of soy-melon-enriched and un-enriched 'gari' using GAB equation. Afr. J. Food Sci. 3, 117–124.

San Martin, M.B., Mate, J.I., Fernandez, T., Virseda, P., 2001. Modelling adsorption equilibrium moisture characteristics of rough rice. Dry. Technol. 19, 681–690.

Moradi, O., 2016. Applicability comparison of different models for ammonium ion adsorption by multi-walled carbon nanotube. Arab. J. Chem. 9, S1170–S1176.

Omotunde, I., Okoronkwo, A., Oluwashina, O., 2018. Derived and thiourea-functionalized silica for cadmium removal: isotherm, kinetic and thermodynamic studies. Appl. Water Sci. 8, 1–13.

Saad, M., Tahir, H., Ali, D., 2017. Green synthesis of Ag-Cr-AC nanocomposites by Azadirachta indica and its application for the simultaneous removal of binary mixture of dyes by ultrasonicated assisted adsorption process using response surface methodology. Ultrason. Sonochem. 38, 197–213.

Karakuş, S., Taşaltın, N., Taşaltın, C., Kilislioğlu, A., 2020. Comparative study on ultrasonic assisted adsorption of basic blue 3, basic yellow 28 and acid red 336 dyes onto hydromagnesite stromatolite: kinetic, isotherm and error analysis. Surf. Interfaces 20, 100528.

Thompson, T.L., Peart, R.M., Foster, G.H., 1968. Mathematical simulation of corn drying–a new model. Trans. ASAE 24, 573–580.

Hawa, L.C., Ubaidillah, U., Damayanti, R., Hendrawan, Y., 2020. Moisture sorption isotherms of modified cassava flour during drying and storage. Heat and Mass Transfer/Waerme- und Stoffuebertragung 56, 2389–2396.

Stępień, A., Witczak, M., Witczak, T., 2020. Moisture sorption characteristics of food powders containing freeze dried avocado, maltodextrin and inulin. Int. J. Biol. Macromol. 149, 256–261.

Chawla, C., Kaur, D., Oberoi, D.P.S., Sogi, D.S., 2008. Drying characteristics, sorption isotherms, and lycopene retention of tomato pulp. Dry. Technol. 26, 1257–1264.

Corrêa et al., n.d. PC Corrêa M Fagundes T Reis GH Horta De Oliveira A Paula L Rodrigues De Oliveira et al Moisture Desorption Isotherms of Cucumber Seeds: Modeling and Thermodynamic Properties 1. SciELO Brasil.

Poursaeidesfahani, A., Andres-Garcia, E., de Lange, M., Torres-Knoop, A., Rigutto, M., Nair, N., et al., 2019. Prediction of adsorption isotherms from breakthrough curves. Microporous Mesoporous Mater. 277, 237–244.

Soukup, K., Hejtmánek, V., Cruz, G.J., Jandová, V., Solcova, O., 2017. Excess adsorption isotherms of hydrogen on activated carbons from agricultural waste materials. Chem. Eng. Technol. 40, 900–906.

Vidoca, L.P., de Almeida, E.S., Cardoso, M.F., Otavio, L., Valadares, L.F., Monteiro, S., 2020. Extraction of carotene from crude hybrid palm oil using polymeric resin. J. Food Eng. 278, 109944.

Koopal, L., Van Riemsdijk, W., De Wit, J., Benedetti, M., 1994. Analytical isotherm equations for multicomponent adsorption to heterogeneous surfaces. J. Colloid Interface Sci. 166, 51–60.

Karoui, S., Arfi, R.B., Mougin, K., Ghorbal, A., Assadi, A.A., Amrane, A., 2020. Synthesis of novel biocomposite powder for simultaneous removal of hazardous ciprofloxacin and methylene blue: central composite design, kinetic and isotherm studies using brouers-sotolongo family models. J. Hazard. Mater. 387, 121675.

Makhlouf, C., Ladhari, N., Braham, D., Roudesli, S., Sakly, F., 2015. The effect of hot water setting treatment on the dyeing properties of grafted polyamide 6.6 microfibres. J. Text. Inst. 106, 986–994.

Bayuo, J., Abukari, M.A., Pelig-Ba, K.B., 2020. Optimization using central composite design (CCD) of response surface methodology (RSM) for biosorption of hexavalent chromium from aqueous media. Appl. Water Sci. 10, 1–12.

Aly-Eldeen, M.A., El-Sayed, A.A., Salem, D.M., El Zokm, G.M., 2018. The uptake of eriochrome black T dye from aqueous solutions utilizing waste activated sludge: adsorption process optimization using factorial design. Egypt. J. Aquat. Res. 44, 179–186.

Ghaleh, S.P., Khodapanah, E., Tabatabaei-Nezhad, S.A., 2020. Comprehensive monolayer two-parameter isotherm and kinetic studies of thiamine adsorption on clay minerals: experimental and modeling approaches. J. Mol. Liq. 306, 112942.

Munagapati, V.S., Wen, J.-C., Pan, C.-L., Gutha, Y., Wen, J.-H., 2019. Enhanced adsorption performance of reactive red 120 azo dye from aqueous solution using quaternary amine modified orange peel powder. J. Mol. Liq. 285, 375–385.

Bilgili, M.S., Varank, G., Sekman, E., Top, S., Özçimen, D., 2012. Modeling 4-chlorophenol removal from aqueous solutions by granular activated carbon. Environ. Model. Assess. 17, 289–300.

Wakkel, M., Khiari, B., Zagrouba, F., 2019. Textile wastewater treatment by agro-industrial waste: equilibrium modelling, thermodynamics and mass transfer mechanisms of cationic dyes adsorption onto low-cost lignocellulosic adsorbent. J. Taiwan Inst. Chem. Eng. 96, 439–452.

Fil, B.A., Bayar, S., Boncukcuoglu, R., Yilmaz, A.E., 2012. Adsorption kinetics and isotherms for the removal of zinc ions from aqueous solutions by an ion-exchange resin. Journal of the Chemical Society of Pakistan 34, 841.

Marczewski, A.W., 2011. Extension of langmuir kinetics in dilute solutions to include lateral interactions according to regular solution theory and the kiselev association model. J. Colloid Interface Sci. 361, 603–611.

Yousef, N., Farouq, R., Hazzaa, R., 2016. Adsorption kinetics and isotherms for the removal of nickel ions from aqueous solutions by an ion-exchange resin: application of two and three parameter isotherm models. Desalin. Water Treat. 57, 21925–21938.
Alahmadi, S., Mohamad, S., Maah, M.J., 2014. Comparative study of tributyltin adsorption onto mesoporous silica functionalized with calix [4] arene, p-tert-butylcalix [4] arene and p-sulfonatocalix [4] arene. Molecules 19, 4524–4547.
Hamidpour, M., Kalbasi, M., Afyuni, M., Shariatmadari, H., Furrer, G., 2011. Sorption of lead on iranian bentonite and zeolite: kinetics and isotherms. Environ. Earth Sci. 62, 559–568.
Han, X., Wang, W., Ma, X., 2011. Adsorption characteristics of methylene blue onto low cost biomass material lotus leaf. Chem. Eng. J. 171, 1–8.
Wang, L.-G., Yan, G.-B., 2011. Adsorptive removal of direct yellow 161dye from aqueous solution using bamboo charcoals activated with different chemicals. Desalination 274, 81–90.
Liu, X., Wan, Y., Liu, P., Zhao, L., Zou, W., 2019b. Optimization of sulfamethazine sodium adsorption onto activated carbon-based Salix psammophila: investigation of adsorption behavior and mechanism. J. Dispers. Sci. Technol. 40, 507–518.
Langmuir, I., 1916. The constitution and fundamental properties of solids and liquids. Part I. Solids. Journal of the American chemical society 38, 2221–2295.
Chanzu, H.A., Onyari, J.M., Shiundu, P.M., 2019. Brewers' spent grain in adsorption of aqueous Congo red and malachite green dyes: batch and continuous flow systems. J. Hazard. Mater. 380, 120897.
Mohammed, B.B., Yamni, K., Tijani, N., Alrashdi, A.A., Zouihri, H., Dehmani, Y., et al., 2019. Adsorptive removal of phenol using faujasite-type Y zeolite: adsorption isotherms, kinetics and grand canonical Monte Carlo simulation studies. J. Mol. Liq. 296, 111997.
Alsuhybani, M., Alshahrani, A., Algamdi, M., Al-Kahtani, A.A., Alqadami, A.A., 2020. Highly efficient removal of pb (II) from aqueous systems using a new nanocomposite: adsorption, isotherm, kinetic and mechanism studies. J. Mol. Liq. 301, 112393.
Sawant, S.V., Banerjee, S., Patwardhan, A.W., Joshi, J.B., Dasgupta, K., 2019. Effect of in-situ boron doping on hydrogen adsorption properties of carbon nanotubes. Int. J. Hydrog. Energy 44, 18193–18204.
Soltani, R., Marjani, A., Shirazian, S., 2019. Facile one-pot synthesis of thiol-functionalized mesoporous silica submicrospheres for tl (I) adsorption: isotherm, kinetic and thermodynamic studies. J. Hazard. Mater. 371, 146–155.
Ghanei, M., Rashidi, A., Tayebi, H.-A., Yazdanshenas, M.E., 2018. Removal of acid blue 25 from aqueous media by magnetic-SBA-15/CPAA super adsorbent: adsorption isotherm, kinetic, and thermodynamic studies. J. Chem. Eng. Data 63, 3592–3605.
Wang, X., Jiang, C., Hou, B., Wang, Y., Hao, C., Wu, J., 2018. Carbon composite lignin-based adsorbents for the adsorption of dyes. Chemosphere 206, 587–596.
Ahsaine, H.A., Zbair, M., Anfar, Z., Naciri, Y., El Alem, N., Ezahri, M., 2018. Cationic dyes adsorption onto high surface area 'almond shell'activated carbon: kinetics, equilibrium isotherms and surface statistical modeling. Mater. Today Chem. 8, 121–132.
Mercado-Borrayo, B., Schouwenaars, R., Litter, M., Montoya-Bautista, C., Ramírez-Zamora, R., 2014a. Metallurgical slag as an efficient and economical adsorbent of arsenic. Water reclamation and sustainability. Elsevier 95–114.
Mercado-Borrayo, B., Schouwenaars, R., Litter, M., Ramirez-Zamora, R., 2014b. Adsorption of boron by metallurgical slag and iron nanoparticles. Adsorp. Sci. Technol. 32, 117–123.
Rezakazemi, M., Shirazian, S., 2019. Lignin-chitosan blend for methylene blue removal: adsorption modeling. J. Mol. Liq. 274, 778–791.
Jhider, N., Bagané, M., 2019. Moisture sorption isotherms and isosteric heat of sorption of tunisian clay product. Heat Mass Transf. 55, 571–579.
Bogoeva, A.L., Durakova, A.G., 2020. Sorption characteristics of full-fatted grape seeds flour of bulgarian origin. J. Agric. Food Res. 2, 100026.
Getahun, E., Gabbiye, N., Delele, M.A., Fanta, S.W., Gebrehiwot, M.G., Vanierschot, M., 2020. Effect of maturity on the moisture sorption isotherm of chili pepper (Mareko fana variety). Heliyon 6, e04608.
Henrique Horta de Oliveira, G., Paula Lelis Rodrigues de Oliveira, A., Vinicius Corrêa de Souza, M., Felipe Neves, R., Mendes Botelho, F., de Carvalho Campos Botelho, S., 2020. Water adsorption isotherms of coffee blends. BrazilianJournal of Development 4, 20988–20997.
Subramanyam, B., Ashutosh, D., 2012. Adsorption isotherm modeling of phenol onto natural soils–applicability of various isotherm models. Int. J. Environ. Res. 6, 265–276.
Ravnote, O.M., Adsorpcijo, N.I.Z., 2013. Evaluation of equilibrium isotherm models for the adsorption of cu and ni from wastewater on bentonite clay. Mater. Tehnol. 47, 481–486.
Goshadrou, A., Moheb, A., 2011. Continuous fixed bed adsorption of CI acid blue 92 by exfoliated graphite: an experimental and modeling study. Desalination 269, 170–176.
Sarici-Özdemir, Ç., Önal, Y., 2014. Error anlaysis studies of dye adsorption onto activated carbon from aqueous solutions. Part. Sci. Technol. 32, 20–27.
Rafati, L., Ehrampoush, M., Rafati, A., Mokhtari, M., Mahvi, A., 2018. Removal of ibuprofen from aqueous solution by functionalized strong nano-clay composite adsorbent: kinetic and equilibrium isotherm studies. Int. J. Environ. Sci. Technol. 15, 513–524.
Şahin, S., SaS, Bayazit, 2020. Recovery of β-carotene on graphene nanoplatelets UiO-66 nanocomposites. J. Chem. Eng. Data 65, 821–827.
Prasad, R.K., Srivastava, S., 2009. Sorption of distillery spent wash onto fly ash: kinetics and mass transfer studies. Chem. Eng. J. 146, 90–97.
Ng, J., Cheung, W., McKay, G., 2002. Equilibrium studies of the sorption of cu (II) ions onto chitosan. J. Colloid Interface Sci. 255, 64–74.
Wu, F.-C., Liu, B.-L., Wu, K.-T., Tseng, R.-L., 2010. A new linear form analysis of redlich-Peterson isotherm equation for the adsorptions of dyes. Chem. Eng. J. 162, 21–27.
Kumar, K.V., de Castro, M.M., Martinez-Escandell, M., Molina-Sabio, M., Silvestre-Albero, J., Rodriguez-Reinoso, F., 2010a. A continuous site energy distribution function from redlich-Peterson isotherm for adsorption on heterogeneous surfaces. Chem. Phys. Lett. 492, 187–192.
Brdar, M., Šćiban, M., Takači, A., Došenović, T., 2012. Comparison of two and three parameters adsorption isotherm for Cr (VI) onto Kraft lignin. Chem. Eng. J. 183, 108–111.
Açıkyıldız, M., Gürses, A., Güneş, K., Yalvaç, D., 2015. A comparative examination of the adsorption mechanism of an anionic textile dye (RBY 3GL) onto the powdered activated carbon (PAC) using various the isotherm models and kinetics equations with linear and non-linear methods. Appl. Surf. Sci. 354, 279–284.
Nakhjiri, M.T., Marandi, G.B., Kurdtabar, M., 2018. Poly (AA-co-VPA) hydrogel cross-linked with N-maleyl chitosan as dye adsorbent: isotherms, kinetics and thermodynamic investigation. Int. J. Biol. Macromol. 117, 152–166.
Pérez-Marín, A., Zapata, V.M., Ortuno, J., Aguilar, M., Sáez, J., Lloréns, M., 2007. Removal of cadmium from aqueous solutions by adsorption onto orange waste. J. Hazard. Mater. 139, 122–131.
Günay, A., Arslankaya, E., Tosun, I., 2007. Lead removal from aqueous solution by natural and pretreated clinoptilolite: adsorption equilibrium and kinetics. J. Hazard. Mater. 146, 362–371.
Rostamian, R., Najafi, M., Rafati, A.A., 2011. Synthesis and characterization of thiol-functionalized silica nano hollow sphere as a novel adsorbent for removal of poisonous heavy metal ions from water: kinetics, isotherms and error analysis. Chem. Eng. J. 171, 1004–1011.
Ahmed, M.J., Dhedan, S.K., 2012. Equilibrium isotherms and kinetics modeling of methylene blue adsorption on agricultural wastes-based activated carbons. Fluid Phase Equilib. 317, 9–14.
Sreńscek-Nazzal, J., Narkiewicz, U., Morawski, A.W., Wróbel, R.J., Michalkiewicz, B., 2015. Comparison of optimized isotherm models and error functions for carbon dioxide adsorption on activated carbon. J. Chem. Eng. Data 60, 3148–3158.
He, Y., Zhang, L., An, X., Wan, G., Zhu, W., Luo, Y., 2019. Enhanced fluoride removal from water by rare earth (La and Ce) modified alumina: adsorption isotherms, kinetics, thermodynamics and mechanism. Sci. Total Environ. 688, 184–198.
Marques, B.S., Frantz, T.S., Junior, T.R.S.A.C., de Almeida Pinto, L.A., Dotto, G.L., 2019. Adsorption of a textile dye onto piaçava fibers: kinetic, equilibrium, thermodynamics, and application in simulated effluents. Environ. Sci. Pollut. Res. 26, 28584–28592.
Ghalandari, V., Hashemipour, H., Bagheri, H., 2020. Experimental and modeling investigation of adsorption equilibrium of CH4, CO2, and N2 on activated carbon and prediction of multi-component adsorption equilibrium. Fluid Phase Equilib. 508, 112433.
Maleki Majd, K., Karparvarfard, S.H., Farahnaky, A., Jafarpour, K., 2013. Thermodynamic of water sorption of grape seed: temperature effect of sorption isotherms and thermodynamic characteristics. Food Biophys. 8, 1–11.
Cruz, F.P.B., Johann, G., de Oliveira, K.C., Palú, F., da Silva, E.A., Guirardello, R., et al., 2017. Crambe grain drying: evaluation of a linear and double resistance driving force model and energetic performance. Renew. Sust. Energ. Rev. 80, 1–8.
Mundada, M., Hathan, B.S., 2012. Studies on moisture sorption isotherms for osmotically pretreated and air-dried pomegranate arils. J. Food Process.Preserv. 36, 329–338.
Zare, D., Ranjbaran, M., Niakousari, M., Javidi, M., 2011. Thin layer drying and equilibrium moisture content equations for canola (Brassica napus L.).
Aharoni, C., Ungarish, M., 1977. Kinetics of activated chemisorption. Part 2. —Theoretical models. J. Chem. Soc., Faraday Trans. 1 73, 456–464.
Kim, Y., Kim, C., Choi, I., Rengaraj, S., Yi, J., 2004. Arsenic removal using mesoporous alumina prepared via a templating method. Environ. Sci. Technol. 38, 924–931.
Krishni, R., Foo, K., Hameed, B., 2014. Adsorption of cationic dye using a low-cost biowaste adsorbent: equilibrium, kinetic, and thermodynamic study. Desalin. Water Treat. 52, 6088–6095.
Hadi, M., Samarghandi, M.R., McKay, G., 2010. Equilibrium two-parameter isotherms of acid dyes sorption by activated carbons: study of residual errors. Chem. Eng. J. 160, 408–416.
Hu, X.-J., Wang, J.-S., Liu, Y.-G., Li, X., Zeng, G.-M., Bao, Z.-L., et al., 2011. Adsorption of chromium (VI) by ethylenediamine-modified cross-linked magnetic chitosan resin: isotherms, kinetics and thermodynamics. Journal of hazardous materials 185, 306–314.
Srivastava, S., Agrawal, S., Mondal, M., 2015. Biosorption isotherms and kinetics on removal of cr (VI) using native and chemically modified Lagerstroemia speciosa bark. Ecol. Eng. 85, 56–66.
Araújo, C.S., Almeida, I.L., Rezende, H.C., Marcionilio, S.M., Léon, J.J., de Matos, T.N., 2018. Elucidation of mechanism involved in adsorption of pb (II) onto Lobeira fruit (Solanum lycocarpum) using langmuirFreundlich and Temkin isotherms. 137, 348–354.
Paluri, P., Ahmad, K.A., Durbha, K.S., 2020. Importance of estimation of optimum isotherm model parameters for adsorption of methylene blue onto biomass derived activated carbons: comparison between linear and non-linear methods. Biomass Convers. Biorefinery 1–18.
Forssén, P., Fornstedt, T., 2015. A model free method for estimation of complicated adsorption isotherms in liquid chromatography. J. Chromatogr. A 1409, 108–115.
Serna-Guerrero, R., Sayari, A., 2010. Modeling adsorption of CO2 on amine-functionalized mesoporous silica. 2: kinetics and breakthrough curves. Chem. Eng. J. 161, 182–190.
Terzyk, A.P., Chatłas, J., Gauden, P.A., Rychlicki, G., Kowalczyk, P., 2003. Developing the solution analogue of the Toth adsorption isotherm equation. Journal of Colloid and Interface Science 266, 473–476 Academic Press Inc.
Feng, Y., Wang, J., Liu, Y., Zheng, Q., 2019. Adsorption equilibrium of hydrogen adsorption on activated carbon, multi-walled carbon nanotubes and graphene sheets. Cryogenics 101, 36–42.
Rocky, K.A., Pal, A., Moniruzzaman, M., Saha, B.B., 2019. Adsorption characteristics and thermodynamic property fields of polymerized ionic liquid and polyvinyl alcohol based composite/CO2 pairs. J. Mol. Liq. 294, 111555.
Wilson, S.M.W., Gabriel, V.A., Tezel, F.H., 2020. Adsorption of components from air on silica aerogels. Microporous Mesoporous Mater. 305, 110297.
Ghazy, M., Askalany, A.A., Saha, B.B., 2020. Maxsorb III/HFC404A as an adsorption pair for renewable energy driven systems. Int. J. Refrig. 120, 12–21.
Vargas, A.M., Cazetta, A.L., Martins, A.C., Moraes, J.C., Garcia, E.E., Gauze, G.F., et al., 2012. Kinetic and equilibrium studies: adsorption of food dyes acid yellow 6, acid yellow

23, and acid red 18 on activated carbon from flamboyant pods. Chem. Eng. J. 181, 243–250.
Balci, B., Erkurt, F.E., 2017. Adsorption of bisphenol-a by eucalyptus bark/magnetite composite: modeling the effect of some independent parameters by multiple linear regression. Adsorp. Sci. Technol. 35, 339–356.
Podder, M., Majumder, C., 2016b. Studies on the removal of as (III) and as (V) through their adsorption onto granular activated carbon/MnFe2O4 composite: isotherm studies and error analysis. Compos. Interfaces 23, 327–372.
Sulthana, R., Taqui, S.N., Zameer, F., Syed, U.T., Syed, A.A., 2018. Adsorption of ethidium bromide from aqueous solution onto nutraceutical industrial fennel seed spent: kinetics and thermodynamics modeling studies. Int. J. Phytoremediation 20, 1075–1086.
Afonso, R., Gales, L., Mendes, A., 2016. Kinetic derivation of common isotherm equations for surface and micropore adsorption. Adsorption 22, 963–971.
Eddy, N.O., Ibok, U.J., Ameh, P.O., Alobi, N.O., Sambo, M.M., 2014. Adsorption and quantum chemical studies on the inhibition of the corrosion of aluminum in HCl by Gloriosa superba (GS) gum. Chem. Eng. Commun. 201, 1360–1383.
Davoudinejad, M., Ghorbanian, S., 2013. Modeling of adsorption isotherm of benzoic compounds onto GAC and introducing three new isotherm models using new concept of adsorption effective surface (AES). Sci. Res. Essays 8, 2263–2275.
Fard, N.E., Fazaeli, R., Ghiasi, R., 2016. Band gap energies and photocatalytic properties of CdS and Ag/CdS nanoparticles for azo dye degradation. Chemical Engineering & Technology 39, 149–157.
Vijayaraghavan, K., 2015. Biosorption of lanthanide (praseodymium) using Ulva lactuca: mechanistic study and application of two, three, four and five parameter isotherm models. J. Environ. Biotechnol. Res. 1, 10–17.
Parker, G.R., 1995. Optimum isotherm equation and thermodynamic interpretation for aqueous 1, 1, 2-trichloroethene adsorption isotherms on three adsorbents. Adsorption 1, 113–132.
Das, D., Das, N., Mathew, L., 2010. Kinetics, equilibrium and thermodynamic studies on biosorption of ag (I) from aqueous solution by macrofungus pleurotus platypus. J. Hazard. Mater. 184, 765–774.
Sivarajasekar, N., Baskar, R., 2014b. Adsorption of basic red 9 onto activated carbon derived from immature cotton seeds: isotherm studies and error analysis. Desalin. Water Treat. 52, 7743–7765.
Fard, N.E., Fazaeli, R., 2018. Optimization of operating parameters in photocatalytic activity of visible light active Ag/TiO 2 nanoparticles. Russ. J. Phys. Chem. A 92, 2835–2846.
Jareteg, A., Maggiolo, D., Larsson, A., Thunman, H., Sasic, S., Ström, H., 2020a. Industrial-scale benzene adsorption: assessment of a baseline one-dimensional temperature swing model against online industrial data. Ind. Eng. Chem. Res. 59, 12239–12249.
Jareteg, A., Maggiolo, D., Sasic, S., Ström, H., 2020b. Finite-volume method for industrial-scale temperature-swing adsorption simulations. Comput. Chem. Eng. 138, 106852.
Kuah, W.C., Effendy, S., Farooq, S., 2018. Industrial scale propylene/propane separation using pressure vacuum swing adsorption. Ind. Eng. Chem. Res. 57, 6451–6463.
Jafari, L., Moradi, H., Tavan, Y., 2020. A theoretical and industrial study of component co-adsorption on 3A zeolite: an industrial case. Chem. Pap. 74, 651–661.
Cardenas, C., Latifi, A.M., Vallières, C., Marsteau, S., Sigot, L., 2021. Analysis of an industrial adsorption process based on ammonia chemisorption: modeling and simulation. Comput. Chem. Eng. 107474.
Zarei, S., Niad, M., 2017. Cystoseira myricaas for mercury (II) uptake: isotherm, kinetics, thermodynamic, response surface methodology and fuzzy modeling. J. Taiwan Inst. Chem. Eng. 81, 247–257.
Podder, M.S., Majumder, C.B., 2015c. SD/MnFe2O4 composite, a biosorbent for As(III) and As(V) removal from wastewater: optimization and isotherm study. J. Mol. Liq. 212, 382–404.
Das, D., Vimala, R., Das, N., 2014. Biosorption of Zn(II) onto pleurotus platypus: 5-level box-behnken design, equilibrium, kinetic and regeneration studies. Ecol. Eng. 64, 136–141.
Sivarajasekar, N., Baskar, R., 2014a. Adsorption of basic red 9 onto activated carbon derived from immature cotton seeds: isotherm studies and error analysis. Desalin. Water Treat. 52, 7743–7765.
Das, D., Basak, G., Lakshmi, V., Das, N., 2012. Kinetics and equilibrium studies on removal of zinc(II) by untreated and anionic surfactant treated dead biomass of yeast: batch and column mode. Biochem. Eng. J. 64, 30–47.
Saravanan, A., Kumar, P.S., Renita, A.A., 2018. Hybrid synthesis of novel material through acid modification followed ultrasonication to improve adsorption capacity for zinc removal. J. Clean. Prod. 172, 92–105.
Yu, W., Sepehrnoori, K., Patzek, T.W., 2016a. Modeling gas adsorption in marcellus shale with langmuir and bet isotherms. SPE Journal. 21, 589–600 Society of Petroleum Engineers.
Navea, J.G., Richmond, E., Stortini, T., Greenspan, J., 2017. Water adsorption isotherms on Fly ash from several sources. Langmuir 33, 10161–10171.
Alyousef, H., Ben Yahia, M., Aouaini, F., 2020. Statistical physics modeling of water vapor adsorption isotherm into kernels of dates: experiments, microscopic interpretation and thermodynamic functions evaluation. Arab. J. Chem. 13, 4691–4702.
Oliveira, E.H.C.D., Marques Fraga, D.M.D.S., Da Silva, M.P., Fraga, T.J.M., Carvalho, M.N., De Luna Freire, E.M.P., et al., 2019. Removal of toxic dyes from aqueous solution by adsorption onto highly recyclable xGnP® graphite nanoplatelets. J. Environ. Chem. Eng. 7, 103001.
Tsui, H.W., Cheng, K.T., Lin, A.Y., Chen, S.C., Hung, Y.L., Chou, P.Y., 2018. Solvent effects on the retention mechanisms of an amylose-based sorbent. J. Chromatogr. A 1556, 64–72.
De Rossi, A., Rigon, M.R., Zaparoli, M., Braido, R.D., Colla, L.M., Dotto, G.L., et al., 2018. Chromium (VI) biosorption by Saccharomyces cerevisiae subjected to chemical and thermal treatments. Environ. Sci. Pollut. Res. 25, 19179–19186.
Kostić, M., Radović, M., Velinov, N., Najdanović, S., Bojić, D., Hurt, A., et al., 2018. Synthesis of mesoporous triple-metal nanosorbent from layered double hydroxide as an efficient new sorbent for removal of dye from water and wastewater. Ecotoxicol. Environ. Saf. 159, 332–341.
Ahmad, M.A., Ahmad, N., Bello, O.S., 2015. Modified durian seed as adsorbent for the removal of methyl red dye from aqueous solutions. Appl Water Sci 5, 407–423.
Njoku, V., Asif, M., Hameed, B., 2015. 2, 4-dichlorophenoxyacetic acid adsorption onto coconut shell-activated carbon: isotherm and kinetic modeling. Desalin. Water Treat. 55, 132–141.
Ahmad, M.A., NAA, Puad, Bello, O.S., 2014b. Kinetic, equilibrium and thermodynamic studies of synthetic dye removal using pomegranate peel activated carbon prepared by microwave-induced KOH activation. Water Resour. Industry 6, 18–35.
Madrakian, T., Afkhami, A., Ahmadi, M., 2012. Adsorption and kinetic studies of seven different organic dyes onto magnetite nanoparticles loaded tea waste and removal of them from wastewater samples. Spectrochim. Acta A Mol. Biomol. Spectrosc. 99, 102–109.
Karoui, S., Ben Arfi, R., Fernández-Sanjurjo, M.J., Nuñez-Delgado, A., Ghorbal, A., Álvarez-Rodríguez, E., 2021. Optimization of synergistic biosorption of oxytetracycline and cadmium from binary mixtures on reed-based beads: modeling study using brouers-sotolongo models. Environ. Sci. Pollut. Res. 28, 46431–46447.
Brouers, F., Al-Musawi, T.J., 2015. On the optimal use of isotherm models for the characterization of biosorption of lead onto algae. J. Mol. Liq. 212, 46–51.
Dron, J., Dodi, A., 2011. Comparison of adsorption equilibrium models for the study of CL −, NO3− and SO42− removal from aqueous solutions by an anion exchange resin. J. Hazard. Mater. 190, 300–307.
Luo, J., Liu, Y., Jiang, C., Chu, W., Jie, W., Xie, H., 2011. Experimental and modeling study of methane adsorption on activated carbon derived from anthracite. J. Chem. Eng. Data 56, 4919–4926.
Ushiki, I., Ota, M., Sato, Y., Inomata, H., 2013. Measurements and dubinin-astakhov correlation of adsorption equilibria of toluene, acetone, n-hexane, n-decane and methanol solutes in supercritical carbon dioxide on activated carbon at temperature from 313 to 353 K and at pressure from 4.2 to 15.0 MPa. Fluid Phase Equilib. 344, 101–107.
Zhao, X., Zeng, X., Qin, Y., Li, X., Zhu, T., Tang, X., 2018. An experimental and theoretical study of the adsorption removal of toluene and chlorobenzene on coconut shell derived carbon. Chemosphere 206, 285–292.
Jribi, S., Miyazaki, T., Saha, B.B., Pal, A., Younes, M.M., Koyama, S., et al., 2017. Equilibrium and kinetics of CO2 adsorption onto activated carbon. Int. J. Heat Mass Transf. 108, 1941–1946.
Singh, V.K., Kumar, E.A., 2017. Experimental investigation and thermodynamic analysis of CO2 adsorption on activated carbons for cooling system. Journal of CO2 Utilization 17, 290–304.
Ahmad, M., Lee, S.S., Rajapaksha, A.U., Vithanage, M., Zhang, M., Cho, J.S., et al., 2013. Trichloroethylene adsorption by pine needle biochars produced at various pyrolysis temperatures. Bioresour. Technol. 143, 615–622.
Vieira, A.P., Santana, S.A., Bezerra, C.W., Silva, H.A., Chaves, J.A., Melo, J.C., et al., 2011. Removal of textile dyes from aqueous solution by babassu coconut epicarp (Orbignya speciosa). Chem. Eng. J. 173, 334–340.
Araga, R., Soni, S., Sharma, C.S., 2017. Fluoride adsorption from aqueous solution using activated carbon obtained from KOH-treated jamun (Syzygium cumini) seed. J. Environ. Chem. Eng. 5, 5608–5616.
James, O., Ajanaku, K., Ogunniran, K., Ajani, O., Siyanbola, T., John, M., 2011. Adsorption behaviour of pyrazolo [3, 4-b] pyridine on corrosion of stainless steel in HCl solutions. Trends in Applied Sciences Research 6, 910–917.
Farooq, M., Jalees, M., Iqbal, A., Zahra, N., Kiran, A., 2019. Characterization and adsorption study of biosorbents for the removal of basic cationic dye: kinetic and isotherm analysis. Des. Water Treat. 160, 333–342.
Jalees, M.I., Farooq, M.U., Basheer, S., Asghar, S., 2019a. Removal of heavy metals from drinking water using chikni mitti (kaolinite): isotherm and kinetics. Arab. J. Sci. Eng. 44, 6351–6359.
Ghanbari, A., Attar, M., Mahdavian, M., 2010. Corrosion inhibition performance of three imidazole derivatives on mild steel in 1 M phosphoric acid. Mater. Chem. Phys. 124, 1205–1209.
Nechifor, G., Pascu, D.-E., Pascu, M., Traistaru, G.A., Albu, P.C., 2015. Comparative study of temkin and flory-huggins isotherms for adsorption of phosphate anion on membranes. Sci. Bull. B [Internet] 77, 63–72.
Hossain, M., Ngo, H., Guo, W., Nguyen, T., 2012. Palm oil fruit shells as biosorbent for copper removal from water and wastewater: experiments and sorption models. Bioresour. Technol. 113, 97–101.
Akinbulumo, O.A., Odejobi, O.J., Odekanle, E.L., 2020. Thermodynamics and adsorption study of the corrosion inhibition of mild steel by Euphorbia heterophylla L. Extract in 1.5 M HCl. Results Mater. 5, 100074.
Mahmoud, M.E., El-Said, G.F., Rashedy, I.R., Abdelfattah, A.M., 2020. Assembly and implementation of an eco-friendly marine nanosediment for adsorptive removal of heptavalent manganese: adsorption isotherm, thermodynamic and kinetics studies. Powder Technol. 359, 247–260.
Khan, T.A., Dahiya, S., Ali, I., 2012. Use of kaolinite as adsorbent: equilibrium, dynamics and thermodynamic studies on the adsorption of rhodamine B from aqueous solution. Appl. Clay Sci. 69, 58–66.
Albatrni, H., Qiblawey, H., Almomani, F., Adham, S., Khraisheh, M., 2019. Polymeric adsorbents for oil removal from water. Chemosphere 233, 809–817.
Pennanen, T., Srivastava, V., Sillanpää, M., Sainio, T., 2020. Compost: potent biosorbent for the removal of heavy metals from industrial and landfill stormwater. J. Clean. Prod. 273, 122736.
Mokkapati, R., Ratnakaram, V., Mokkapati, J., 2018. Utilization of agro-waste for removal of toxic hexavalent chromium: surface interaction and mass transfer studies. Int. J. Environ. Sci. Technol. 15, 875–886.

Myśliwiec, D., Chylińska, M., Szymańska-Chargot, M., Chibowski, S., Zdunek, A., 2016. Revision of adsorption models of xyloglucan on microcrystalline cellulose. Cellulose 23, 2819–2829.
Chen, Z., Darancet, P., Wang, L., Crowther, A.C., Gao, Y., Dean, C.R., et al., 2014. Physical adsorption and charge transfer of molecular br 2 on graphene. ACS Nano 8, 2943–2950.
Koubaissy, B., Joly, G., Batonneau-Gener, I., Magnoux, P., 2011. Adsorptive removal of aromatic compounds present in wastewater by using dealuminated faujasite zeolite. Ind. Eng. Chem. Res. 50, 5705–5713.
Yonli, A.H., Kabore, H.A., Koulidiati, J., 2014. α-endosulfan removal from water by adsorption over natural clays from Burkina Faso: an isothermal study. J. Mater. Sci. Chem. Eng. 2, 49.
Hatch, C.D., Greenaway, A.L., Christie, M.J., Baltrusaitis, J., 2014. Water adsorption constrained Frenkel–Halsey–Hill adsorption activation theory: montmorillonite and illite. Atmos. Environ. 87, 26–33.
Laaksonen, A., 2015. A unifying model for adsorption and nucleation of vapors on solid surfaces. J. Phys. Chem. A 119, 3736–3745.
Kim, K.-M., Oh, H.-T., Lim, S.-J., Ho, K., Park, Y., Lee, C.-H., 2016. Adsorption equilibria of water vapor on zeolite 3A, zeolite 13X, and dealuminated Y zeolite. J. Chem. Eng. Data 61, 1547–1554.
Sadeek, S.A., Negm, N.A., Hefni, H.H., Wahab, M.M.A., 2015. Metal adsorption by agricultural biosorbents: adsorption isotherm, kinetic and biosorbents chemical structures. Int. J. Biol. Macromol. 81, 400–409.
Ahmad, R., Mirza, A., 2017. Adsorption of pb (II) and cu (II) by alginate-au-mica bionanocomposite: kinetic, isotherm and thermodynamic studies. Process Saf. Environ. Prot. 109, 1–10.
Akpa, O.M., Unuabonah, E.I., 2011. Small-sample corrected akaike information criterion: an appropriate statistical tool for ranking of adsorption isotherm models. Desalination 272, 20–26.
Toor, M., Jin, B., 2012. Adsorption characteristics, isotherm, kinetics, and diffusion of modified natural bentonite for removing diazo dye. Chem. Eng. J. 187, 79–88.
Alver, E., Metin, A.Ü., 2012. Anionic dye removal from aqueous solutions using modified zeolite: adsorption kinetics and isotherm studies. Chem. Eng. J. 200, 59–67.
Anirudhan, T., Ramachandran, M., 2015. Adsorptive removal of basic dyes from aqueous solutions by surfactant modified bentonite clay (organoclay): kinetic and competitive adsorption isotherm. Process Saf. Environ. Prot. 95, 215–225.
Khan, T.A., Chaudhry, S.A., Ali, I., 2015. Equilibrium uptake, isotherm and kinetic studies of cd (II) adsorption onto iron oxide activated red mud from aqueous solution. J. Mol. Liq. 202, 165–175.
Singh, D., Mishra, S., 2010. Synthesis and characterization of Hg (II)-ion-imprinted polymer: kinetic and isotherm studies. Desalination 257, 177–183.
Gao, Z.P., Yu, Z.F., Yue, T.L., Quek, S.Y., 2013. Adsorption isotherm, thermodynamics and kinetics studies of polyphenols separation from kiwifruit juice using adsorbent resin. J. Food Eng. 116, 195–201.
Ghaedi, M., Hajati, S., Karimi, F., Barazesh, B., Ghezelbash, G., 2013. Equilibrium, kinetic and isotherm of some metal ion biosorption. J. Ind. Eng. Chem. 19, 987–992.
Nilchi, A., Dehaghan, T.S., Garmarodi, S.R., 2013. Kinetics, isotherm and thermodynamics for uranium and thorium ions adsorption from aqueous solutions by crystalline tin oxide nanoparticles. Desalination 321, 67–71.
Khataee, A., Vafaei, F., Jannatkhah, M., 2013. Biosorption of three textile dyes from contaminated water by filamentous green algal spirogyra sp.: kinetic, isotherm and thermodynamic studies. Int. Biodeterior. Biodegradation 83, 33–40.
Amela, K., Hassen, M.A., Kerroum, D., 2012. Isotherm and kinetics study of biosorption of cationic dye onto banana peel. Energy Procedia 19, 286–295.
Kim, H., Kang, S.-O., Park, S., Park, H.S., 2015. Adsorption isotherms and kinetics of cationic and anionic dyes on three-dimensional reduced graphene oxide macrostructure. J. Ind. Eng. Chem. 21, 1191–1196.
Vučurović, V.M., Razmovski, R.N., Tekić, M.N., 2012. Methylene blue (cationic dye) adsorption onto sugar beet pulp: equilibrium isotherm and kinetic studies. J. Taiwan Inst. Chem. Eng. 43, 108–111.
Bhatti, H.N., Jabeen, A., Iqbal, M., Noreen, S., Naseem, Z., 2017. Adsorptive behavior of rice bran-based composites for malachite green dye: isotherm, kinetic and thermodynamic studies. J. Mol. Liq. 237, 322–333.
Gautam, P.K., Gautam, R.K., Banerjee, S., Lofrano, G., Sanroman, M.A., Chattopadhyaya, M.C., et al., 2015. Preparation of activated carbon from alligator weed (Alternenthera philoxeroids) and its application for tartrazine removal: isotherm, kinetics and spectroscopic analysis. J. Environ. Chem. Eng. 3, 2560–2568.
Daneshvar, E., Kousha, M., Sohrabi, M.S., Khataee, A., Converti, A., 2012. Biosorption of three acid dyes by the brown macroalga stoechospermum marginatum: isotherm, kinetic and thermodynamic studies. Chem. Eng. J. 195, 297–306.
Rout, P.R., Bhunia, P., Dash, R.R., 2014. Modeling isotherms, kinetics and understanding the mechanism of phosphate adsorption onto a solid waste: ground burnt patties. J. Environ. Chem. Eng. 2, 1331–1342.
de Luna, M.D.G., Flores, E.D., Genuino, D.A.D., Futalan, C.M., Wan, M.-W., 2013. Adsorption of eriochrome black T (EBT) dye using activated carbon prepared from waste rice hulls—Optimization, isotherm and kinetic studies. J. Taiwan Inst. Chem. Eng. 44, 646–653.
Setiabudi, H., Jusoh, R., Suhaimi, S., Masrur, S., 2016. Adsorption of methylene blue onto oil palm (Elaeis guineensis) leaves: process optimization, isotherm, kinetics and thermodynamic studies. J. Taiwan Inst. Chem. Eng. 63, 363–370.
Nassaji Jahromi, L., Fazaeli, R., Behjatmanesh-Ardakani, R., Taghdiri, M., 2020. Photocatalytic mineralization of disperse red 167.1 by cubic Cu2O nanoparticles: experimental and theoretical approach. J. Photochem. Photobiol. A Chem. 392, 112425.
Hashem, A., Hammad, H.A., Al-Anwar, A., 2016. Modified camelorum tree particles as a new adsorbent for adsorption of Hg(II) from aqueous solutions: kinetics, thermodynamics and non-linear isotherms. Desalin. Water Treat. 57, 23827–23843.
Asgarzadeh, S., Rostamian, R., Faez, E., Maleki, A., Daraei, H., 2016. Biosorption of Pb(II), Cu(II), and Ni(II) ions onto novel lowcost P. Eldarica leaves-based biosorbent: isotherm, kinetics, and operational parameters investigation. Desalin. Water Treat. 57, 14544–14551.
Nascimento, G.Ed., Duarte, M.M.M.B., Campos, N.F., Barbosa, C.M.Bd.M., 2014. Silva VLd. Adsorption of the reactive gray BF-2R dye on orange peel: kinetics and equilibrium studies. Desalin. Water Treat. 52, 1578–1588.
Schouwenaars, R., Montoya-Bautista, C.V., Isaacs-Páez, E.D., Solís-López, M., Ramírez-Zamora, R.M., 2017. Removal of arsenic III and V from laboratory solutions and contaminated groundwater by metallurgical slag through anion-induced precipitation. Environ. Sci. Pollut. Res. 24, 25034–25046.
Din, M.I., Hussain, Z., Mirza, M.L., Shah, A.T., Athar, M.M., 2014. Adsorption optimization of Lead (II) using saccharum bengalense as a non-conventional low cost biosorbent: isotherm and thermodynamics modeling. Int. J. Phytoremediation 16, 889–908.
Rangabhashiyam, S., Balasubramanian, P., 2018. Adsorption behaviors of hazardous methylene blue and hexavalent chromium on novel materials derived from pterospermum acerifolium shells. J. Mol. Liq. 254, 433–445.
Hisham, J., Elsousy, K.M., Hartany, K.A., 2016. Kinetics, equilibrium, and isotherm of the adsorption of cyanide by MDFSD. Arab. J. Chem. 9, S198–S203.
Ameh, P.O., Eddy, N.O., 2014. Commiphora pedunculata gum as a green inhibitor for the corrosion of aluminium alloy in 0.1 M HCl. Res. Chem. Intermed. 40, 2641–2649.
Rossi, E., Montoya Rojo, Ú., Cerrutti, P., Foresti, M.L., Errea, M.I., 2018. Carboxymethylated bacterial cellulose: an environmentally friendly adsorbent for lead removal from water. J. Environ. Chem. Eng. 6, 6844–6852.
Shen, W., Li, X., Lu, X., Guo, W., Zhou, S., Wan, Y., 2018. Experimental study and isotherm models of water vapor adsorption in shale rocks. J. Nat. Gas Sci. Eng. 52, 484–491.
García-Tejeda, Y.V., Barrera-Figueroa, V., 2019. Least squares fitting-polynomials for determining inflection points in adsorption isotherms of spray-dried açaí juice (Euterpe oleracea Mart.) and soy sauce powders. Powder Technol. 342, 829–839.
Ma, X., Shen, W., Li, X., Hu, Y., Liu, X., Lu, X., 2020. Experimental investigation on water adsorption and desorption isotherms of the longmaxi shale in the Sichuan BasinChina. 10, 1–12.
Singh, P., Talukdar, P., 2020. Determination of desorption isotherms of potato using gravimetric method and fast isotherm method. Heat Transfer Eng. 41, 513–521.
Zungur Bastıoğlu, A., Koç, M., Kaymak, Ertekin F., 2017. Moisture sorption isotherm of microencapsulated extra virgin olive oil by spray drying. J. Food Meas. Charact. 11, 1295–1305.
de Oliveira, G.H.H., Corrêa, P.C., de Oliveira, A.P.L.R., Reis, R.Cd., Devilla, I.A., 2017. Application of GAB model for water desorption isotherms and thermodynamic analysis of sugar beet seeds. J. Food Process Eng. 40, e12278.
Mikšík, F., Miyazaki, T., Thu, K., 2020. Adsorption isotherm modelling of water on Nanotailored mesoporous silica based on distribution function. Energies 13, 4247.
Khan, T.A., Nazir, M., Khan, E.A., 2013. Adsorptive removal of rhodamine B from textile wastewater using water chestnut (Trapa natans L.) peel: adsorption dynamics and kinetic studies. Toxicol. Environ. Chem. 95, 919–931.
Khalili, M.S., Zare, K., Moradi, O., Sillanpää, M., 2018. Preparation and characterization of MWCNT–COOH–cellulose–MgO NP nanocomposite as adsorbent for removal of methylene blue from aqueous solutions: isotherm, thermodynamic and kinetic studies. J. Nanostruct Chem. 8, 103–121.
Shahnaz, T., Sharma, V., Subbiah, S., Narayanasamy, S., 2020. Multivariate optimisation of cr (VI), co (III) and cu (II) adsorption onto nanobentonite incorporated nanocellulose/chitosan aerogel using response surface methodology. J. Water Process. Eng. 36, 101283.
Manjunatha, C., Nagabhushana, B., Raghu, M.S., Pratibha, S., Dhananjaya, N., Narayana, A., 2019. Perovskite lanthanum aluminate nanoparticles applications in antimicrobial activity, adsorptive removal of direct blue 53 dye and fluoride. Mater. Sci. Eng. C 101, 674–685.
Tümsek, F., Oz, Avcı, 2013. Investigation of kinetics and isotherm models for the acid orange 95 adsorption from aqueous solution onto natural minerals. J. Chem. Eng. Data 58, 551–559.
Arslan-Tontul, S., 2020a. Moisture sorption isotherm and thermodynamic analysis of quinoa grains. Heat Mass Transf. 1–8.
Thalerngnawachart, S., Duangmal, K., 2016. Influence of humectants on the drying kinetics, water mobility, and moisture sorption isotherm of osmosed air-dried papaya. Dry. Technol. 34, 574–583.
Chen, Q., Wang, G., Ma, X.X., Chen, M.L., Fang, C.H., Fei, B.H., 2020. The effect of graded fibrous structure of bamboo (Phyllostachys edulis) on its water vapor sorption isotherms. Ind. Crop. Prod. 151, 112467.
Gürses, A., Hassani, A., Kranşan, M., Açşl, Ö., Karaca, S., 2014. Removal of methylene blue from aqueous solution using by untreated lignite as potential low-cost adsorbent: kinetic, thermodynamic and equilibrium approach. J. Water Process. Eng. 2, 10–21.
Shi, Q., Lin, W., Zhao, Y., Zhang, P., Wang, R., 2016. Moisture adsorption isotherms and thermodynamic properties of Penaeus vannamei meat with and without maltodextrin addition. J. Aquat. Food Prod. Technol. 25, 1348–1367.
Arthur, E., Tuller, M., Moldrup, P., de Jonge, L.W., 2016. Evaluation of theoretical and empirical water vapor sorption isotherm models for soils. Water Resour. Res. 52, 190–205.
Fideles, R.A., Ferreira, G.M.D., Teodoro, F.S., Adarme, O.F.H., da Silva, L.H.M., Gil, L.F., et al., 2018. Trimellitated sugarcane bagasse: a versatile adsorbent for removal of cationic dyes from aqueous solution. Part I: batch adsorption in a monocomponent system. J. Colloid Interface Sci. 515, 172–188.
Ahmad, M., Moon, D.H., Vithanage, M., Koutsospyros, A., Lee, S.S., Yang, J.E., et al., 2014a. Production and use of biochar from buffalo-weed (Ambrosia trifida L.) for trichloroethylene removal from water. J. Chem. Technol. Biotechnol. 89, 150–157.
Ashiq, A., Sarkar, B., Adassooriya, N., Walpita, J., Rajapaksha, A.U., Ok, Y.S., et al., 2019. Sorption process of municipal solid waste biochar-montmorillonite composite for ciprofloxacin removal in aqueous media. Chemosphere 236, 124384.

Dehghani, M.H., Dehghan, A., Najafpoor, A., 2017. Removing reactive red 120 and 196 using chitosan/zeolite composite from aqueous solutions: kinetics, isotherms, and process optimization. J. Ind. Eng. Chem. 51, 185–195.

Lin, G., Hu, T., Wang, S., Xie, T., Zhang, L., Cheng, S., et al., 2019. Selective removal behavior and mechanism of trace Hg (II) using modified corn husk leaves. Chemosphere 225, 65–72.

Makhlouf, C., Ladhari, N., Roudesli, S., Sakly, F., 2012. Influence of grafting with acrylic acid on the dyeing properties of polyamide 6.6 fibres. Color. Technol. 128, 176–183.

Balasubramani, K., Sivarajasekar, N., Naushad, M., 2020. Effective adsorption of antidiabetic pharmaceutical (metformin) from aqueous medium using graphene oxide nanoparticles: equilibrium and statistical modelling. J. Mol. Liq. 301, 112426.

Rafati, L., Ehrampoush, M.H., Rafati, A.A., Mokhtari, M., Mahvi, A.H., 2016. Modeling of adsorption kinetic and equilibrium isotherms of naproxen onto functionalized nanoclay composite adsorbent. J. Mol. Liq. 224, 832–841.

Kumar, P.S., Varjani, S.J., Suganya, S., 2018. Treatment of dye wastewater using an ultrasonic aided nanoparticle stacked activated carbon: kinetic and isotherm modelling. Bioresour. Technol. 250, 716–722.

Kalhor, M.M., Rafati, A.A., Rafati, L., Rafati, A.A., 2018. Synthesis, characterization and adsorption studies of amino functionalized silica nano hollow sphere as an efficient adsorbent for removal of imidacloprid pesticide. J. Mol. Liq. 266, 453–459.

Arabloo, M., Ghazanfari, M.H., Rashtchian, D., 2015. Spotlight on kinetic and equilibrium adsorption of a new surfactant onto sandstone minerals: a comparative study. J. Taiwan Inst. Chem. Eng. 50, 12–23.

Bekkouche, S., Baup, S., Bouhelassa, M., Molina-Boisseau, S., Petrier, C., 2012. Competitive adsorption of phenol and heavy metal ions onto titanium dioxide (Dugussa P25). Desalin. Water Treat. 37, 364–372.

Kumar, P.S., Ramalingam, S., Senthamarai, C., Niranjanaa, M., Vijayalakshmi, P., Sivanesan, S., 2010b. Adsorption of dye from aqueous solution by cashew nut shell: studies on equilibrium isotherm, kinetics and thermodynamics of interactions. Desalination 261, 52–60.

Mandal, A., Singh, N., 2016. Kinetic and isotherm error optimization studies for adsorption of atrazine and imidacloprid on bark of Eucalyptus tereticornis L. J. Environ. Sci. Health B 51, 192–203.

Mpatani, F.M., Aryee, A.A., Kani, A.N., Wen, K., Dovi, E., Qu, L., et al., 2020. Removal of methylene blue from aqueous medium by citrate modified bagasse: kinetic, equilibrium and thermodynamic study. Bioresour. Technol. Rep. 11, 100463.

Supelano, G., Cuaspud, J.G., Moreno-Aldana, L.C., Ortiz, C., Trujillo, C., Palacio, C., et al., 2020. Synthesis of magnetic zeolites from recycled fly ash for adsorption of methylene blue. Fuel 263, 116800.

Pei, J., Zhang, J.S., 2012. Determination of adsorption isotherm and diffusion coefficient of toluene on activated carbon at low concentrations. Build. Environ. 48, 66–76.

Baseri, H., Tizro, S., 2017. Treatment of nickel ions from contaminated water by magnetite based nanocomposite adsorbents: effects of thermodynamic and kinetic parameters and modeling with langmuir and freundlich isotherms. Process Saf. Environ. Prot. 109, 465–477.

Sandberg, T., Weinberger, C., Karaman, D.Ş., Rosenholm, J.M., 2018. Modeling of a hybrid langmuir adsorption isotherm for describing interactions between drug molecules and silica surfaces. J. Pharm. Sci. 107, 1392–1397.

Srilakshmi, C., Saraf, R., 2016. Ag-doped hydroxyapatite as efficient adsorbent for removal of Congo red dye from aqueous solution: synthesis, kinetic and equilibrium adsorption isotherm analysis. Microporous Mesoporous Mater. 219, 134–144.

Ali, M., Mahmud, H.B., 2015. The effects of concentration and salinity on polymer adsorption isotherm at sandstone rock surface. IOP Conference Series: Materials Science and Engineering. 78. IOP Publishing, p. 012038.

Ganesan, P., Kamaraj, R., Vasudevan, S., 2013. Application of isotherm, kinetic and thermodynamic models for the adsorption of nitrate ions on graphene from aqueous solution. J. Taiwan Inst. Chem. Eng. 44, 808–814.

Milmile, S.N., Pande, J.V., Karmakar, S., Bansiwal, A., Chakrabarti, T., Biniwale, R.B., 2011. Equilibrium isotherm and kinetic modeling of the adsorption of nitrates by anion exchange indion NSSR resin. Desalination 276, 38–44.

Pandiarajan, A., Kamaraj, R., Vasudevan, S., Vasudevan, S., 2018. OPAC (orange peel activated carbon) derived from waste orange peel for the adsorption of chlorophenoxyacetic acid herbicides from water: adsorption isotherm, kinetic modelling and thermodynamic studies. Bioresour. Technol. 261, 329–341.

Deyab, M., 2014. Adsorption and inhibition effect of ascorbyl palmitate on corrosion of carbon steel in ethanol blended gasoline containing water as a contaminant. Corros. Sci. 80, 359–365.

Ghasemi, M., Naushad, M., Ghasemi, N., Khosravi-Fard, Y., 2014. Adsorption of pb (II) from aqueous solution using new adsorbents prepared from agricultural waste: adsorption isotherm and kinetic studies. J. Ind. Eng. Chem. 20, 2193–2199.

Singh, A.K., Quraishi, M., 2010. Effect of cefazolin on the corrosion of mild steel in HCl solution. Corros. Sci. 52, 152–160.

Reddy, Y.S., Magdalane, C.M., Kaviyarasu, K., Mola, G.T., Kennedy, J., Maaza, M., 2018. Equilibrium and kinetic studies of the adsorption of acid blue 9 and safranin O from aqueous solutions by MgO decked FLG coated Fuller's earth. J. Phys. Chem. Solids 123, 43–51.

Sumathi, S., Bhatia, S., Lee, K., Mohamed, A., 2010. Adsorption isotherm models and properties of SO2 and NO removal by palm shell activated carbon supported with cerium (Ce/PSAC). Chem. Eng. J. 162, 194–200.

Hyder, A., Begum, S.A., Egiebor, N.O., 2015. Adsorption isotherm and kinetic studies of hexavalent chromium removal from aqueous solution onto bone char. J. Environ. Chem. Eng. 3, 1329–1336.

Owalude, S.O., Tella, A.C., 2016. Removal of hexavalent chromium from aqueous solutions by adsorption on modified groundnut hull. Beni-Seuf Univ. J. Appl. 5, 377–388.

Swain, S.K., Sarkar, D., 2013. Study of BSA protein adsorption/release on hydroxyapatite nanoparticles. Appl. Surf. Sci. 286, 99–103.

Egbosiuba, T., Abdulkareem, A., Kovo, A., Afolabi, E., Tijani, J., Auta, M., et al., 2020. Ultrasonic enhanced adsorption of methylene blue onto the optimized surface area of activated carbon: adsorption isotherm, kinetics and thermodynamics. Chem. Eng. Res. Des. 153, 315–336.

Ren, H., Gao, Z., Wu, D., Jiang, J., Sun, Y., Luo, C., 2016. Efficient pb (II) removal using sodium alginate–carboxymethyl cellulose gel beads: preparation, characterization, and adsorption mechanism. Carbohydr. Polym. 137, 402–409.

Huang, Z., Li, Y., Chen, W., Shi, J., Zhang, N., Wang, X., et al., 2017. Modified bentonite adsorption of organic pollutants of dye wastewater. Mater. Chem. Phys. 202, 266–276.

Nasuha, N., Hameed, B., 2011. Adsorption of methylene blue from aqueous solution onto NaOH-modified rejected tea. Chem. Eng. J. 166, 783–786.

Sivarajasekar, N., Baskar, R., 2015. Biosorption of basic violet 10 onto activated Gossypium hirsutum seeds: batch and fixed-bed column studies. Chin. J. Chem. Eng. 23, 1610–1619.

Podder, M., Majumder, C., 2015a. Removal of arsenic by a Bacillus arsenicus biofilm supported on GAC/MnFe2O4 composite. Groundw. Sustain. Dev. 1, 105–128.

Podder, M., Majumder, C., 2015b. SD/MnFe2O4 composite, a biosorbent for as (III) and as (V) removal from wastewater: optimization and isotherm study. J. Mol. Liq. 212, 382–404.

Podder, M., Majumder, C., 2016a. Investigation on elimination of as (III) and as (V) from wastewater using bacterial biofilm supported on Sawdust/MnFe 2 O 4 composite. Water Conserv. Sci. Eng. 1, 21–48.

Neeli, S.T., Ramsurn, H., Ng, C.Y., Wang, Y., Lu, J., 2020. Removal of cr (VI), as (V), cu (II), and pb (II) using cellulose biochar supported iron nanoparticles: a kinetic and mechanistic study. J. Environ. Chem. Eng. 8, 103886.

GHH, de Oliveira, APLR, de Oliveira, MVC, de Souza, Neves, R.F., Botelho, F.M., Botelho, S., 2020. Water adsorption isotherms of coffee blends. Embrapa Agrossilvipastoril-Artigo em periódico indexado (ALICE).

Saha, D., Deng, S., 2011. Hydrogen adsorption on Pd-and Ru-doped C60 fullerene at an ambient temperature. Langmuir 27, 6780–6786.

Gazor, H.R., Eyvani, A., 2011. Adsorption isotherms for red onion slices using empirical and neural network models. Int. J. Food Eng. 7.

Jamaluddin, N., Razak, N., Shaari, A., 2020. Moisture adsorption isotherms of dried Ficus deltoidea herbal leaves. IOP Conference Series: Materials Science and Engineering. 932. IOP Publishing, p. 012025.

Eyni, H., Tahermansouri, H., Kiani, F., Jahangiri, M., 2019. Kinetics, equilibrium and isotherms of Pb2+ adsorption from aqueous solutions on carbon nanotubes functionalized with 3-amino-5a, 10a-dihydroxybenzo [b] indeno [2, ld] furan-10-one. New Carbon Mater. 34, 512–523.

Parsa, M.M., Pourfakhar, H., Baghdadi, M., 2020. Application of graphene oxide nanosheets in the coagulation-flocculation process for removal of Total organic carbon (TOC) from surface water. J. Water Process Eng. 37, 101367.

Auta, M., Hameed, B., 2012. Modified mesoporous clay adsorbent for adsorption isotherm and kinetics of methylene blue. Chem. Eng. J. 198, 219–227.

Wang, Z., Yin, P., Qu, R., Chen, H., Wang, C., Ren, S., 2013. Adsorption kinetics, thermodynamics and isotherm of hg (II) from aqueous solutions using buckwheat hulls from jiaodong of China. Food Chem. 136, 1508–1514.

Shahmohammadi-Kalalagh, S., Babazadeh, H., 2014. Isotherms for the sorption of zinc and copper onto kaolinite: comparison of various error functions. Int. J. Environ. Sci. Technol. 11, 111–118.

Vilela, P.B., Matias, C.A., Dalalibera, A., Becegato, V.A., Paulino, A.T., 2019. Polyacrylic acid-based and chitosan-based hydrogels for adsorption of cadmium: equilibrium isotherm, kinetic and thermodynamic studies. J. Environ. Chem. Eng. 7, 103327.

Roghanizad, A., Abdolmaleki, M.K., Ghoreishi, S.M., Dinari, M., 2020. One-pot synthesis of functionalized mesoporous fibrous silica nanospheres for dye adsorption: isotherm, kinetic, and thermodynamic studies. J. Mol. Liq. 300, 112367.

Mangwandi, C., Kurniawan, T.A., Albadarin, A.B., 2020. Comparative biosorption of chromium (VI) using chemically modified date pits (CM-DP) and olive stone (CM-OS): kinetics, isotherms and influence of co-existing ions. Chem. Eng. Res. Des. 156, 251–262.

Zhang, H., Wu, D., Huang, Q., Liu, Z., Luo, X., Xiong, S., et al., 2020. Adsorption kinetics and thermodynamics of yeast β-glucan for off-odor compounds in silver carp mince. Food Chem. 319, 126232.

Subbaiah, M.V., Kim, D.-S., 2016. Adsorption of methyl orange from aqueous solution by aminated pumpkin seed powder: kinetics, isotherms, and thermodynamic studies. Ecotoxicol. Environ. Saf. 128, 109–117.

de Franco, M.A.E., de Carvalho, C.B., Bonetto, M.M., de Pelegrini, Soares R., Féris, L.A., 2017. Removal of amoxicillin from water by adsorption onto activated carbon in batch process and fixed bed column: kinetics, isotherms, experimental design and breakthrough curves modelling. J. Clean. Prod. 161, 947–956.

Juhola, R., Runtti, H., Kangas, T., Hu, T., Romar, H., Tuomikoski, S., 2020. Bisphenol a removal from water by biomass-based carbon: isotherms, kinetics and thermodynamics studies. Environ. Technol. 41, 971–980.

Feng, L., Shen, Y., Wu, T., Liu, B., Zhang, D., Tang, Z., 2020. Adsorption equilibrium isotherms and thermodynamic analysis of CH 4, CO 2, CO, N 2 and H 2 on NaY zeolite. Adsorption 26, 1101–1111.

Bagheri, H., Mohebbi, A., Mirzaie, M., Ghalandari, V., 2021. Mathematical modeling of reactor for water remediation. Appl. Water Sci. Remediat. Technol. 2, 107–170.

Contreras, A.P., Mendoza, J.S., Lozano, K.C., Paternina, M.G., 2017. Characterization and desorption isotherm modeling of cassava bagasse (Manihot esculenta Crantz). Starch-Stärke 3, n/a-n/a.

Ma, C.M., Chen, H.W., Hong, G.B., 2016. Moisture sorption isotherm characteristics of hemerocallis fulva and cymbopogon. Asia Pac. J. Chem. Eng. 11, 757–765.

Sharma, R., Srivastava, T., Saxena, D., 2019. Moisture sorption isotherm modeling approach and effect of packaging material on quality changes in extruded product stored under controlled conditions. J. Packag. Technol. Res. 3, 57–65.

Chisté, R.C., Silva, P.A., Lopes, A.S., da Silva, Pena R., 2012. Sorption isotherms of tapioca flour. Int. J. Food Sci. Technol. 47, 870–874.
Sun, S., Su, Z., Cui, S., 2017. Study on the continuing education innovative talents training mode of civil engineering major. IOP Conference Series: Earth and Environmental Science. 100. IOP Publishing, p. 012197.
Arslan-Tontul, S., 2020b. Moisture sorption isotherm, isosteric heat and adsorption surface area of whole chia seeds. LWT 119, 108859.
Garnier, C., Finqueneisel, G., Zimny, T., Pokryszka, Z., Lafortune, S., Défossez, P., et al., 2011. Selection of coals of different maturities for CO2 storage by modelling of CH4 and CO2 adsorption isotherms. Int. J. Coal Geol. 87, 80–86.
Duran, C., Ozdes, D., Gundogdu, A., Senturk, H.B., 2011. Kinetics and isotherm analysis of basic dyes adsorption onto almond shell (Prunus dulcis) as a low cost adsorbent. J. Chem. Eng. Data 56, 2136–2147.
Shrestha, S., Son, G., Lee, S.H., Lee, T.G., 2013. Isotherm and thermodynamic studies of zn (II) adsorption on lignite and coconut shell-based activated carbon fiber. Chemosphere 92, 1053–1061.
Ismail, B., Hussain, S.T., Akram, S., 2013. Adsorption of methylene blue onto spinel magnesium aluminate nanoparticles: adsorption isotherms, kinetic and thermodynamic studies. Chem. Eng. J. 219, 395–402.
Masoumi, A., Ghaemy, M., 2014. Removal of metal ions from water using nanohydrogel tragacanth gum-g-polyamidoxime: isotherm and kinetic study. Carbohydr. Polym. 108, 206–215.
Bordoloi, N., Goswami, R., Kumar, M., Kataki, R., 2017. Biosorption of Co (II) from aqueous solution using algal biochar: kinetics and isotherm studies. Bioresour. Technol. 244, 1465–1469.
Hajahmadi, Z., Younesi, H., Bahramifar, N., Khakpour, H., Pirzadeh, K., 2015. Multicomponent isotherm for biosorption of zn (II), CO (II) and cd (II) from ternary mixture onto pretreated dried aspergillus Niger biomass. Water Resour. Ind. 11, 71–80.
Mahmoud, H.R., Ibrahim, S.M., El-Molla, S.A., 2016. Textile dye removal from aqueous solutions using cheap MgO nanomaterials: adsorption kinetics, isotherm studies and thermodynamics. Adv. Powder Technol. 27, 223–231.
Shin, H.S., Kim, J.-H., 2016. Isotherm, kinetic and thermodynamic characteristics of adsorption of paclitaxel onto diaion HP-20. Process Biochem. 51, 917–924.
Subramani, S., Thinakaran, N., 2017. Isotherm, kinetic and thermodynamic studies on the adsorption behaviour of textile dyes onto chitosan. Process Saf. Environ. Prot. 106, 1–10.
Chakraborty, R., Verma, R., Asthana, A., Vidya, S.S., Singh, A.K., 2021. Adsorption of hazardous chromium (VI) ions from aqueous solutions using modified sawdust: kinetics, isotherm and thermodynamic modelling. Int. J. Environ. Anal. Chem. 101, 911–928.
Jalees, M.I., Farooq, M.U., Basheer, S., Asghar, S., 2019;;. Removal of heavy metals from drinking water using chikni mitti (Kaolinite): isotherm and kinetics. Arab. J. Sci. Eng. 44.
Vergis, B.R., Kottam, N., Krishna, R.H., Nagabhushana, B., 2019. Removal of Evans blue dye from aqueous solution using magnetic spinel ZnFe2O4 nanomaterial: adsorption isotherms and kinetics. Nano-Struct. Nano-Objects 18, 100290.
Kavci, E., 2021. Malachite green adsorption onto modified pine cone: isotherms, kinetics and thermodynamics mechanism. Chem. Eng. Commun. 208, 318–327.
Hassan, W., Noureen, S., Mustaqeem, M., Saleh, T.A., Zafar, S., 2020. Efficient adsorbent derived from haloxylon recurvum plant for the adsorption of acid brown dye: kinetics, isotherm and thermodynamic optimization. Surf. Interfaces 20, 100510.
Patil, S.R., Sutar, S.S., Jadhav, J.P., 2020. Sorption of crystal violet from aqueous solution using live roots of Eichhornia crassipes: kinetic, isotherm, phyto and cyto-genotoxicity studies. Environ. Technol. Innov. 18, 100648.
Liu, Y., Xiong, Y., Xu, P., Pang, Y., Du, C., 2020. Enhancement of pb (II) adsorption by boron doped ordered mesoporous carbon: isotherm and kinetics modeling. Sci. Total Environ. 708, 134918.
Hashem, A., Taha, G.M., Fletcher, A.J., Mohamed, L.A., Samaha, S.H., 2020. Highly efficient adsorption of Cd(II) onto carboxylated camelthorn biomass: applicability of three-parameter isotherm models, kinetics, and mechanism. J. Polym. Environ. 1–13.
Son, K.N., Richardson, T.M.J., Cmarik, G.E., 2019. Equilibrium adsorption isotherms for H 2 O on zeolite 13X. J. Eng. Data 64, 1063–1071.
Sridhar, P., Kaisare, N.S., 2020. A critical analysis of transport models for refueling of MOF-5 based hydrogen adsorption system. J. Ind. Eng. Chem. 85, 170–180.
Behloul, S., Hamitouche, A.-E., Haffas, M., Boudjemaa, A., Benammar, S., Sehailia, M., et al., 2018. Removal of methyl violet dye by a low-cost waste (Ajuga pseudo-Iva): kinetic and equilibrium isotherm study. Can. J. Chem. Eng. 96, 2282–2291.
Diaz de Tuesta, J.L., Silva, A.M.T., Faria, J.L., Gomes, H.T., 2020. Adsorption of Sudan-IV contained in oily wastewater on lipophilic activated carbons: kinetic and isotherm modelling. Environ. Sci. Pollut. Res. 27, 20770–20785.
Moreno-Piraján, J., Giraldo, L., 2010. Adsorption of copper from aqueous solution by activated carbons obtained by pyrolysis of cassava peel. J. Anal. Appl. Pyrolysis 87, 188–193.
Moreno-Piraján, J., Giraldo, L., 2011. Activated carbon obtained by pyrolysis of potato peel for the removal of heavy metal copper (II) from aqueous solutions. J. Anal. Appl. Pyrolysis 90, 42–47.
Kashi, N., Fard, N.E., Fazaeli, R., 2017. Empirical modeling and CCD-based RSM optimization of cd (II) adsorption from aqueous solution on clinoptilolite and bentonite. Russ. J. Appl. Chem. 90, 977–992.